Salt Functionalization System for Protection against Airborne Diseases

by

Ilaria Rubino

A thesis submitted in partial fulfillment of the requirements for the degree of

Doctor of Philosophy

in

Chemical Engineering

Department of Chemical and Materials Engineering
University of Alberta

Abstract

Infectious respiratory diseases, caused by viruses and bacteria that attack the respiratory system, constitute a serious threat in public health around the world. Pathogens can be transmitted in the air though large droplets or aerosols. As aerosols can linger in the environment for a prolonged time and travel long distances, airborne transmission causes fast and efficient transmission. Infection prevention plays a critical role against airborne particles in healthcare and for the public. In particular, respiratory protective devices, such as the commonly used N95 respirator and surgical mask, are the first line of defense during outbreaks and in susceptible settings. In spite of their indispensable function in infection control and emergency preparedness, masks have experienced limited progress over the years. Currently available masks exhibit unresolved technical challenges, including survival of the collected pathogens, filtration efficiency limited by breathability, and restriction to a single use of the devices. These lead to the risk of cross-infection from pathogen-laden filters, low effectiveness in infection prevention, low compliance to the recommended modes of use, and shortages of masks during outbreaks. Therefore, our research objective was the development of universal infection control measures against pathogenic aerosols. To this end, we successfully coated fibrous polymeric substrates with salt crystal films to produce highly effective, pathogen-inactivating filters.

Formulations were identified to develop coatings based on different salt candidates, and formation of the salt coatings were confirmed by scanning electron microscopy (SEM), energy dispersive X-ray (EDX) and X-ray diffraction (XRD) analysis. We hypothesized that salt coatings inactivate pathogens by first dissolving upon contact with the pathogenic aerosols, and then physically damaging the pathogens during the evaporation-induced salt recrystallization. For demonstration of the concept, surgical mask filters were coated with sodium chloride salt.

Successful, quick pathogen inactivation was demonstrated both *in vitro* (by hemagglutinin activity (HA), virus titer, native fluorescence and nile red fluorescence measurements) and *in vivo* against aerosols of multiple strains of influenza virus. Additionally, our preliminary investigation showed that sodium chloride-coated filters have high filtration efficiency and stability after prolonged incubation at 37 °C and 70% relative humidity.

Next, non-functional fibrous membranes were coated with uniform layers of sodium chloride, potassium sulfate and potassium chloride. The filtration efficiency tested against bacterial aerosols showed that the salt coatings turned the inert membranes into filters with high pathogen capture performance. Simultaneously, the pressure drop measured across the salt-coated filters at a breathing air flow did not increase compared the bare membranes. Following exposure to both virus and bacteria aerosols, all the developed salt coatings caused rapid pathogen inactivation, as measured by HA titer/virus titer and colony forming units (CFU) measurements, respectively. The physical damage on the pathogens was observed by transmission electron microscopy (TEM). Furthermore, the salt-coated filters were observed to be stable and functional following storage at 37 °C and 70, 80 and 90% relative humidity.

Finally, the pathogen inactivation mechanism was analyzed by focusing on the interaction between salt powders and bacteria aerosols over time. It was observed that the salt recrystallization kinetics well matched the pathogen inactivation behaviors. Additionally, the salt recrystallization was observed to be the primary pathogen inactivation mechanism, although the high salt concentration during the aerosol evaporation was found to have a minor effect.

Overall, this thesis has developed a technology for production of highly effective, low-cost infection control devices with universal pathogen inactivation and safe reusability, which can be used to tackle public health issues related to respiratory disease transmission worldwide.

Preface

Part of the research conducted for this thesis is associated with research collaborations, led by Dr. Hyo-Jick Choi at the University of Alberta, with Dr. Sang-Moo Kang at Georgia State University (Atlanta, GA, U.S.), Dr. Fu-Shi Quan at Kyung Hee University (Seoul, Korea), Dr. Byeong Hwa Jeon at University of Minnesota (Minneapolis, MN, U.S.; previously at University of Alberta), and Dr. Chun Il Kim at University of Alberta. Part of the influenza virus growth and inactivation experiments referred to in Chapters 2 and 3 were implemented by myself, with the assistance of Dr. S.-M. Kang; I completed the remaining myself. The animal studies were conducted by Dr. F.-S. Quan and the data analysis was completed by myself (Chapters 2 and 3). All animal protocols were approved by the Kyung Hee University (KHU) Institutional Animal Care and Use Committee (IACUC); all animal experiments and husbandry were conducted under the approved protocols and guidelines of KHU IACUC; KHU IACUC operates under National Veterinary Research and Quarantine Service (NVRQS), and animal welfare law and regulations of the WOAH-OIE (World organization for animal health). I conducted part of the bacteria work referred to in Chapter 3 with the assistance of Dr. B. H. Jeon; I completed the remaining myself. The literature review in Chapter 1, methods design and data analysis in Chapters 2 and 3, and concluding analysis in Chapter 4 are my original work.

Section 1.5 of this thesis has been adapted from the journal article published as I. Rubino, and H.-J. Choi, “Respiratory Protection against Pandemic and Epidemic Diseases”, Trends in Biotechnology, vol. 35, issue 10, 907-910 (2017). I contributed as first author and was responsible for literature review and writing the manuscript; H.-J. Choi was the corresponding author and assisted in writing the manuscript.

Chapter 2 of this thesis has been published as F.-S. Quan, I. Rubino, S.-H. Lee, B. Koch, and H.-J. Choi, "Universal and Reusable Virus Deactivation System for Respiratory Protection", Scientific Reports, vol. 7, 39956 (2017). I contributed as co-first author and was responsible for performing experiments, data analysis, and writing the manuscript. F.-S. Quan and B. Koch assisted with performing experiments, data analysis, and manuscript editing. S.-H. Lee assisted with performing experiments and data analysis. H.-J. Choi was the corresponding author, was involved with conceiving and designing the experiments, and assisted with performing experiments, data analysis, and writing the manuscript.

Section 3.1 of this thesis has been adapted from the manuscript under consideration for publication as I. Rubino, E. Oh, S. Han, S. Kaleem, A. Hornig, S.-H. Lee, H.-J. Kang, D.-H. Lee, K.-B. Chu, S. Kumaran, S. Armstrong, R. Lalani, S. Choudhry, C. I. Kim, F.-S. Quan, B. H. Jeon, and H.-J. Choi, "Salt coatings functionalize inert membranes into high-performing filters against infectious respiratory diseases". I was responsible for designing and performing experiments, data analysis, and writing the manuscript. E. Oh, S. Han, S. Kaleem, A. Hornig, S.-H. Lee, H.-J. Kang, D.-H. Lee, K.-B. Chu, S. Kumaran, S. Armstrong, R. Lalani, S. Choudhry, C. I. Kim, F.-S. Quan, and B. H. Jeon assisted with performing the experiments, data analysis, and/or manuscript editing. H.-J. Choi was the corresponding author, was involved with conceiving and designing the experiments, and assisted with performing experiments, data analysis, and writing the manuscript.

"Credo di poter affermare che nella ricerca scientifica, né il grado di intelligenza né la capacità di eseguire e portare a termine con esattezza il compito intrapreso siano i fattori essenziali per la riuscita e la soddisfazione personale. Nell'una e nell'altra contano maggiormente la totale dedizione e il chiudere gli occhi davanti alle difficoltà: in tal modo possiamo affrontare problemi che altri, più critici e acuti, non affronterebbero."

"I have become persuaded that, in scientific research, neither the degree of one's intelligence nor the ability to carry out one's tasks with perfection are factors essential to personal success and fulfilment. More important for the attaining of both ends are total dedication and a tendency to underestimate difficulties, which cause one to tackle problems that other, more critical and acute persons instead opt to avoid."

Rita Levi-Montalcini

Acknowledgments

I would like to sincerely thank my supervisor, Dr. Hyo-Jick Choi, without whom this work would not have been possible. He personally taught me research skills in the lab and beyond. His supervision has shaped this journey of discovery that my PhD has been, and for that I am grateful. I thank my supervisory committee members, Dr. Janet Elliott and Dr. Hasan Uludag, for their valuable advice and support on my thesis project, which encouraged me to improve at every turn.

A huge thank you goes to my groupmates, present and past, for their continued friendship and help in and outside of the lab; Bahman, Harish, Manika, Sumin, Euna, Surjith, Matthew, Ankit, and Chengmeng, I am confident our paths will cross again. I will never forget the inspiration from mentoring undergraduate and high school students; Sally, Sarah, Sana, Romani, Miyoung, Iryna, Shivanjali, Alex, and Minho, you have each left an important mark on this work.

Additionally, I am most appreciative of our collaborators at the University of Alberta and around the world. Dr. Sang-Moo Kang welcomed me to his lab at Georgia State University (U.S.) and I am thankful for his support as he went above and beyond to ensure I had a successful experience and progress on my thesis; I would like to also thank his group, Yu-Jin, Youri, Ki-Hye, Noopur, Bo, Jeeva, YoungMan, and Zhuo for their exceptional help on the virology techniques, as well as for making me feel at home in Atlanta. I am grateful to Dr. Fu-Shi Quan (Kyung Hee University, Korea) for her outstanding support and assistance in the project and during my research visit; a special thank you to her group, Su-Hwa, Hae-Ji, Dong-Hun, and Ki-Back, for their tireless contribution as well as for showing me all the best Korean foods. Dr. Byeong Hwa Jeon (currently at University of Minnesota, U.S.) was an invaluable

collaborator and I would like to thank him to enable my work in his microbiology lab at the University of Alberta; his group was phenomenal in helping me in the bacteria work and always welcomed me. I would also like to thank Dr. Chun Il Kim at the University of Alberta for the valuable discussions and suggestions.

I would like to extend my thanks to my undergraduate supervisor, Dr. Paola Petrini, for initiating me into research at the Politecnico di Milano (Milan, Italy) and encouraging my plans for graduate school, instilling that interest that has carried me here.

Last but not least, I would like to express my gratitude to my loved ones. Nick, the love we share has prevailed over distance and time, across multiple countries; thank you for your kindness and adventurous view on life. I would like to also thank Nick's family, for your warmth and always being interested in my achievements. To my American family, thank you for your generosity and energetic spirit. To my friends, old and new, in Edmonton, Sarzana, Milan, Cape Cod and across the world, I carry with me all the laughs, hugs, and thoughtful words. Il ringraziamento più sentito va alla mia famiglia; a mamma e papà, per credere in me ad ogni passo e per il vostro appoggio incondizionato; ai miei nonni, che mi hanno insegnato il senso dell'impegno e che sono i miei modelli di vita; a tutti i miei zii, cugini, parenti e amici, per il vostro affettuoso sostegno.

Table of Contents

List of Tables

List of Figures

1 Introduction

The ease and rapidness of airborne transmission calls for effective infection prevention and control measures against respiratory diseases and beyond, as seen in past and recent experiences of pandemic and epidemic outbreaks, rising antibiotic resistance and risk of nosocomial (i.e., hospital-associated) infections. At the point of outbreak and in susceptible settings, respiratory protective devices are essential first lines of defense against pathogen-carrying aerosols. Unfortunately, the available technologies have several shortcomings, which hinder their safe use and defy their protective purpose. As such, there is a strong need for alternative systems that can overcome the current challenges of personal and public infection control measures. In this Chapter, first the background of aerosol transmission of diseases and the related burden in health care settings is discussed, followed by an overview of current respiratory protective technologies, their role in pandemic and epidemic preparedness, and the status of the research efforts. Finally, the concept, hypothesis and goals of our novel respiratory protective system are introduced.

1.1 Airborne transmission

1.1.1 Aerosols and droplets

Up until the first few decades of the 1900s, airborne transmission of diseases was strongly opposed in public health, and results from indirect studies to demonstrate infection by droplet nuclei were disregarded or considered inconclusive [1]. Following the direct demonstration of airborne transmission of tuberculosis (TB) in guinea pigs in 1957, influenza, smallpox, and measles were the first infectious diseases to be accepted as transmitted through the air by small droplets, due to studies published between 1968 and 1978 [1].

Aerosols are two-phase systems of solid or liquid particles suspended in a gas (commonly air) [2]. Thus, aerosols can have variable stability of a few seconds to more than a year and can be in the particle size range of 0.002 to more than 100 μm. They can be divided into primary and secondary aerosols. Particles of primary aerosols are directly introduced into the air, whereas particles of secondary aerosols derive from a chemical reaction in the air where gas in converted into particle. Aerosols are commonly polydisperse, i.e. they include various particle sizes. The size of the particles is the property that has the most influence on the aerosol behavior. For instance, particles with size greater than 10 μm have limited stability [2]. Depending on the origin, aerosols can be of different types, such as bioaerosol, cloud, dust, fume, haze, mist/fog, smog, smoke, and spray. Focusing on health science and health care settings, bioaerosols are the most relevant. They have a biological origin, including viruses, bacteria, fungi, and fungal spores [2]. Particle size is strictly correlated with the route of infection, since it determines the number of pathogens the particle can carry, how far from its source it can travel, and which part of the respiratory tract it can deposit on [3].

In light of this, infectious particles expelled by infected subjects during actions such as coughing or sneezing can be divided based on size into splashes (>100 μm), droplets (5–100 μm) and aerosols (<5–10 μm) [3]. Splashes are airborne suspended for a few seconds, similarly to droplets bigger than 20 μm. On the other hand, droplets smaller than 20 μm can be airborne suspended for up to many minutes. For instance, the settling time of a 20-μm droplet from a height of 3 m (approximate height of a room) is 4 min [4]. Droplets and splashes deposit in the mucosal surface of the upper airways passages (nose, esophagus and trachea) by impaction due to the high air speed and tortuosity of the nasopharyngeal airway [5]. This type of transmission has a high efficiency since big particles can carry a high number of pathogens, but only if the distance form the subject is less than about 1 m [3]. Notably, it has been observed that droplets that deposit in the upper respiratory tract can subsequently reach the gastrointestinal tract, causing infections [6]. Aerosols are stable over long periods of time and distances. As an example, a 5-μm particle settles from a 3-m height in over 1 h [4]. Aerosols can penetrate into the tracheobronchial and, if particle size is <0.5 μm, alveolar regions [5]. In these regions of the respiratory tract, air velocity is low and aerosols can deposit by sedimentation (0.003–5 μm) and diffusion (<0.5 μm). To put this into context, the size of virus aerosols is in the range of 0.01 to 0.3 μm, and bacteria aerosols are about 0.3 to 10 μm in size [2]. Notably, aerosols can be generated not only through coughing and sneezing but also from certain procedures, including intubation, resuscitation, bronchoscopy, and laser surgery.

Due to the long travelling distance and respirability of aerosols, airborne transmission can occur without a direct encounter with the infected subject, as opposed to droplet transmission [7]. Additionally, droplets can evaporate before falling out of suspension, becoming droplet nuclei, which contribute to airborne transmission of infection. This process takes less than 1 s for a

particle that has an initial size smaller than 20 μm, resulting in a particle that has half of its initial size [4,8].

Infections that can transmit via aerosols include influenza, measles, TB, chickenpox, and coronavirus-associated diseases (i.e., some common colds, severe acute respiratory syndrome (SARS), Middle East respiratory syndrome (MERS), and coronavirus disease 2019 (COVID-19)) [3,9-12]. In the specific case of influenza, three modes of transmission have been proposed, namely aerosols, droplets and contact transmission (self-inoculation of the nasal mucosa by contaminated hands), where aerosol transmission has been demonstrated to have an important role [4]. Influenza aerosols have low infection doses. The airborne infective dose 50% (ID_{50}) was determined to be 0.6–3 50% tissue culture infective dose ($TCID_{50}$), as opposed to a nasal ID_{50} of 100–1000 $TCID_{50}$ [13] (representing the main transmission pathway of droplets [7]). Notably, subjects have been determined to exhale virus aerosols at a rate of up to 4 $TCID_{50}$/h even during tidal breathing [4]. Even though ventilation and other engineering control methods could reduce risk of exposure to aerosols (air changes at 1 h frequency can each reduce the number of particles by 63% [14]), the possibility of disease transmission by aerosols at a close distance from the source still remains.

Virus, bacterial and fungal aerosol stability is affected by several factors, including temperature, relative humidity (RH), composition of fluid (e.g., saliva), atmospheric gases, irradiation (e.g., UV, microwave), pathogen type (e.g., enveloped and non-enveloped viruses, or Gram-positive and Gram-negative bacteria), and meteorological factors (e.g., precipitation, wind speed, air fronts) [6,15-17]. In particular, RH is a prominent factor in aerosol stability [7]. For instance, at low RH conditions influenza virus aerosols have low death-rate constants (including at humidity conditions typical of indoor environments) [18], and maintain the ability to infect

mice for up to 24 h after generation [19]. At 80% RH, the maximum survival time has been observed to be 1 h [7]. When on surfaces, survival times of influenza A virus, for instance, are up to 12 and 48 h for porous and non-porous surfaces, respectively [20].

1.1.2 Health care facilities

Aerosolized pathogen particles represent major routes of infection and transmission of bacterial infectious diseases, threatening personal safety in private and public settings. Specifically, nosocomial bacterial diseases such as methicillin-resistant *Staphylococcus aureus* (MRSA), transmissible by air [21], pose an imminent danger to public health. MRSA is recognized as one of the most detrimental multidrug-resistant bacterial strains, which causes 20 to above 80% of *Staphylococcus aureus* (*S. aureus*) nosocomial infections worldwide, constituting one of the top pathogens causing nosocomial infections [22]. For instance, infections with MRSA were found to be up to ~60% of all *S. aureus* infections in U.S. hospitals [23]. In Canada, MRSA has been reported to cause 150–400 infections every year, out of which ~70% are contracted in a clinical setting [24]. Another nosocomial bacterial infection showing dangerous levels of drug resistance is due to *Klebsiella pneumoniae (K. pneumoniae)*. Nosocomial infections with *K. pneumoniae* can have mortality rates as high as 50%, and the World Health Organization (WHO) has reported worldwide resistance to third-generation cephalosporins and carbapenem in 30–60% and up to 50% of cases, respectively [22]. In the U.S., the Centers for Disease Control and Prevention (CDC) had indicated as carbapenem-resistant 8% of *K. pneumoniae* infections in hospitals, making it one of the most important carbapenem-resistant bacterial species [25]. Prominent issues due to drug-resistant bacterial infections include the use of more expensive drugs compared to the first-line drugs used against the counterpart pathogens not showing resistance, with higher toxicity for the patient as well as

higher mortality rates [25,26]. For instance, an increase in mortality rate by 64% is observed for MRSA [26]. Additionally, new drug-resistant strains can emerge in response to the widespread use of second-line drugs [22]. Since droplets and skin particles carrying bacteria such as *S. aureus* and *K. pneumoniae* can transmit infections through the air, including in hospital settings (e.g., operating theatres, and intensive care, burn and orthopedic units) [27-29], respiratory protection has a primary role in infection prevention in healthcare.

Another airborne pathogen responsible for serious nosocomial outbreaks is *Mycobacterium tuberculosis*. Ranking among the top 10 causes of death in the world, TB was reported to infect over 10 million people and to cause ~1.5 million deaths worldwide in 2018 alone [30]. Notably, TB was the first infectious disease to be directly demonstrated to transmit by the aerosol route due to a study carried out in a hospital TB ward at the end of the 1950s [31]. Airborne transmission in poorly ventilated and/or overcrowded wards, and lack of proper infection prevention and isolation practices are at the basis of nosocomial outbreaks. For instance, in the last three decades large cases of TB nosocomial outbreaks were reported in Italy and South Africa [32,33]. In the U.S., out of the ~65,000 cases of TB infections that occurred in 2010–2016, 4% were reported among health care workers [34]. Furthermore, multidrug-resistance adds to the burden of TB infections, with as low as 39% success rate of treatment in the case of extremely drug-resistant strains of TB (XDR-TB) [30].

1.2 Respiratory protection

1.2.1 Classification in health care settings

Two types of devices are used in health care settings for respiratory protection: surgical masks and respirators [35]. Figure 1.1 shows a classification of the devices, drawn by considering which of the existing respirators for industrial purposes are used in health care settings [36]. Unlike surgical masks, respirators are identified as respiratory protective equipment as they can protect the wearer from inhalation of pathogens [3]. In general, respirators can work based on two principles: they either remove the contaminants from the ambient air by filtration (air purifying respirators), or provide air from a source that is not the surrounding air (atmosphere-supplying respirators) [37].

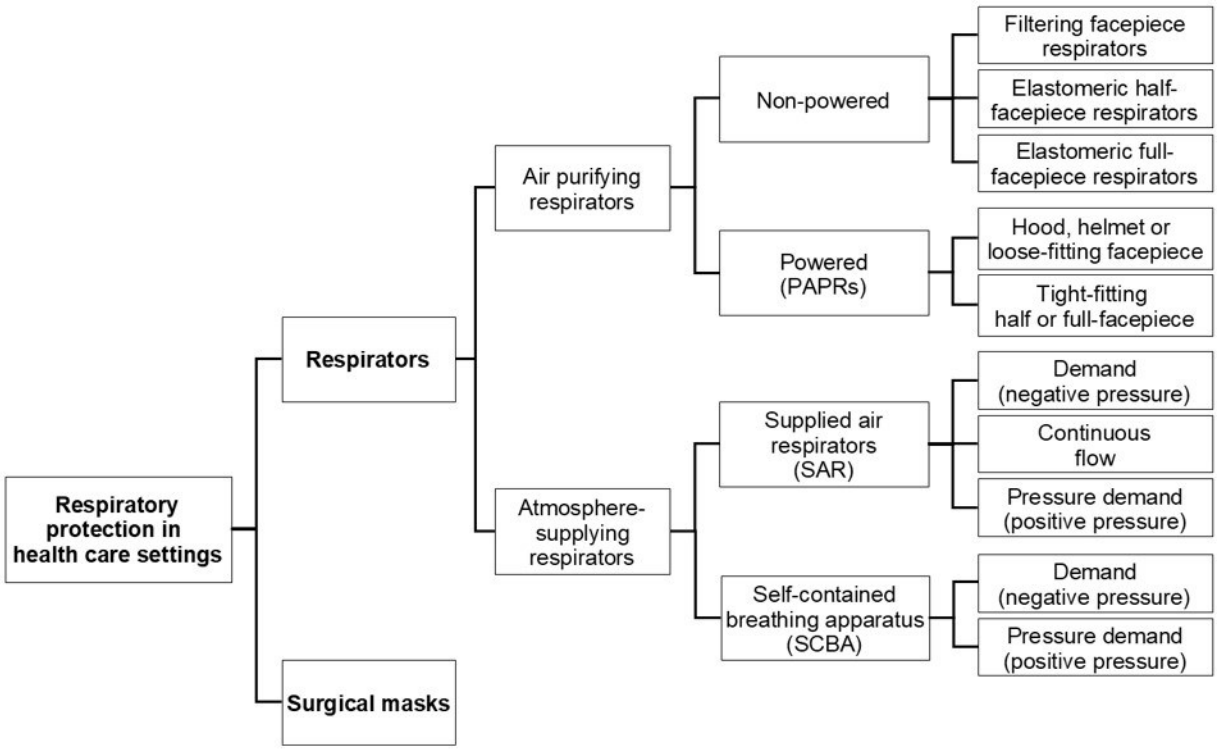

Figure 1.1 Schematic classification of respiratory protective devices used in health care settings.

Air purifying respirators can be powered, meaning that they can include a blower that draws the air through the filter before it flows into the facepiece [37]. Compared to non-powered respirators, where the user has to exert a substantial effort for the air to cross the decontaminating element, powered devices are more comfortable since the blower facilitates breathing, decreasing the burden on the wearer's cardiovascular system. Moreover, powered respirators do not require fit testing and are reusable. Nonetheless, decontamination can be problematic and the issue of potential cross infection persists [3]. Irrespective of the presence of a powered mechanism, filtration remains the basic element of protection of this type of apparatus, which is discussed more thoroughly in Section 1.2.3.

Atmosphere-supplying respirators provide superior protection than air-purifying respirators, but maintenance and cost are greater [36]. The air can be received from a distant source (supplied air respirators (SAR)) or from cylinders carried by the wearer (self-contained breathing apparatuses (SCBA)). The common advantage for the two types is that protection is provided irrespective of the contaminants, since the breathing air comes from a clean source, with no dependence on the choice of filter media. This aspect can be particularly beneficial against exposure to unidentified agents. SCBAs do not have the limitations on movement imposed in SARs by the element connecting to the distant decontaminated source of air; however, the carried air supply has a maximum duration of approximately 4 hours and can weigh up to 7 kg [37]. Notably, in atmosphere supplying respirators with demand mode, the air flows into the facepiece when pressure inside the facepiece is negative compared to the outer environment (i.e., during inhalation); differently, in pressure demand mode, the pressure in the facepiece is always maintained positive, and even more air is provided during inhalation, This way, pressure demand mode generates higher protection from contaminants in the outer

environment than demand mode. Overall, SCBAs with pressure demand mode offer the highest level of protection out of all respirators [36,38].

Another broad categorization of respirators is based on the type of facepiece, which can cover varying portions of the face [36]. Half facepiece respirators fit over the nose and under the chin. Due to the lower level of protection they can guarantee, they are not used in atmosphere-supplying respirators. Higher performance is achieved by full facepiece respirators, which cover from the hairline to below the chin, including a barrier for the eyes. They are used in both air-purifying and supplying respirators. Finally, loose-fitting designs usually include the head, neck and shoulders. Under certain conditions, they can provide enough protection to be considered hoods and helmets, which are commonly used in air-supplying respirators.

Apart from the described categorizations based on mode of use and facepiece designs, respiratory protective devices employed in health care settings are subject to regulations from different agencies, which aim to control the performance of the technology, while providing a classification based on parameters that determine their protective efficacy. As such, a further classification in health care settings can be made by discerning between surgical masks, N95 respirators and surgical N95 respirators.

1.2.2 Regulatory agencies, testing and standards

In the U.S., surgical masks are approved by the Food and Drug Administration (FDA) as medical equipment, based on fluid resistance, differential pressure, flammability and filtration efficiency [39-43]. In particular, filtration efficiency includes two tests, i.e. particulate and bacterial [39]. The former determines the mask penetration of latex microspheres with sizes 0.1–5 μm at 0.5–25 cm/s [44,45]. On the other hand, bacterial filtration efficiency tests compare expelled bacteria by subjects talking inside a chamber before and after donning a mask [46].

Alternatively, the mask is exposed to 3-μm bacterial aerosols at 28.3 L/min, and the ratio of bacteria concentration upstream to downstream is calculated [47,48].

The differential pressure test evaluates the pressure drop of the flowing air due to the mask [39]. It correlates with its breathability and comfort, since an increased resistance to the air flow causes greater difficulty in inhaling and exhaling, and a higher perception of heat. The recommended standard is MIL-M-36945C 4.4.1.1.1, Method 1 Military Specifications: Surgical Mask, Disposable (June 12, 1975), where the mask sample is exposed to a fixed flow rate and the pressure on the two sides is measured [49].

The National Institute for Occupational Safety and Health (NIOSH), part of the CDC, certifies respirators by identification with a letter followed by a number [50]. The letter defines whether the filter is resistant to oil substances (R and P series respirators) or not (N series), based on the particle material used for testing (dioctyl phthalate oil or sodium chloride (NaCl), respectively). The number (95, 99 or 100) is the filtration efficiency at 85 L/min against particles with size distributions (count median diameters) of 75 ± 20 and 185 ± 20 nm for N and R/P series, respectively [51-59]. In health care settings, respirators must additionally receive FDA approval, as it is the case of the commonly used surgical N95 respirator [39].

Several aspects determine the protection that respiratory protective devices can provide and regulatory agencies make strong efforts in defining standards to ensure safety. Nonetheless, the basic principle for masks and air-purifying respirators is filtration.

1.2.3 Filtration mechanisms

Fibrous filters are meshes constituted by randomly organized fibers, with varying sizes of pores and fiber diameters. In general, filtration is based on interactions between a particle and the fibers, and the driving mechanisms are diffusion, interception, inertial impaction and sedimentation. Additionally, if the filter possesses electrical charges, there can be substantial contribution to filtration from electrostatic forces.

The total collection efficiency of a filter can be determined by modeling the fibers as cylinders. Considering a flow carrying particles through cylindrical fibers, the total collection efficiency η_t is a function of the collection efficiency of a single fiber η and physical properties of the filter (fiber diameter d_f, volume fraction of fibers α and thickness of filter L) [60]:

$$\eta_t = 1 - \exp\left(-\frac{4\eta L}{\pi d_f}\frac{\alpha}{(1-\alpha)}\right) \quad (1.1)$$

where the volume fraction of fibers (i.e., solid fraction of the filter) α can be expressed in terms of d_f and the total length of fiber per unit volume of filter L_f:

$$\alpha = \frac{\pi d_f^2 L_f}{4} \quad (1.2)$$

Specifically, a greater volume fraction of fibers and filter thickness correspond to higher filtration efficiency. In contrast, fibers with greater average diameter achieve a lower filtration performance. The predominant factor is the filtration efficiency of a single fiber η, which is the sum of the contributions of mechanical (diffusion (η_d), interception (η_{int}), inertial impaction (η_{imp}), sedimentation (η_g)) and, where applicable, electrostatic (η_e) filtration mechanisms [37,61]:

$$\eta = \eta_d + \eta_{int} + \eta_{imp} + \eta_g + \eta_e \quad (1.3)$$

Capture by diffusion is based on the non-deterministic Brownian motion of small particles with diameter <0.5 μm [60,62]. The random path of particles affected by diffusion does

not follow that of the fluid streamline, and may cause the fiber to intercept the particles. Several theoretical equations have been derived to analyze this phenomenon [63-68]; Lee *et al.* [67] expressed η_d as:

$$\eta_d = 2.6\left(\frac{1-\alpha}{K}\right)^{1/3} Pe^{-2/3} \quad (1.4)$$

where K is a function of α and Pe is the Peclet number:

$$K = -\frac{1}{2}\ln\alpha - 0.75 + \alpha - \frac{1}{4}\alpha^2 \quad (1.5)$$

$$Pe = \frac{u(2R_f)}{D} \quad (1.6)$$

where u is the flow velocity, R_f is the fiber radius, and D is the diffusion coefficient.

The mechanism of interception is based on the principle that a particle is captured if at a distance from the fiber that is less than its own radius [67]. η_{int} is expressed as [67]:

$$\eta_{int} = \frac{1-\alpha}{K}\frac{\left(R_p/R_f\right)^2}{1+\left(R_p/R_f\right)} \quad (1.7)$$

where R_p is the particle radius. η_{int} is higher at greater particle sizes (most effective at diameters >1 μm [60]), since a lower critical distance between particle and fiber is permitted before collection occurs.

Capture by inertial impaction is due to the inertia of the particle. The streamline carrying the particle changes direction as it encounters a fiber, but due to inertia the particle may not change direction with the streamline, and be intercepted by the fiber [37]. A study on the filtering efficiency due to inertial impaction was done by Zhu *et al.* [61], where the following equation for η_{imp} was determined:

$$\eta_{imp} = \frac{2(1-\alpha)\sqrt{\alpha}}{K} Stk\left(\frac{d_p}{d_f}\right) + \frac{(1-\alpha)\alpha}{K} Stk^2 \quad (1.8)$$

where d_p is the particle diameter and Stk is the Stokes number:

$$Stk = \frac{C_c \rho_p d_p^2 u}{18 \mu d_f} \quad (1.9)$$

where C_c is the Cunningham slip factor (correction factor taking into account the drag force on a particle moving in a fluid), ρ_p is the particle density, and μ is the air viscosity. Along with properties of the flowing fluid and particle/fiber sizes, the expression has the additional contribution of particle density. Increased mass density implies a greater filtration efficiency. Similarly to interception, inertial impaction is more effective against particles with diameters greater than 1 μm [60].

A further mechanical mechanism that can favor collection of particles is sedimentation, where gravitational force acts on the particle, and by modifying its path can bring the particle into contact with the fiber [37]. Sedimentation is more effective in the particle diameter range 0.2 to 2 μm [69]. η_g is significant if air velocity u is low and terminal velocity of the particle V_t is high, which in turn is directly proportional to the particle diameter d_p and density ρ_p and acceleration of gravity g, and inversely proportional to the air viscosity μ [70]:

$$V_t = \frac{d_p^2 g \rho_p}{18 \mu} \quad (1.10)$$

Electrically charged filters have an additional element in their total collection efficiency given by electrostatic filtration mechanisms. Due to the charge of the fiber, two forces can act on the particle: coulomb and induced-dipole forces. If the particle is charged, there is an interaction with the charged fiber determined by Coulomb force [62]. Filtration efficiency of a particle by a cylindrical fiber due to Coulomb force is mainly dependent on the charges of the particle and fiber, which generate the electrostatic force, and the air resistance existing at the specific relative

velocity between the streamline and fiber [70,71]. In the case that the particle is not charged, the electric field generated by the fiber can induce a dipole in the particle, which in turn can be attracted by the charge on the fiber [62]. Electrostatic filtration is more effective on particles with a diameter range of 0.01 to 5 μm [60].

Due to the mechanisms filtration relies on, the filter characteristics, choice of materials and fabrication methods greatly impact their performance. For this reason, the offered level of protection varies among devices. Moreover, it is worth noting that the mechanisms can collect particles by mechanical or, at best, electrostatic interactions. In the case of pathogens, filtration alone does not address potential risks of secondary exposure and contamination.

1.3 Surgical masks

1.3.1 Background

Surgical masks have been in use ever since the beginning of the 1900s as barrier for the spread of contaminants from the wearer's mouth and nose to avoid development of infections during surgical procedures [35,72]. Their use has expanded to provide protection of the wearer against infectious droplets due to their fluid resistance [3], for instance in medical examinations of patients suffering or suspected to suffer from airborne transmissible diseases [73]. However, surgical masks are not designed to offer protection of the wearer against pathogenic aerosols [3].

Despite their different intended use, recently there has been an increasing adoption of surgical masks as replacements of respirators, partly due to shortages of respirators, and lower cost and higher comfort of surgical masks. This practice has been observed in both health care workers and the general public during epidemics and pandemics. Recent instances are SARS [74], H1N1 swine flu [75-77], MERS [78,79], and COVID-19 [80]. However, the use of surgical masks as protective means against diseases remains highly controversial [9,10,14,35,80-90], and surgical masks are not classified as respiratory protective equipment.

Surgical masks are widely used, and can be found in different health care settings, such as isolation, procedure and dental masks, and in varying designs (duck bill, flat pleated, cone shaped and pouch) [39], which can affect the adherence to the wearer's face and level of leakages [9]. In any case, they are limited to a single use, but inexpensive (about $0.70 per mask [91]). The choice of materials has evolved over the decades, from the early attempts with gauze, paper and glass-fiber mats to the more recent spread of synthetic polymers [72].

1.3.2 Materials

Currently, surgical masks are produced from polymeric fibers. Suitable materials include polypropylene, polystyrene, polycarbonate, polyethylene, polyester, polyurethane and polyamides [92,93], but polypropylene is the most widely used material due to properties that make it favorable for the manufacture of inexpensive, single-use microfibrous filters.

Surgical masks usually have a three-ply system (Figure 1.2). The inner layer is in contact with the face and helps support the mask, the middle layer is the main filtration unit, and the outer layer provides exterior protection from wear and tear [86]. Inner, middle and outer layers are usually made in non-woven polypropylene fabrics with weights of 20, 25 and 20 g/m^2, respectively [92]. Polypropylene confers hydrophobicity to the mask layers [94], which enhances the function of the inner and outer layers in protecting the middle filter. Hydrophobicity of the outer layer can reduce the penetration of aerosols by capillary motion [95]. The fluid resistance of the inner layer decreases the wetting process of the mask due to exhaled air during breathing or talking, with consequently lower spread of aerosols by capillary motion [95].

The integrity of the mask should not be disrupted during use to prevent compromising its protective function. Polypropylene fibers exhibit good chemical resistance [96], which entails that the fibers do not tend to deteriorate easily because of chemicals, environment and other detrimental exterior conditions. This helps maintain the desired filtering efficiency of the mask. A further property of polypropylene fibers is their low cost. Due to non-recyclability and the high consumption volume, surgical masks need to be inexpensive. Thus, the lower cost of polypropylene fibers as compared to other materials, such as polyester and polyamides, renders it more advantageous for this application [97]. Another factor that favors cost containment of masks is the use of non-woven fabrics [92].

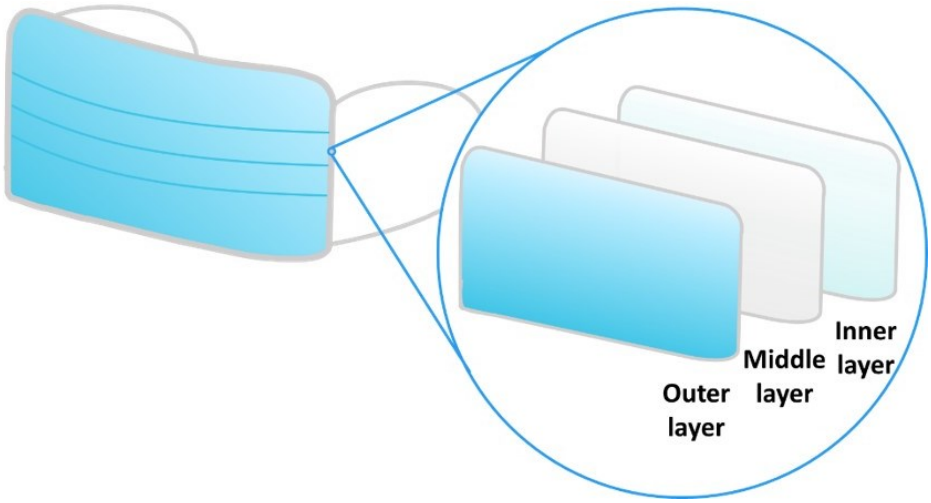

Figure 1.2 Typical three-ply structure of surgical masks. The inner and outer layer protect the middle layer from scratches and physical damage; the middle layer filters big droplets.

1.3.3 Fiber fabrication methods

Fabrics can be broadly categorized into knitted, woven and non-woven types. In non-woven fabrics, fibers are connected physically through entanglements or contact adhesion, while knitted and woven fabrics present various forms of knitting and stitching [98]. Non-woven fabrics have several advantages over the other two that make it the fabric of choice for surgical masks, such as higher breathability, no defects due to yarn slippage that could lower the filtration efficiency, and lower cost and time for the production process [92,99]. Among the different manufacturing technologies of non-woven fabrics, the inner and outer layers of surgical masks are mostly produced by spunbonding, while the middle filter is made by meltblowing [92,100,101].

In spunbonding, the polymer melt is extruded from spinnerets to form a curtain of filaments, which are subsequently drawn by air at high speed through the cooling chamber [102]. The filaments are then exposed to high velocity and low pressure, and consequently they spread

out randomly. Finally, the filaments in this configuration are collected on a belt, and connected through thermal bonding by using calenders [103].

Meltblowing is a technology that derives from spunbonding and differs from it in two aspects: the temperature and volume of air that draws the fibers, and where it is applied with respect to the spinneret [104] (Table 1.1). Spunbonding employs small quantities of air at ambient temperature, which is not applied close to the spinneret. Conversely, meltblowing is performed with larger volumes of air at the same temperature of the polymer melt, and applied in proximity to the die tip.

As a result, spunbond fibers are stronger than meltblown fibers due to a higher level of fiber orientation, whereas meltblown fibers can achieve diameters smaller than 10 μm [104]. Therefore, it is worth noting that the inner and outer layers, which are spunbond, have grater physical properties than the middle filter, and can provide it protection from mechanical damage. On the other hand, the meltblown middle layer can achieve greater filtration efficiency due to smaller fiber diameters. The physical characteristics of finalized masks available in the literature are listed in Table 1.2, divided into the three layers.

Table 1.1 Differences in the fabrication process of spunbond and meltblown fibers.

Process	**Air**		**Location of draw force**	**Property of fibers**
	Temperature	**Volume**		
Spunbonding	Ambient	Small	Not in proximity to die tip, after polymer has cooled	Strength
Meltblowing	Temperature of polymer melt	Large	In proximity to die tip, while polymer is in molten state	Micro-size

Table 1.2 Physical characteristics of surgical mask.

	Outer layer	Middle layer	Inner layer	General/Total
Fiber diameter	-	14–20 μm [105]	-	2–20 μm [106,107]
Pore diameter	-	-	-	16–51 μm [108]
Thickness	0.43 mm [93]	0.225 mm [93]	0.15 mm [93]	0.2339–0.803 mm [108]
Fabric weight	20 g/m^2 [92]	25 g/m^2 [92]	20 g/m^2 [92]	-

1.3.4 Performance

The minimum performance of surgical masks for their intended purpose is tested by manufacturers in accordance with the standards for certification determined by the regulatory agencies, as described in Section 1.2.2. Additionally, substantial scientific efforts have been made to probe the effective level of filtration efficiency offered by available masks against multiple types of pathogens, aerosols and particles

Chen and Willeke [86] exposed tightly sealed surgical masks to corn oil aerosols at different flow rates. The filter penetration by 0.3-μm particles was found to be 25% and 65% at flow rates of 5 and 100 L/min, respectively. Balazy *et al.* [81] evaluated the filtration efficiency of surgical masks sealed to a manikin against MS2 virus aerosols (size range of 10 to 80 nm), at a flow rate of 85 L/min. Although the two tested surgical masks were from the same manufacturer, they exhibited the two significantly different penetration levels of 21% and 85%. When tested with sodium chloride aerosols as described by the NIOSH certification requirements for N-series respirators (see Section 1.2.2), Qian *et al.* [109] found that surgical masks exhibit the unsuccessful filtration efficiency of 71%. Weber *et al.* [9] found that filter penetration by

submicron-sized corn oil aerosols varied from 20% to 100%, suggesting inability of surgical masks to protect against infectious aerosols at submicron sizes.

Overall, a great variety of filtration efficiency results have been observed for surgical masks. Several factors affecting the performance can be identified in the literature. First, filtration generally shows dependence on particle size, which is of particular importance when considering viruses. Depending on the air flow rate, mask performance varies, implying that the provided protection is influenced by breathing patterns and work load. In general, surgical masks have shown a performance that is unsatisfactory compared to the minimum filtration requirements set forth by the regulatory agencies (NIOSH/FDA) for respiratory protective equipment. In the literature, there is overwhelming evidence of the inadequacy of currently available surgical masks to provide the wearer protection against infectious aerosols.

1.4 N95 respirators

1.4.1 Background

N95 respirators fall under the category of air purifying respirators, which remove the contaminants from the ambient air by filtration. Specifically, they are filtering facepiece respirators, in that the whole facepiece functions as filtration medium, as opposed to elastomeric respirators, which have a rubber or silicone facepiece complemented with filter pads [110]. While the facepiece of elastomeric respirators is reusable and the filters can be replaced, filtering facepiece respirators are meant for single use only [73]. Thus, risk of contamination during disinfection due to collected particles on the surface of the device is avoided in the case of filtering facepiece respirators. However, a possible source of cross infection remains during removal and disposal [14].

Along with R and P series, N series respirators were first introduced by NIOSH in 1995 as part of 42 CFR Part 84 regulations on non-powered air purifying respirators, which substituted the previous 30 CFR Part 11 regulations [111]. Out of the nine categories that were established, N95 respirators have the overall lowest performance level, but they are the most commonly used ones in health care settings, and have gradually replaced the dust/mist and dust/mist/fume respirators certified under the former regulations [109]. N95 respirators are tested against aerosols with count median diameter of about 100 nm. They have a minimum filtration efficiency of 95%, and are certified to have degradation resistance against solid particles, since they are challenged with NaCl aerosols during testing. N95 respirators are designed to fit tightly on the wearer's face, and fit testing is required prior to use. In particular, surgical N95 respirators are the ones broadly used to provide protection to health care workers. As it emerges from the following Sections, they are similar to surgical masks in the choice of materials and

manufacturing technologies. However, a number of differences exist that determine the applicability of N95 respirators as respiratory protective equipment against airborne pathogens.

1.4.2 Materials

N95 respirators have 3 filter layers. The inner and outer layers mostly have the function to cover the middle layer, which is the main filtration unit [109]. Generally, the three layers are made of polypropylene [94,109,112,113], although other polymers are used, such as polyethylene for the inner layer [114]. An additional middle layer can be part of the mask, either between the outer and middle filter layers [94] or middle and inner filter layers [112]. In this case, the purpose is to provide a defined shape and mechanical support to the mask, and the employed materials are mainly cellulose and polyester [94,112].

It is of interest to characterize the interaction of water with the materials of respirators to better understand the possible behavior of aerosols once collected. Viscusi *et al.* [113] studied the hydrophobicity properties of the three filtration layers. The results determined that the outer and middle layers are hydrophobic, whereas hydrophobic properties of the inner layers showed dependency on the model. Hydrophobic outer layers can provide improved protection by avoiding further penetration of the collected aerosols due to capillary motion [95]. However, aerosols tend to accumulate on the surface of the outer layer [94]. Thus, risks arise of contact contamination, and reaerosolization caused by mechanical agitation due to breathing, coughing or sneezing [115]. With decreased wetting due to condensation of breathing air, hydrophobic inner layers have lower penetration of aerosols due to capillary motion [95]. Concurrently, hydrophobicity could cause increased temperature and humidity inside the respirator and the filter pores could be blocked, leading to discomfort and difficulty in breathing [116]. As for the middle filter layer, its main characteristic is that it is made of charged fibers.

1.4.3 Fiber fabrication methods

Similarly to surgical masks, N95 respirator filters are produced by spunbonding (outer and inner layers) and meltblowing (middle layer) technologies [94,112]. The physical characteristics are summarized in Table 1.3. In the middle layer, the fiber diameter is smaller and the thickness is greater compared to those of the outer and inner layers, emphasizing its function as filter medium as opposed to the protection role of the other two. By comparing with the values reported in Table 1.2, it is worth noting that the fiber diameter in the middle layer of N95 respirators is smaller compared to that of surgical masks. Moreover, the pore diameters in the surgical mask are generally greater and the thickness smaller than in the N95 respirator. Considering the effects of these physical properties on the filtration mechanisms, these differences can be partially ascribed for the increased protection guaranteed by N95 respirators compared to surgical masks. This suggests that controlling parameters such as filter thickness can have a substantial effect on performance. However, this gain in performance is achieved at the cost of lower breathability. Finally, N95 respirators have a superficial charge density of 2.5–7.0×10^{-5} C/m^2 due to charging mechanisms applied during the fabrication process [117].

In general, electrical enhancements can be applied to filters by (i) application of an external voltage to the filter by using electrodes in different configurations, (ii) charge of the particles before filtration, or (iii) charged fibers. The latter is the only solution applicable in respirators. The middle layer of N95 respirators is often referred to as an electret filter, where an electret is a dielectric material with the ability to stay charged for a relatively long time [118]. Charged fibers of electret filters can be produced in three ways, namely corona charging, tribocharging, and electrostatic fiber spinning [119], out of which the method used for meltblown fibers is corona charging by plasma generation [62,120].

Table 1.3 Physical characteristics of N95 respirator.

	Outer layer	Middle layer	Inner layer	General/Total
Fiber diameter	39.49 μm [114]	7.84 μm [114]	40.88 μm [114]	-
Pore diameter	-	22.7–24.1 μm [117]	-	0.3–0.5 μm [121]
Thickness	0.31 mm [114]	1.77 mm [114]	1.05 mm [114]	-
Fabric weight	46.67 g/m^2 [114]	110.67 g/m^2 [114]	191.67 g/m^2 [114]	-
Charging density	-	2.5–7.0×10^{-5} C/m^2 [117]	-	-

During this process, various mechanisms contribute to the final polarization of the fibers [122]: (i) charges are trapped on the crystalline-amorphous phase boundaries; (ii) charges are captured by traps (defects in the structure of the polymer, contaminants, voids, terminal groups); (iii) formation of electron defects due to localization of electrons in the bulk of the material, functioning as traps; (iv) thermooxidative degradation of the polymer, where heat reaches a level such that the bonds on the polymer melt are extended to the point of breaking, with formation of polar functional groups and charged fragments; (v) oxidation of the macromolecules and formation of polar groups due to the formation of ozone, atomic oxygen and nitrogen oxides in the air caused by the electric field; and (vi) heterolytic breaking of the chemical bonds of the polymer, which turns the macromolecules into charged fragments.

1.4.4 Performance

There has been a broad focus on testing the protective efficacy of N95 respirators under multiple conditions and possible settings of use. Moreover, the performance of N95 respirators has been often evaluated in comparison with surgical masks under the same challenging conditions to provide means to decide which device is more appropriate in specific situations.

An early study by Qian *et al.* [109] evaluated the filtration efficiency of N95 respirators shortly after the 42 CFR Part 84 regulations were approved and N series respirators were established. The performance of N95 respirators was tested under the conditions determined by NIOSH and compared with that of dust/mist and dust/fume/mist respirators (certified under the previous regulations) and surgical masks. N95 respirators resulted to be the only devices to have the minimum required filtration efficiency, with values between 95% and 96% against 0.1 to 0.3-μm particles. However, it has been shown that even though the penetration of aerosols may be overall below the 5% limit, spatial variability in the filter medium due to the manufacturing process may lead to local particle penetrations that exceed the threshold [123].

Lee *et al.* [124] conducted an *in vivo* study on the overall protection provided by N95 respirators and surgical masks against particles in the size range 0.04–1.3 μm. The protection factors, considering both filtration efficiency and faceleaks, were calculated as the ratio of the concentration of particles outside and inside the masks. N95 respirators resulted to have a protection factor 8 to 12 times greater than surgical masks. However, only 71% of the tested N95 respirators had protection factors greater than the minimum U.S. Occupational Safety and Health Administration (OSHA) requirement of 10 [125], indicating that the actual protection guaranteed by this class of respirators may be lower than expected.

Studies on N95 respirators have raised concerns over their minimum filtration efficiency against nano-sized particles. Balazy *et al.* [114] conducted this type of study with 10–600-nm NaCl particles, which showed that particle penetration in the range 30–70 nm can be >5%. In a similar study [81], the group used MS2 virus (size 10–80 nm) as challenging particles. Although N95 respirators exhibited an exceedingly better filtration performance than surgical masks, for some models the filtration efficiency against MS2 virus was lower than 95%.

1.5 Respiratory protection against pandemic and epidemic diseases: status

Respiratory protection against airborne pathogens is crucial for pandemic and epidemic preparedness in the context of personal protection, healthcare systems, and governance. We expect that the development of technologies that overcome the existing challenges in current respiratory protective devices will lead to a timely and effective response to the next outbreak.

1.5.1 Role of respiratory protection in pandemic and epidemic preparedness

Influenza, a major respiratory disease, poses great risks to global health. Influenza epidemics and pandemics are responsible for 250,000–500,000 deaths each year [126] and >50 million fatalities worldwide in the past century [127], respectively. The next influenza pandemic is estimated to cause ~60 million deaths [128]. Ideally, vaccination within 2 months of the outbreak can provide effective protection [129]. However, because several months are necessary for vaccine development and administration, the infection risk is heightened during the non-vaccine period. This is further supported by the outcomes of the 2002–2003 SARS outbreak that originated in China, in which the disease was transmitted globally within a few weeks, but the first vaccine Phase I clinical study began a year after the outbreak [130]. Logistically, an effective pandemic preparedness plan should include both vaccination and alternative mitigation methods (pharmaceutical—antiviral; non-pharmaceutical—isolation, administrative control, personal protective measures). Therefore, respiratory protection devices are a key non-pharmaceutical intervention that is essential to the global strategy for pandemic readiness.

The parameters behind respiratory protection and airborne transmission intertwine in a complex system that can be broken down into four bidirectional components: (i) release, (ii) infection, (iii) filtration, and (iv) protection (Figure 1.3). Once a subject is infected, nanometer-to-millimeter-sized pathogenic particles can be released while breathing, speaking, sneezing, or

coughing, and infect a host respiratory tract via different mechanisms that depend on the aerodynamic size of the particles (d_a <5 μm, lower respiratory tract; 5 < d_a < 100 μm, upper respiratory tract). Similarly to infection, current respiratory protection devices filter infectious particles in a size-dependent manner. Filtration efficiency, comfort (e.g., breathability), and fit at the face-mask interface govern technical performance. While effective management and availability of control measures are crucial to an outbreak response, the pathogens (virus/ bacteria/fungi) captured on filters are an intrinsic concern because of fear of cross-infection, new aerosol release, and contaminated waste.

Recurrent recommendations regarding respiratory protective measures by the CDC and the WHO emphasize their prominent role in emergency preparedness. Nonetheless, fewer scientific efforts have been focused on respiratory protection technologies compared to vaccine development technologies. We present here an overview of currently available respiratory intervention technologies and their implications for future research directions in response to pandemic and epidemic outbreaks.

1.5.2 Limitations of current technologies

Surgical masks have been in use for over 100 years as barriers against the development of infection via large droplets produced during surgery. N95 filtering facepiece respirators were introduced in 1995 as part of the NIOSH 42 Code of Federal Regulations (CFR) Part 84 on non-powered air-purifying respirators [111]. Currently, surgical masks and N95 respirators are the two main intervention measures for personal respiratory protection. Nonetheless, technical challenges exist, some of which are shared by both devices: (i) filtration efficiency, (ii) cross-infection, (iii) recyclability, and (iv) faceseal.

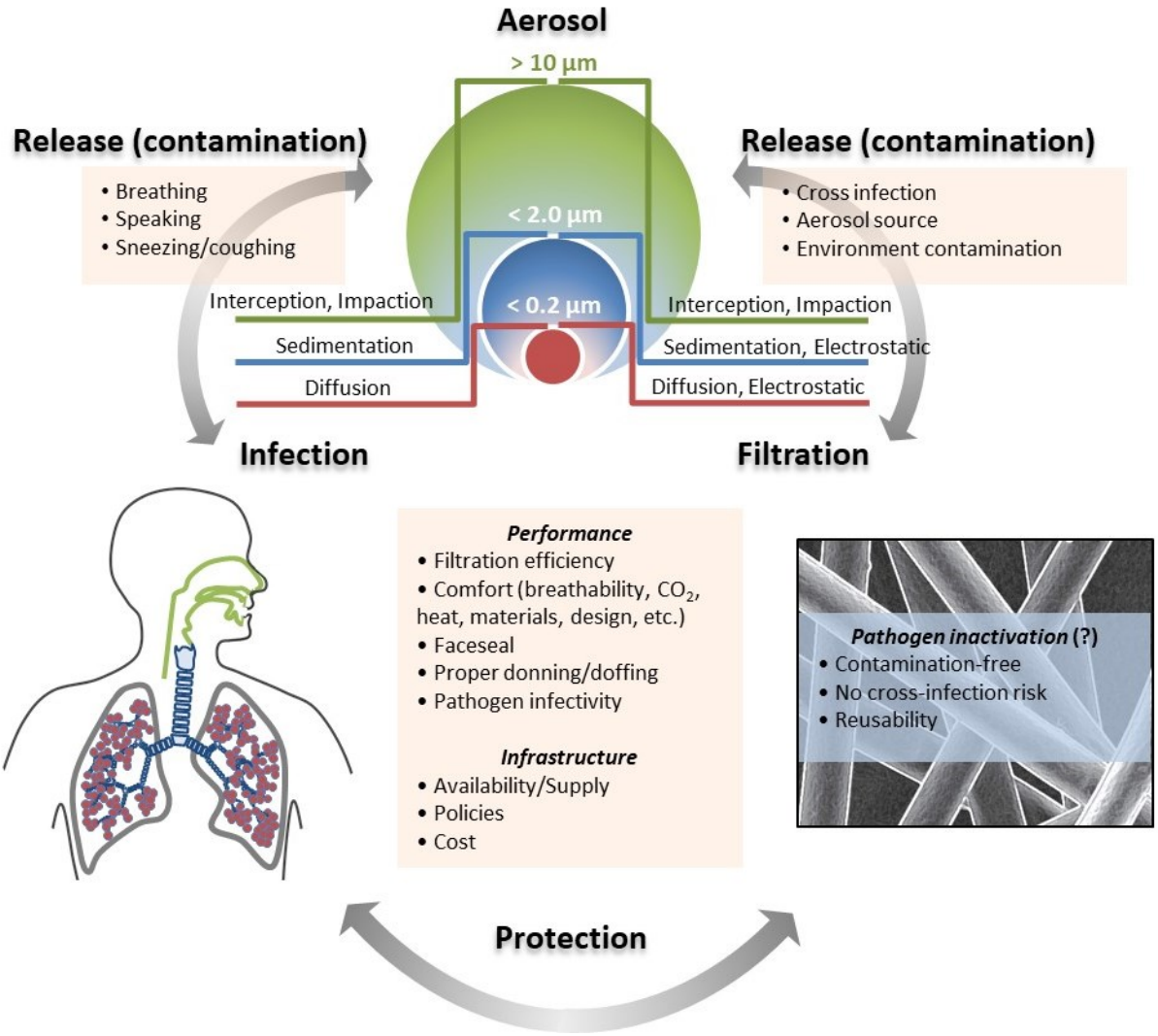

Figure 1.3 Principles guiding filtration and airborne transmission of infection. An infected subject releases pathogenic aerosols by breathing, talking, sneezing, and coughing. Depending on the size, the particles deposit in different levels of the respiratory tract—upper respiratory tract (green), tracheobronchial region (blue), and alveolar region (red)—as a result of different mechanisms (i.e., interception, impaction, sedimentation, and diffusion). Based on the same mechanisms, with additional electrostatic interactions of charged fibers, masks offer respiratory protection by filtration. The degree of respiratory protection is affected by the technical performance of the mask (filtration efficiency, comfort, faceseal, proper donning/doffing, and pathogen infectivity), as well as the infrastructure (available supplies, policies, and cost). In addition, because virus/bacteria infectivity is maintained on the fibers, the filter becomes a source of cross-infection, re-aerosolization, and environmental contamination. Neutralization of the pathogens on respiratory protective devices is an approach that can bridge this gap towards pandemic and epidemic preparedness.

A primary issue concerning the efficacy of surgical masks against airborne pathogens is low filtration efficiency. Although performance can vary drastically among models, inconsistent reports on surgical mask efficacy are probably associated with improper application, resulting in performance mismatch. Another crucial issue is cross-infection/transmission. Because viruses and microorganisms can survive for at least a few hours to several days [131], masks and respirators become a source of infection for the wearer and others, thus limiting them to single use. Infectious aerosols on filters can also be re-released into the environment (i.e., re-aerosolization), for example through accidents. With a particle diameter of 1.15 μm, re-aerosolization from N95 respirators as a result of a fall (drop height, 0.76 m) was between 0.002% and 0.012% [132].

Various sterilization methods (e.g., ethylene oxide, formalin, UV, bleach, hydrogen peroxide) have been tested to recycle respirators. However, the drawbacks of each method, such as performance deterioration and generation of toxic residues, have restricted their application. As an example, decontamination of N95 respirators by autoclave, 160 ℃ dry heat, 70% isopropanol, and soap and water lowered the filtration efficiency [133]. Ethylene oxide treatment of respirators caused deposition of hazardous residues of 2-hydroxyethyl acetate on the straps, and bleach, oxidants, or dimethyldioxirane raised issues of sharp odor and incompatibility with staples/nosepiece [134]. Despite the need for further research, with safety as a preponderant concern, mask recyclability would be beneficial because it would reduce the amount of biohazardous waste and derived risks. In addition, reusability would naturally address a shortage of respirators during pandemics.

Furthermore, aerosols penetrate through loose-fitting masks/respirators, based on wearer facial features, movement, proper and timely fit testing/check, aerosol size, and mask shape.

Particles <10 μm enter through faceleaks 5–6-fold and up to 10-fold more than through the filter of surgical masks and N95 respirators, respectively [135]. Thus, although improving filtration efficiency is necessary, better fitting should be a primary objective to fully address aerosol penetration.

Additionally, although N95 respirators offer a superior respiratory performance, they have additional issues compared to surgical masks. N95 respirators are unpractical over long periods of time due to difficulty in breathing and heat buildup [136]. Health care providers caring for patients with SARS in a hospital in Toronto in 2003 reported a high level of stress caused by wearing respirators during 12-h shifts [137]. 60% of health care workers participating in a study on tolerability of N95 respirators could not wear them for 8 h [138]. Thus, the discomfort may compromise the protective efficacy of respirators in relation to wearer's compliance. Furthermore, this could particularly affect the health of members of society at higher risk of infection, such as the elderly and children [139], or people suffering from respiratory diseases, such as asthma [140], who would unlikely be able to wear a respirator for several hours.

Interestingly, the general public tends to disregard infection control guidelines. As such, although respirators are recommended when airborne transmission is possible, surgical masks have experienced greater acceptance because of advantages such as comfort, availability, and cost. However, inappropriate application of devices may not provide consistent protection. This in turn stimulates research and development of new technologies to close the gap between guideline and practice.

1.5.3 How can we move towards safer and more effective respiratory protection for a timely emergency response?

Different methods have been investigated to improve the performance of respiratory protection devices (Table 1.4), such as higher filtration efficiency without sacrificing breathability. Representative examples include fabrication using nanofibers (size range of 10–200 nm) [141,142] and incorporation of electric charge by plasma treatment [143] and charge-carrying agents [144]. Nanofibers can constitute filters with a large specific surface area and small pore sizes, which are both advantageous to filtration efficiency [145]. A method of producing non-woven fabrics using nanofibers is electrospinning, which could also be used for production of electrically charged filters for respiratory protection applications, although melt-blowing and multicomponent fiber spinning are also commonly used for nanofibrous filtration media [146]. Qin *et al.* [147] produced nanofibrous filters by electrospinning PVA fibers on spunbond and meltblown polypropylene substrates, respectively. Filtration efficiency was greater in the obtained filters compared to the substrates alone. Similarly, an increase in filtration efficiency was observed by Podgórski *et al.* by including meltbown nanosized fibers on a microfibrous substrate [146].

However, major technical challenges remain to be addressed for effective preparedness from the standpoint of contamination and infrastructure. Hence, production of a filter that inactivates the collected pathogens would bring key improvements to current surgical masks and respirators, resulting in increased protection, reduced risk of cross-infection, and recyclability without decontamination (Figure 1.4).

Table 1.4 Performance of respiratory protection. The key technical components of the performance of current respiratory protection devices are filtration efficiency, fit, and comfort. Each has a significant role in protection efficacy, and specific parameters can be tuned to improve them.

Fit

Non-filtered air entering through poor seal between mask and face is a prominent concern. The efforts made towards reducing faceleaks can be grouped into:

- Material selection that allows customizable mask shape/tightness;
- Investigation of wearers facial features, and modeling of leaks spatial distribution to guide mask design; and
- Fit testing/training optimization to increase efficacy/compliance.

Filtration efficiency

Whereas N95 respirators have certified filtration efficiency of 95%, surgical masks have low performance. Several major parameters can be controlled to decrease particles penetration:

- Decreasing diameter of fibers;
- Decreasing the size of filter pores;
- Controlling fibers electrical charge through manufacturing process/material selection; and
- Increasing thickness of filters.

User comfort

Wearer's perception of comfort is critical to correct practices and effective protection. Tolerability during mask use is often limited by:

- Reduced breathability caused by pressure drop across the mask;
- Heat build-up inside the mask due to increased temperature/humidity;
- Carbon dioxide rebreathing;
- Discomfort from prolonged contact between skin and rough materials; and
- Difficulty in communicating.

To inactivate pathogens, antimicrobial treatments have been investigated for filters utilizing halogens, metals, quaternary ammonium compounds, and antibody-antigen reaction. Chlorine compounds such as N-halamines and iodine-treated filters have been assessed against bacteria (*Micrococcus luteus, S. aureus* and *Escherichia coli*) [148]. Chlorine is a halogen with well-known antimicrobial properties as it causes irreversible oxidation of sulfhydryl groups of bacterial enzymes [149]. It can be included in compounds such as N-halamines, where chlorine

is covalently bonded to nitrogen to form a chloramine group [150]. N-halamines have been incorporated on polypropylene filters by radical graft polymerization during fiber extrusion [151], by producing a semi-interpenetrating network of polyacrylamide immobilized onto polypropylene woven fabric [152], or by coating N-halamine polyelectrolytes onto meltblown polypropylene fabrics [153]. Iodine resins can be obtained by forming a complex with tri-iodide (I_3^-) or penta-iodide (I_5^-) ions and quaternary ammonium. They act as a disinfectant with a release-demand mechanism, where the negatively charged pathogens in proximity to the complexes displace the I^- ion/s and capture I_2 molecules, which cause oxidation and protein denaturation on the pathogens [148,154]. Additionally, surgical masks functionalized with quaternary ammonium inactivated *Acinetobacter baumannii*, *Enterococcus faecalis*, and *S. aureus* by membrane permeability damage (~92% reduction in 1 h) [155].

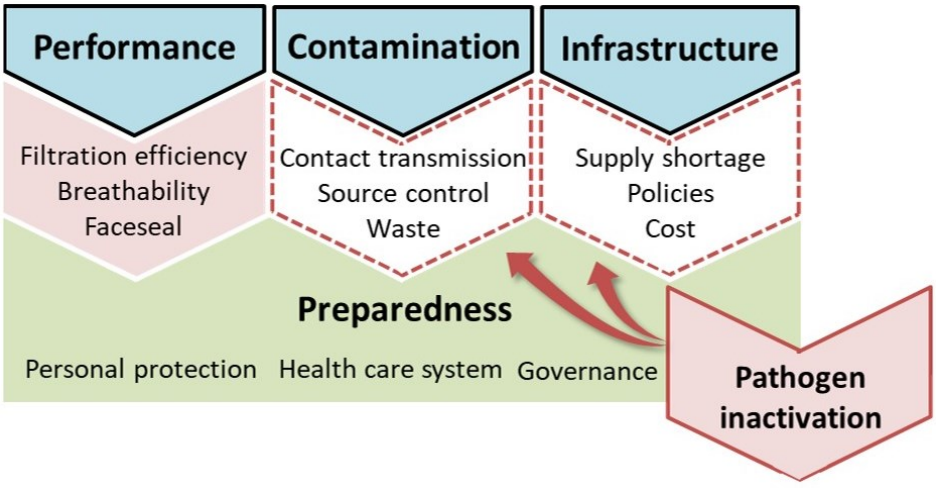

Figure 1.4 Pandemic and epidemic preparedness in the context of personal protection, health care system, and governance. Three major aspects make up pandemic and epidemic preparedness from the perspective of respiratory protection: performance of the technology, contamination by infective pathogens, and infrastructure. Whereas extensive focus has been directed towards technical improvement of filtration efficiency, faceseal, and breathability of masks, several challenges currently exist in the other two fields, creating a gap towards preparedness. Neutralization of the pathogens on respiratory protective devices is an approach that can bridge this gap.

A mask with antiviral properties was produced by treating the inner layer with copper and zinc ions, which disrupt structural components of virus such as lipid envelopes and nucleic acids [94]. Additionally, the outer layer was coated with citric acid to expose pathogens to a low-pH environment, which affects the structure of lipids causing virus denaturation. Another anti-virus mask was developed by incorporating copper and copper oxide particles in the meltblown middle and spunbond outer/inner layers, respectively [112,156]. Silver was also investigated by coating the outer layer of masks with silver nitrate nanoparticles, with the ability to inactivate bacteria (*Escherichia coli* and *S. aureus*) in 48 h by interaction with thiol groups of proteins and enzymes [157].

However, antimicrobial technologies based on silver/copper, reactive oxygen molecules, iodine, and titanium dioxide did not exhibit inactivation properties against MS2 virus [158]. Another approach to inhibit virus transmission involves modification of the filter surface with the antigen-specific antibodies [159]. Despite the merits of each approach, effective protection against virus aerosols is still limited by slow action (rapid inactivation should occur in the order of minutes, not hours) or binding specificity. Notably, most studies have focused on the functionalization of the outermost and middle layers of the mask. The final design of the protection device layers should consider the spatial deposition of aerosols within masks and their contact surface.

Based on the above observations, we identify three central parameters in developing pathogen-inactivating filters. First, an inactivation mechanism should act rapidly to avoid cross-infection. Although additional aspects are involved (e.g., fraction of transferred pathogens, surface area), unsafe handling and people's tendency to touch their face every ~4 minutes lead to a risk of contact transmission from a pathogen-laden mask or respirator [160]. Second, pathogens

should be neutralized in a strain-nonspecific way. The pathogen type/strain responsible for the next pandemic cannot be exactly predicted because of continuous mutation. As such, antibody-functionalized protective devices that target a strain-specific virus would delay the emergency response. Thus, the pathogen-killing mechanism should guarantee broad-spectrum protection. Third, the ideal technology should be device-independent. In the case of a pandemic outbreak, time-consuming production and cost are major limitations to respirator use. Although a certified respirator is recommended, considering the heavy use of surgical masks and scarcity of respirators, the technology should be easily extendable to masks and other existing infection control measures. Therefore, the aforementioned factors outline the considerations that can enhance respiratory protection for a timely emergency response.

The unpredictable nature of airborne pandemic diseases and their impact on our economy and society present a big challenge at the national and global level. Only a prompt and coordinated response among different sectors of society can maintain security from this threat, which can be implemented through the help of technological innovations and comprehensive planning. Unfortunately, despite being recognized as a key technical element in pandemic and epidemic preparedness, innovation in the design of respiratory protection devices has been sparse. In alignment with the strategic plan for pandemic and epidemic preparedness, we anticipate that incorporation of efficient pathogen-neutralization mechanisms can overcome the existing technical (contact transmission, source control, waste) and non-technical (supply shortage, policies, cost) challenges in respiratory protection. Thus, we expect this engaging field to expand further, with the promise to offer enhanced protection to the global population.

1.6 Novel respiratory protection system

Creating a highly effective, low-cost method for protection against infectious aerosols is considered a major challenge in public health. This research aimed to develop a universal, recyclable pathogen negation system, which efficiently captures and inactivates aerosol transmissible diseases on a filter, providing complete protection. Our technology was designed to tackle the aforementioned technical hurdles of respiratory protection systems, namely filtration efficiency, breathability, cross infection and recyclability. To this end, we developed salt coating formulations to apply crystal films on the surface of polymeric meshes. The coating formulations were selected based on safety, cost effectiveness, and environmental response. Our system provides both active and passive protection to the public against all forms of airborne pathogens. Therefore, the overall goal of this research was directed toward development of disease control and prevention technologies to prepare for future epidemics and pandemics and mitigate infection transmission in susceptible settings.

Hypothesis: Salt coatings applied on polymeric fibrous substrates were hypothesized to (1) enhance the filtration efficiency of the challenge aerosols without compromising breathability, and (2) cause inactivation of the pathogens transmitted through aerosols via two successive processes: i) the salt on the fiber dissolves upon exposure to the pathogenic aerosols and ii) salt crystallizes as aerosols evaporate.

Overall, this work was divided into multiple research goals:

1. Development of salt coating formulation and fabrication of prototype sodium chloride-functionalized virus-inactivating surgical mask filter;
2. *In vitro* and *in vivo* demonstration of the proof-of-concept salt recrystallization-based pathogen inactivation mechanism to provide superior protection compared to current technologies;
3. Production of filters functionalized with varying salt candidates to optimize the coating formulation to meet diverse application-specific requirements (i.e., environmental stability);
4. Evaluation of performance (filtration efficiency and breathability) of the fibrous substrates following salt functionalization;
5. Assessment of universal pathogen inactivation against multiple pathogen types (bacteria/viruses) and strains;
6. Evaluation of the environment-dependent performance to determine optimal salt system/s for specific environmental conditions;
7. Examination of the salt-dependent pathogen inactivation behavior.

2 Demonstration of salt functionalization-based pathogen inactivation technology

Aerosolized pathogens are a leading cause of respiratory infection and transmission. Currently employed protective measures pose a potential risk of infection/cross-infection and transmission. Here, we report the development of a universal, reusable virus inactivation system by functionalization of the main fibrous filtration unit of surgical masks with sodium chloride salt. The salt coating on the fiber surface dissolves upon exposure to virus aerosols and recrystallizes during drying, destroying the pathogens. When tested with tightly sealed sides, salt-coated filters showed remarkably higher filtration efficiency than the conventional mask filtration layer, and 100% survival rate was observed in mice infected with virus penetrated through salt-coated filters. Viruses captured on salt-coated filters exhibited rapid infectivity loss compared to gradual decrease on bare filters. Salt-coated filters proved highly effective in inactivating influenza viruses regardless of subtypes and following storage in harsh environmental conditions. Our results can be applied in obtaining a broad-spectrum, airborne pathogen prevention device in preparation for epidemics and pandemics of respiratory diseases.

2.1 Background

Aerosols take a prominent role in airborne transmission of respiratory diseases. Droplets with aerodynamic size (d_a) < 10 μm and 10 < d_a < 100 μm are known to infect the alveolar regions and upper respiratory tract, respectively [7,19]. Notably, aerosols can also be a route of infection in diseases that, contrary to for instance influenza, do not specifically target the respiratory tract, as it could be the case of Ebola virus [161]. While vaccination can greatly reduce morbidity and mortality, during a pandemic or epidemic new vaccines matching the specific strain would be available, at the earliest, six months after the initial outbreak. Additionally, following development of an effective viral vaccine, several potential problems would remain, such as limited supply due to insufficient production capacity and time-consuming manufacturing processes. As a result, individuals close to the point of an outbreak would be in imminent danger of exposure to infectious diseases during the non-vaccine period. In the absence of vaccination, respirators and masks can be worn to prevent transmission of airborne pathogenic aerosols and control diseases, such as influenza [162].

The main alternative, the N95 respirator, requires training prior to use, must be expertly fitted to address the risk of faceseal leakage at the face-mask interface, and must be disposed of as a biohazard [163]. Due to these factors, the use of N95 respirators on a large scale is impractical and expensive during an epidemic or pandemic. Past experiences of SARS, H1N1 swine flu in 2009, and MERS indicate that surgical masks have been most widely adopted by the public as personal protective measure, despite controversy on their effectiveness [14,74,81,82]. Currently, among other factors, filtration in respirators and masks depends on filter characteristics, including fiber diameter, packing density, charge of fibers and filter thickness, as well as particle properties, such as diameter, density and velocity [61,67,70,71,164]. However, in

the lack of a system to inactivate the collected pathogens, safety concerns naturally arise about cross infection and contamination from virus-laden filter media during utilization and disposal. Furthermore, since re-sterilization is not possible without causing damage, respirators and masks are recommended for single use only [3,14,165]. Scientific efforts have been focused on treatment of filters with materials possessing well-known antimicrobial properties, such as iodine, chlorine and metals [94,112,148,151-154,156,157], although with limited effectiveness against virus aerosols [158,166,167]. Therefore, a key challenge is the development of an easy-to-use, universal virus negation system, which is reusable without reprocessing and capable of inactivating pathogens, thereby reducing potential risk of cross infection and transmission.

Here, we report a simple but efficient virus inactivation system exploiting the naturally occurring salt recrystallization. Our strategy is to modify the surface of the fibrous filtration layer within masks with a continuous salt film for virus inactivation via two successive processes: i) salt is locally dissolved by the viral aerosols and ii) supersaturation is followed by evaporation-induced salt recrystallization. Consequently, viruses are exposed to increasingly higher concentrations of saline solution during drying and physically damaged by recrystallization.

2.2 Methods

2.2.1 Bare and salt-coated filter samples preparation

The commercial surgical masks (Fisherbrand Facemasks; Fisher Scientific, Pittsburgh, PA, USA) had a three-ply structure. The middle layer is the filter media, whereas the inner and outer layers provide support and protect the filter against wear and tear. The metal nose clips and elastic ear loops were removed and circular samples (radius = 3 cm) were cut from the masks. The polypropylene filters (middle layer) were isolated by removing the inner and outer protective layers (bare filters, $Filter_{bare}$). The coating solution was prepared by dissolving sodium chloride (NaCl; Sigma Aldrich, St. Louis, MO) in filtered DI water (0.22 μm pore size; Corning, Tewksbury, MA) under stirring at 400 rpm and 90 °C, followed by the addition of Tween 20 (Fisher Scientific) to a final concentration of 29.03 w/v% of NaCl and 1 v/v% of Tween 20. To obtain the salt-coated filters, the mask bare polypropylene filters were pre-wet to contain approximately 600 μL of coating solution by incubating overnight at room temperature (RT). Any remaining dry areas were removed by applying gentle strokes with tweezers to the filters while immersed in the coating solution. Subsequently, the filters were deposited in the desired volume of coating solution (0, 100, 300, 600, 900 and 1200 μL, of which corresponding membranes are abbreviated as $Filter_{wet}$, $Filter_{wet+100\mu L}$, $Filter_{wet+300\mu L}$, $Filter_{wet+600\mu L}$, $Filter_{wet+900\mu L}$, and $Filter_{wet+1200\mu L}$, respectively) on petri dishes (60 × 15 mm; Fisher Scientific) to control the amount of NaCl per unit area and dried in an oven (Isotemp Incubator, Fisher Scientific) at 37 °C for 1 day.

2.2.2 Influenza virus preparation

Influenza viruses A/California/04/2009 (CA/09, H1N1), A/Puerto Rico/8/34 (PR/34, H1N1) and A/Vietnam/1203/2004 (VN/04, H5N1) were grown in 10-day old embryonated hen eggs, in which H5N1 virus was derived by reverse genetics from HPAI A/Vietnam/1203/2004 [168]. Influenza viruses were purified from allantoic fluid using discontinuous sucrose gradient (15%, 30% and 60%) layers following the previously reported procedure [169].

2.2.3 Aerosols exposure to filters

For experiments involving aerosols exposure, an aerosol chamber (L × W × H = 145 × 145 × 150 mm; Emka Inc., Middletown, PA) was used. It has a connection to the vacuum line and a circular aperture in the top wall (diameter = 22 mm) to exactly accommodate the cylindrical part (diameter = 20 mm, height = 20 mm) of the nebulizer unit that is below the aerosol generator (Aeroneb Lab Nebulizer System; Aerogen, Galway, Ireland). Bleach was used as trap between the chamber and the vacuum pump (Welch 2522C-10, 22 L/min; Niles, IL). The filters were placed on top of the chamber aperture and the nebulizer unit was inserted, ensuring the tight seal of the filters against the side of the aperture. 5 μL of virus stock were added to the nebulizer unit, aerosols (diameter = 2.5–4 μm from manufacturer specifications) were generated for 30 sec and subsequently the desired vacuum level (3, 10 or 17 kPa) was applied, by manual control, three times in 1 sec cycles. Notably, in the case of bare filters, pressure was only applied for filtration efficiency tests.

For all assays and analysis, suspensions of the filters were prepared as follows, unless otherwise indicated. To reconstitute virus adsorbed onto filters, virus-laden filters were immersed in 400 μL of sterilized DI water for about 5 min, and then removed after vortexing

from the suspension. The virus suspension was centrifuged at 19,800 g and 4 °C for 10 min (Centrifuge 5810 R, Eppendorf, Hauppauge, NY), followed by resuspension of pellets in 70 μL of DI water to eliminate any interference from materials in the supernatant during assays.

Henceforth, multiple filter samples were tested for each condition and the controls/stocks were tested repeatedly to monitor batch-to-batch quality; *n* for all conditions/controls/stocks is reported in each figure (minimum–maximum values).

2.2.4 Filtration efficiency tests

The filters were exposed to the virus aerosols at 3, 10 and 17 kPa (as measured by the vacuum pump gauge) and suspensions of the filters were obtained, as described above. The filtration efficiency was calculated as the ratio of the amount of virus (i.e., total proteins measured from the virus) reconstituted from the filter to that from the virus in the exposure aerosols. To collect all the virus in the exposure aerosols upstream, the virus stock was aerosolized without filters and the protein concentration was measured. To do this, viral aerosols were generated into a 15-mL centrifuge tube, containing 1 mL of DI water. After vortexing, virus concentrations (i.e., total protein concentration) were measured with bicinchoninic acid assay (BCA protein assay kit; Thermo Fischer scientific, Waltham, IL) with bovine serum albumin as a standard. Briefly, the samples/standard were mixed with the assay reagent at a 1:1 ratio and incubated before measuring absorbance at the wavelength instructed by the manufacturer's protocol; the standard was measured in 2× dilutions. Virus-laden filter suspensions were replaced with DI water prior to BCA assay.

2.2.5 *In vivo* infection tests

Lethal infectivity of influenza viruses (CA/09 H1N1) was examined in 8-week old female inbred BALB/c mice (Nara Biotech; Seoul, Korea) by using the intranasal route. For bare and salt-coated filters, 12 mice per group were infected with individual penetration dosage of influenza virus through each filter. The penetration dosage of the virus through the filters ($Filter_{bare}$, $Filter_{wet}$, $Filter_{wet+600\mu L}$, and $Filter_{wet+1200\mu L}$) was calculated from the filtration efficiency at 10 kPa (near breathing pressure [170]) using the relationship: penetration dosage = virus dosage in lethal aerosol × penetration efficiency (%)/100, where penetration efficiency (%) = 100 – filtration efficiency (%). To examine the effects of the aerosolization process on the viral infectivity change, two mice groups were infected with a lethal dose of virus before and after aerosol formation, which served as negative control groups. Body weight changes and survival rate of mice were monitored daily for 15 days. Mice with body weight loss greater than 25% were euthanized. On day 4 after infection, 6 mice of each group were sacrificed for the collection of lung samples. Lung virus titers were measured on six-well plates containing confluent Madin-Darby Canine Kidney (MDCK) cell monolayers. Inflammatory cytokines (interferon-γ (IFN-γ)) were determined using BD OptEIA mouse IFN-γ ELISA kit (BD Biosciences, San Jose, CA) following the manufacturer's procedure. For body weight measurements $n = 12$ before sacrifice and $n = 6$ after sacrifice, for lung tissue assays $n = 6$; off-trend measurements were not considered, and n is reported for each figure. All animal protocols were approved by the Kyung Hee University (KHU) Institutional Animal Care and Use Committee (IACUC). All animal experiments and husbandry involved in this work were conducted under the approved protocols and guidelines of KHU IACUC. KHU IACUC operates under National Veterinary Research and

Quarantine Service (NVRQS), and animal welfare law and regulations of the WOAH-OIE (World organization for animal health).

To test strain-dependent lethal infection behavior, mice (12 per group) were infected with the penetrated dosage of viral aerosols (PR/34 H1N1 and VN/04 H5N1) through $Filter_{wet+600\mu L}$ at 10 kPa. Body weight change was monitored in the same manner described above.

2.2.6 Test of viral infectivity change on filters

To investigate the effects of salt-coating on viral infectivity loss, lethal influenza aerosols were exposed to four different types of filters ($Filter_{bare}$, $Filter_{wet}$, $Filter_{wet+600\mu L}$, and $Filter_{wet+1200\mu L}$). Since $Filter_{bare}$ exhibited almost complete penetration upon pressure application, aerosols were exposed to the bare filter in the absence of pressure and samples were carefully handled to prevent mechanical agitation. To measure time-dependent stability change of virus, virus-laden filters were incubated at ambient conditions for 0, 5, 15, and 60 min after aerosol exposure, and suspended in DI water to reconstitute virus at each time point. *In vitro* stability of virus was characterized by measuring hemagglutinin activity (HA) and virus titers at the same concentration as lethal dose [171]. The conformational stability of antigenic proteins was characterized by measuring intrinsic fluorescence using 0.1 mg/mL of virus suspension [172]. To investigate morphological change of virus, lipid stability of the viral wall was characterized by nile red fluorescence (Sigma Aldrich), a fluorescent lipid stain, following the manufacturer's protocol [173]. A decrease in fluorescence intensity can be used to examine the level of disintegration of the virus. Both intrinsic and nile red fluorescence were measured by using a fluorimeter (LB 50B; PerkinElmer, Waltham, MA). Intensity changes of fluorescent spectra were compared relative to those of a control from the virus stock.

To test the infectivity difference observed from *in vitro* findings, an *in vivo* study was performed for the virus reconstituted from the filters ($Filter_{bare}$, $Filter_{wet}$, $Filter_{wet+600\mu L}$, and $Filter_{wet+1200\mu L}$) after incubation for 60 min at RT (aerosol exposure at 10 kPa, except for $Filter_{bare}$). 12 mice per group were infected with a lethal dose of virus collected from each type of filter. Body weight change and lung virus titers were measured as described above.

2.2.7 Effects of environmental conditions on the performance of salt-coated filters

Salt-coated filters ($Filter_{wet}$, $Filter_{wet+600\mu L}$, and $Filter_{wet+1200\mu L}$) were stored at 37 °C, 70% RH in an incubator (Maru Max; Rcom, Gyeonggi-do, South Korea) for 15 days. Every day, the filters were collected and incubated at ambient conditions for 5 min. At 1-day incubation, filtration efficiency was measured at 10 kPa from $Filter_{wet+600\mu L}$, followed by *in vivo* infection test. Lethal infectivity between two different filter groups (before and after incubation at 37 °C, 70% RH) was compared by measuring body weight change and survival rate of mice after exposure to lethal CA/09 H1N1 aerosols. X-ray diffraction (XRD) analysis was performed to salt-coated filters incubated for 1 and 15 days, and scanning electron microscopy (SEM) and energy dispersive X-ray (EDX) mapping analysis for 15-day incubated samples.

2.2.8 Contact angle measurements and imaging of aerosols

The bare and salt-coated filters were fixed with carbon tape (Ted Pella, Inc., Redding, CA) to a metal, flat substrate and 3 μL of DI water were added on the surface of the filters. The contact angles were measured from images collected with an optical microscope (10× lens, Motic SMZ-140; Motic, Richmond, Canada) at RT. Images of aerosols on filter fibers were obtained using a dispersive Raman microscope (Nicolet Almega XR; Fisher Scientific).

2.2.9 Aerosol drying time on filters

The bare and salt-coated filters were fixed with carbon tape to a metal, flat substrate and exposed to aerosols generated from 5 μL of Sulforhodamine B Dye solution (1 mM, Sigma-Aldrich). Aerosol drying time was determined with a timer by observation with optical microscope.

2.2.10 Electron microscopy analysis

For virus stability tests, bare and salt-coated filters were exposed to CA/09 H1N1 aerosols and, after 5 and 60 min incubation, the virus was recovered by suspension of the filters, as described above. To study the effects of the coating formulation during aerosol drying independently from crystal growth, bare and salt-coated filters were immersed in DI water and removed after 60 min. Subsequently, the virus was incubated in the obtained suspension for 60 min. Additionally, the virus suspension was centrifuged at 19,800 g and 4 °C for 10 min to collect the samples and suspend them in DI water. For transmission electron microscopy (TEM) analysis (200 kV, JEOL JEM 2100; JEOL, Peabody, MA), samples were deposited on copper grid (Electron Microscopy Sciences, Hatfield, PA) and negatively stained with solution comprised of phosphotungstic acid hydrate (1.5 w/v%, pH = 7.0; Sigma-Aldrich, Oakville, Canada).

To identify the morphology of salt-coated filters and recrystallized salts, SEM/EDX analysis was performed for bare and salt-coated filters after coating with 10-nm thick gold layer. SEM analysis (Hitachi S-3000N; Toronto, Canada) was operated in secondary electron mode at 20 kV and EDX analysis was obtained with EDX detector (Oxford Instruments, Concord, MA).

2.2.11 XRD analysis

To confirm formation of crystalline NaCl coating and its stability during storage at 37 °C and 70% RH, XRD analysis (θ–2θ mode, CuKα radiation; BRU-1098, Bruker, Billerica, MA) was performed at different coating conditions on filters (1 × 1 cm) mounted on a slide glass.

2.2.12 Statistical analysis

To compare multiple conditions, Student's t-test, one-way analysis of variance (ANOVA), and general linear model were used (Minitab release 14; Minitab, State College, PA). *P* value of less than 0.05 was considered to be significant.

2.3 Results

2.3.1 Preparation and characterization of salt-functionalized filters

To demonstrate the concept of a pathogen inactivation system based on salt recrystallization, the middle layer of three-ply surgical mask (polypropylene microfiber filter) was coated with NaCl salt as an active virus negation unit (see Figure 2.1 for bare polypropylene filter). The coating formulations contained surfactant to enhance wetting of saline solution on the surface of hydrophobic polypropylene fibers. Bare polypropylene filters (abbreviated as $Filter_{bare}$) were pre-wet to contain about 600 μL of coating solution (abbreviated as $Filter_{wet}$). The amount of NaCl salt (W_{salt} in mg/cm^2) coated on the filter per unit area, considering that the filter thickness is constant, was easily controlled by changing the coating solution volume (V_{salt} in μL) during drying of pre-wet filter (radius = 3 cm; $W_{salt} = 3.011 + 0.013 \times V_{salt}$, $n = 7$) (Figure 2.2). Scanning electron microscopy (SEM) and energy dispersive X-ray (EDX) mapping analysis showed the formation of homogeneous NaCl coating during drying, as also confirmed by X-ray diffraction (XRD) (Figure 2.3 and Figure 2.4). Both the formation of NaCl coating on polypropylene fibers and the presence of surfactant in the coating formulation appeared to alter the filter surface properties from hydrophobic (bare filter; contact angle, $\theta_c = 133.0 \pm 4.7°$) to completely hydrophilic (salt-coated filter; $\theta_c \sim 0°$, $n = 10$) (Figure 2.5). The hydrophilic nature of the salt coating can greatly improve adhesion of viral aerosols to polypropylene fibers compared to $Filter_{bare}$, as seen in Raman microscope images (Figure 2.6).

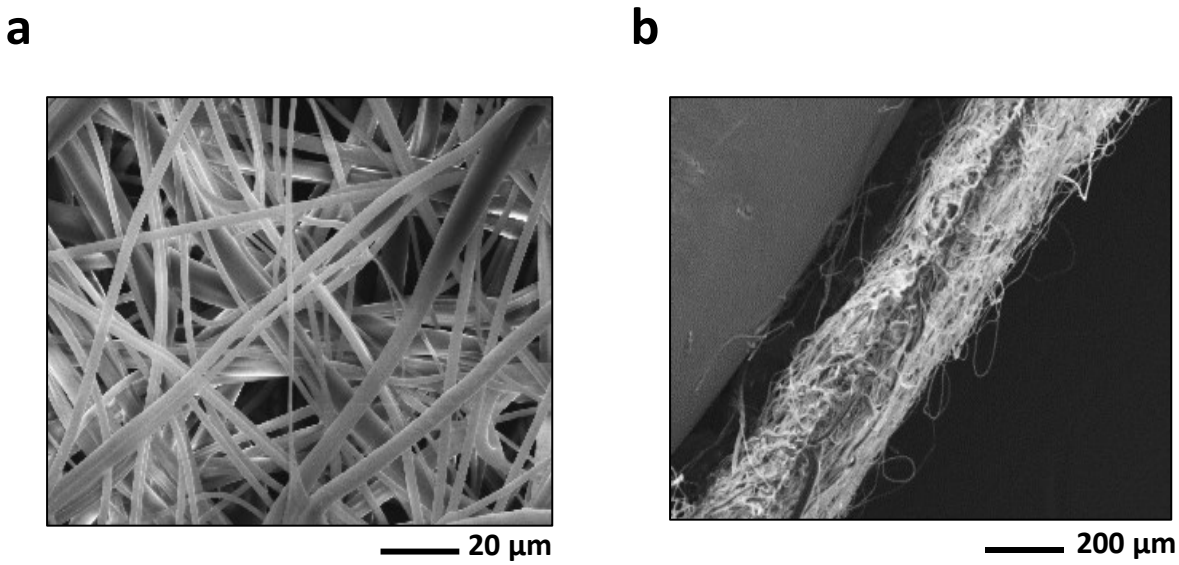

Figure 2.1 SEM micrographs of polypropylene filter of bare surgical mask ($Filter_{bare}$). Top view **(a)** and cross-sectional view **(b)**.

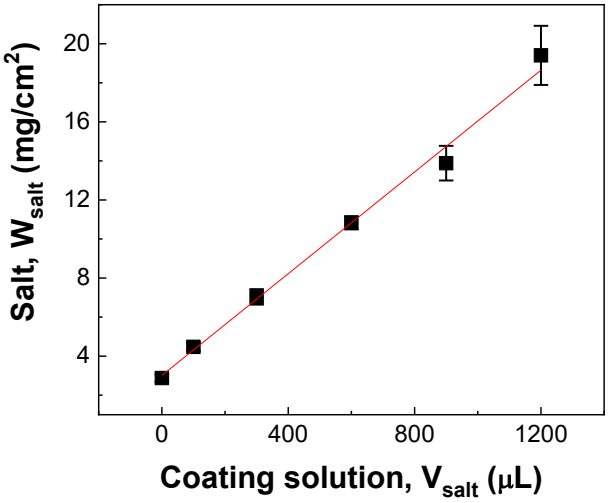

Figure 2.2 Plot showing the relationship between the volume of coating solution used for drying of pre-wet filters (V_{salt}) and amount of coated salts (W_{salt}) (n = 7, mean ± standard deviation (SD)).

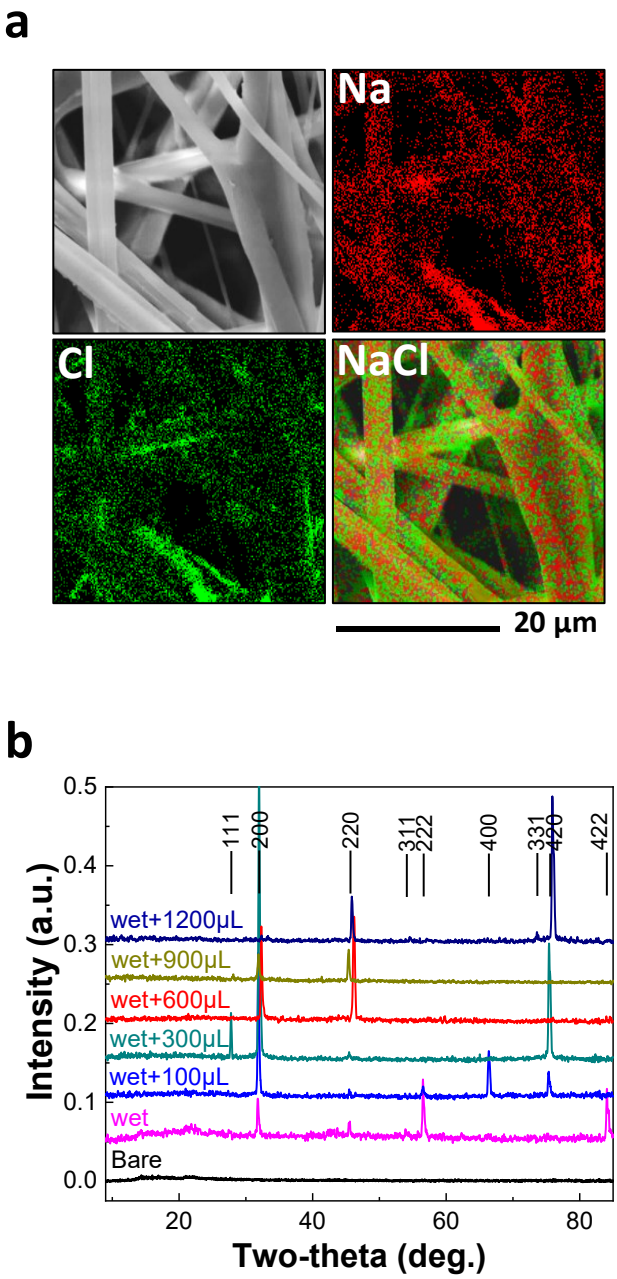

Figure 2.3 Successful preparation of mask salt-coated filter for prevention and inactivation of airborne pathogens. **(a,b)** SEM image of $Filter_{wet+600\mu L}$ (top left) and EDX mapping images of Na (red), Cl (green), and NaCl (combination of Na and Cl mapping images) **(a),** showing the formation of NaCl coating, as also confirmed by XRD spectra **(b)** of $Filter_{bare}$, $Filter_{wet}$, $Filter_{wet+100\mu L}$, $Filter_{wet+300\mu L}$, $Filter_{wet+600\mu L}$, $Filter_{wet+900\mu L}$ and $Filter_{wet+1200\mu L}$ (labelled as Bare, wet, wet+100µL, wet+300µL, wet+600µL, wet+900µL and wet+1200µL, respectively; Miller indices corresponding to NaCl crystal are shown at the top of XRD spectra for each position).

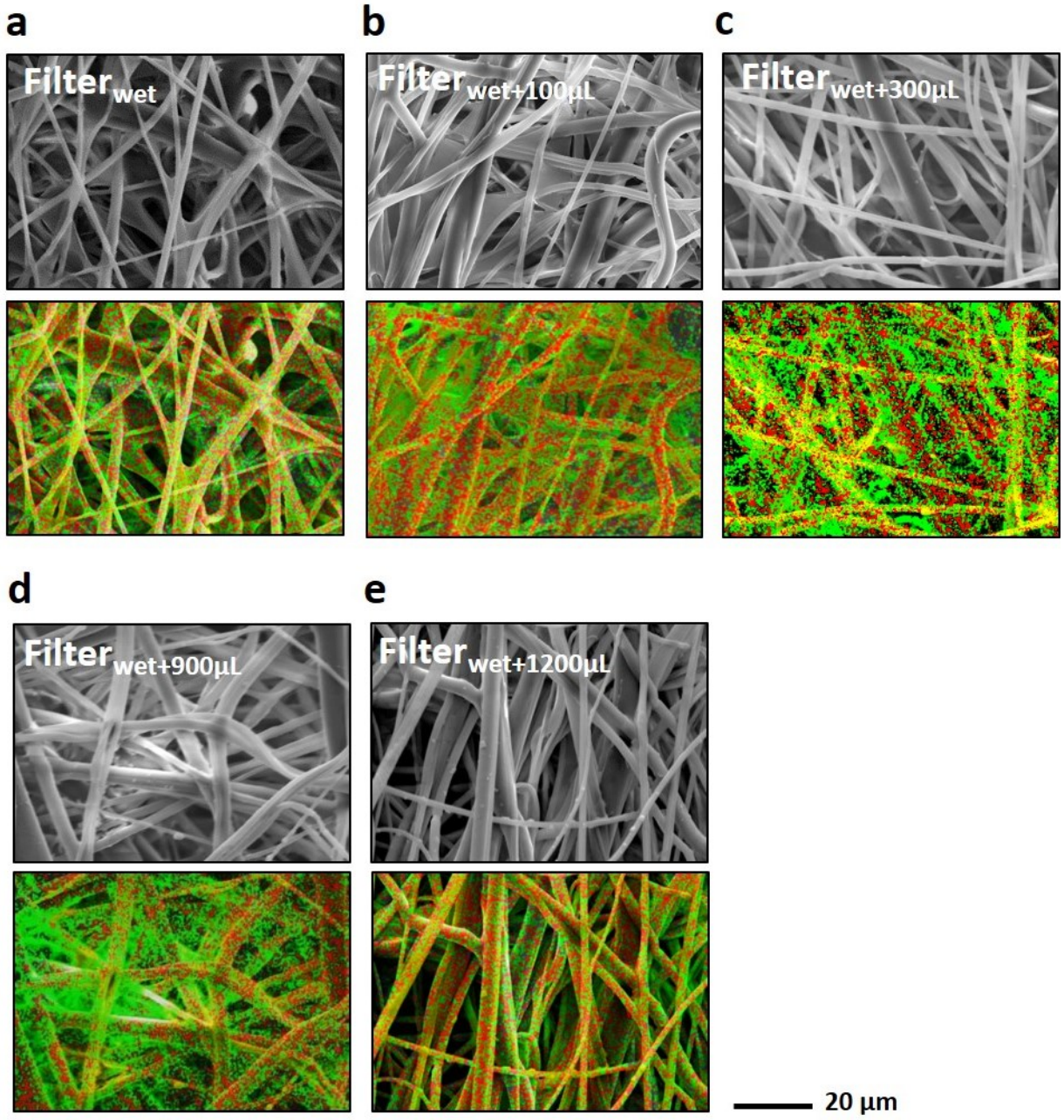

Figure 2.4 Representative SEM/EDX mapping images of salt-coated filters. (**a**) $Filter_{wet}$, (**b**) $Filter_{wet+100\mu L}$, (**c**) $Filter_{wet+300\mu L}$, (**d**) $Filter_{wet+900\mu L}$, and (**e**) $Filter_{wet+1200\mu L}$ (top: SEM, bottom: EDX mapping).

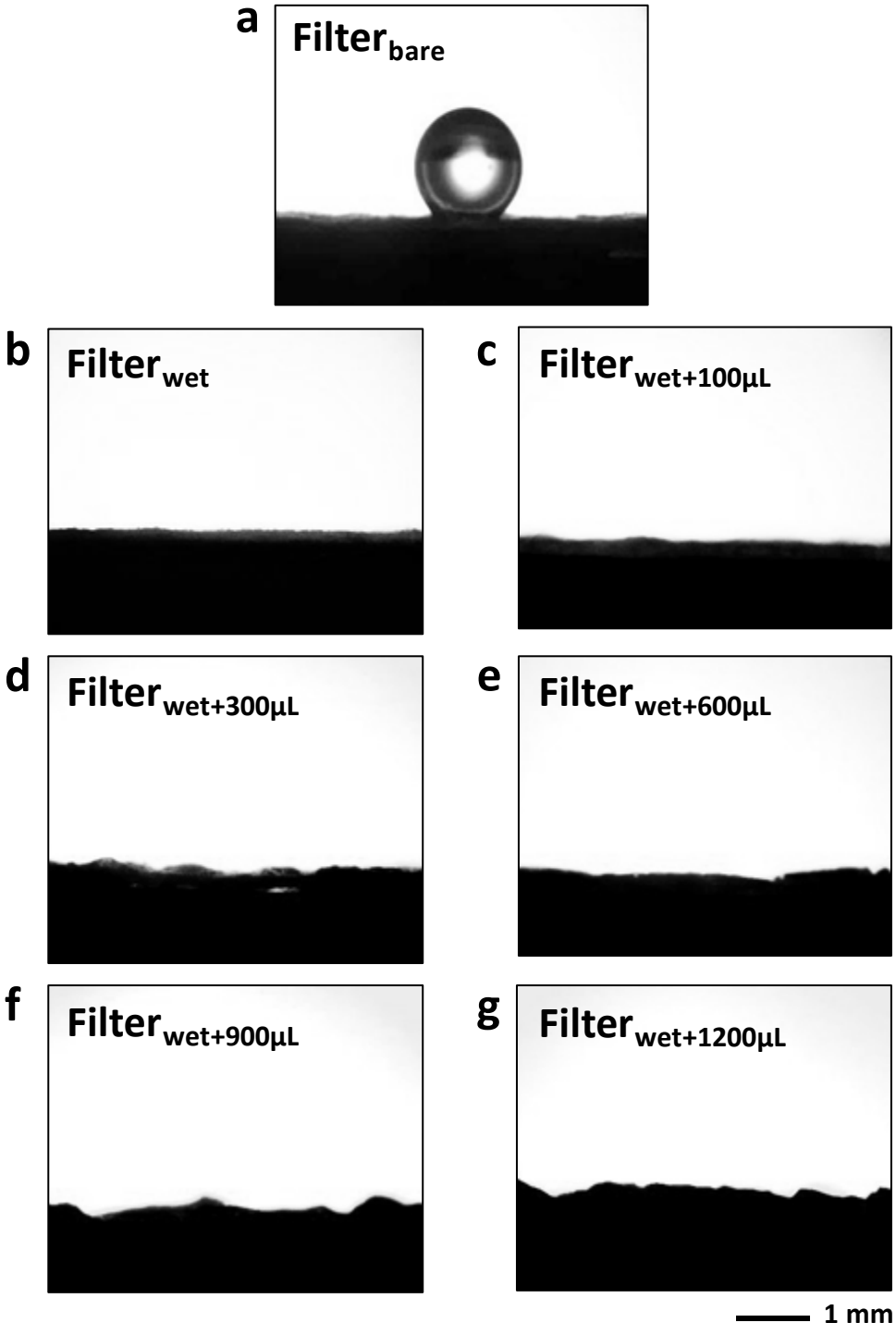

Figure 2.5 Optical microscope images of cross-sectional view of salt-coated filters after applying a drop of DI water (3 µL) for contact angle measurements. **(a)** $Filter_{bare}$, **(b)** $Filter_{wet}$, **(c)** $Filter_{wet+100\mu L}$, **(d)** $Filter_{wet+300\mu L}$, **(e)** $Filter_{wet+600\mu L}$, **(f)** $Filter_{wet+900\mu L}$, and **(g)** $Filter_{wet+1200\mu L}$. All salt-coated filters exhibited complete wetting (n = 10).

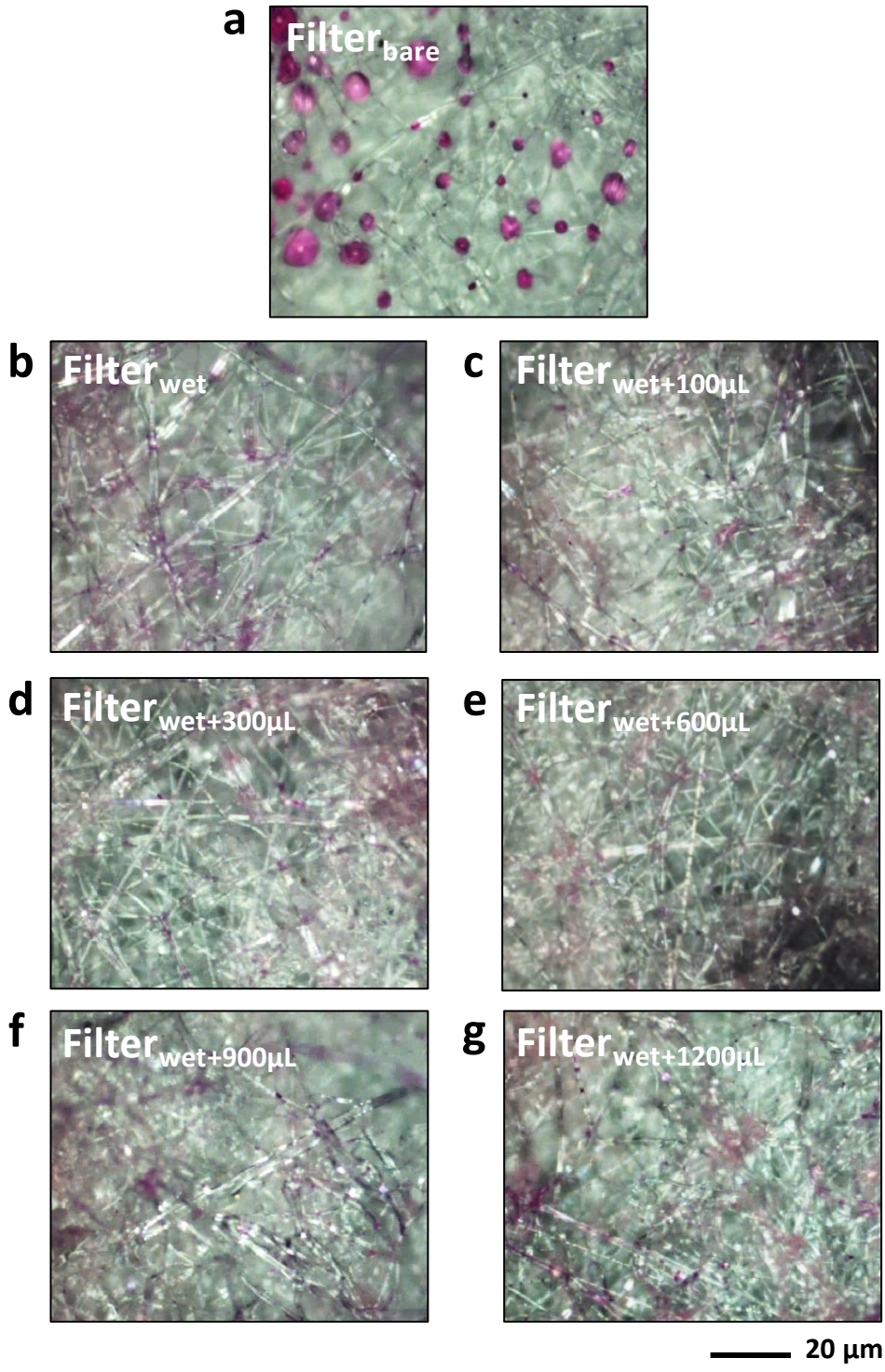

Figure 2.6 Optical microscope images of the top view of salt-coated filters right after exposure to aerosols. **(a)** $Filter_{bare}$, **(b)** $Filter_{wet}$, **(c)** $Filter_{wet+100\mu L}$, **(d)** $Filter_{wet+300\mu L}$, **(e)** $Filter_{wet+600\mu L}$, **(f)** $Filter_{wet+900\mu L}$, and **(g)** $Filter_{wet+1200\mu L}$. All salt-coated filters exhibited complete wetting (n = 10).

2.3.2 Filtration efficiency against viral aerosols and protective efficacy *in vivo*

Filtration efficiency of salt-coated filters was tested against aerosols with volumetric mean diameter (VMD) of 2.5–4 μm containing H1N1 pandemic influenza virus (A/California/04/2009, abbreviated as CA/09) at different pressure conditions. Interestingly, as shown in Figure 2.7, $Filter_{bare}$ did not exhibit any significant level of resistance against penetration of virus under our experimental conditions (i.e., 0% filtration efficiency). Conversely, salt-coated filters showed substantially increasing filtration efficiency with pressure and amount of coated salt. In particular, in the case of $Filter_{wet+600\mu L}$, filtration efficiency varied from 43 to 70%, with increasing pressure from 3 to 17 kPa, and $Filter_{wet+1200\mu L}$ exhibited persistent, high-level efficiency (~85%) (one-way ANOVA, $P = 0.85$). To probe the effects of filtration efficiency on protective efficacy, *in vivo* experiments were performed using mice intranasally (IN) infected with penetrated dosages of H1N1 virus under breathing pressure (~10 kPa) [170]. As shown in Figure 2.8a, similarly to negative control groups (mice infected with a lethal dose of virus stock and aerosolized virus), mice exposed to a dose penetrated through the bare filter showed rapid body weight loss, followed by death within 10 days after infection, in good agreement with the observed 0% filtration efficiency (Figure 2.7). In contrast, mice groups exposed to virus derived from salt-coated filters resulted in 100% survival rate (Figure 2.8b). Furthermore, lungs of mice from negative control groups exhibited severe lung infection 4 days after challenge (Figure 2.8c). Conversely, mice groups exposed to virus derived from salt-coated filters showed significantly lower levels of lung viral titers (t-test, $P < 0.005$). This is consistent with lower levels of inflammatory cytokines, interferon-γ (IFN-γ), from salt-coated filter groups compared to negative control and bare filter groups (t-test, $P < 0.001$) (Figure 2.8d).

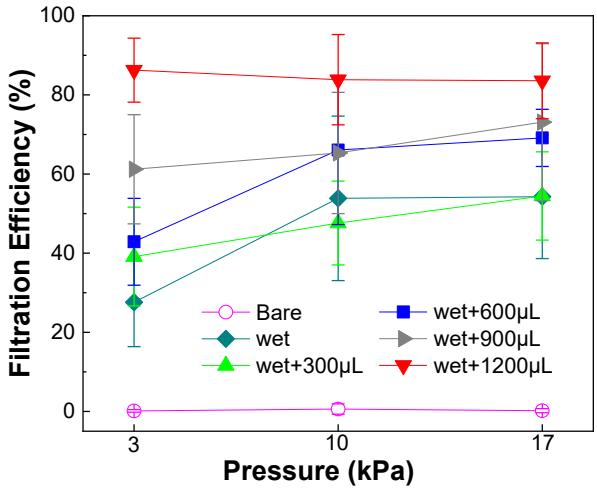

Figure 2.7 Pressure-dependent viral filtration efficiency (n = 8–10, mean ± SD).

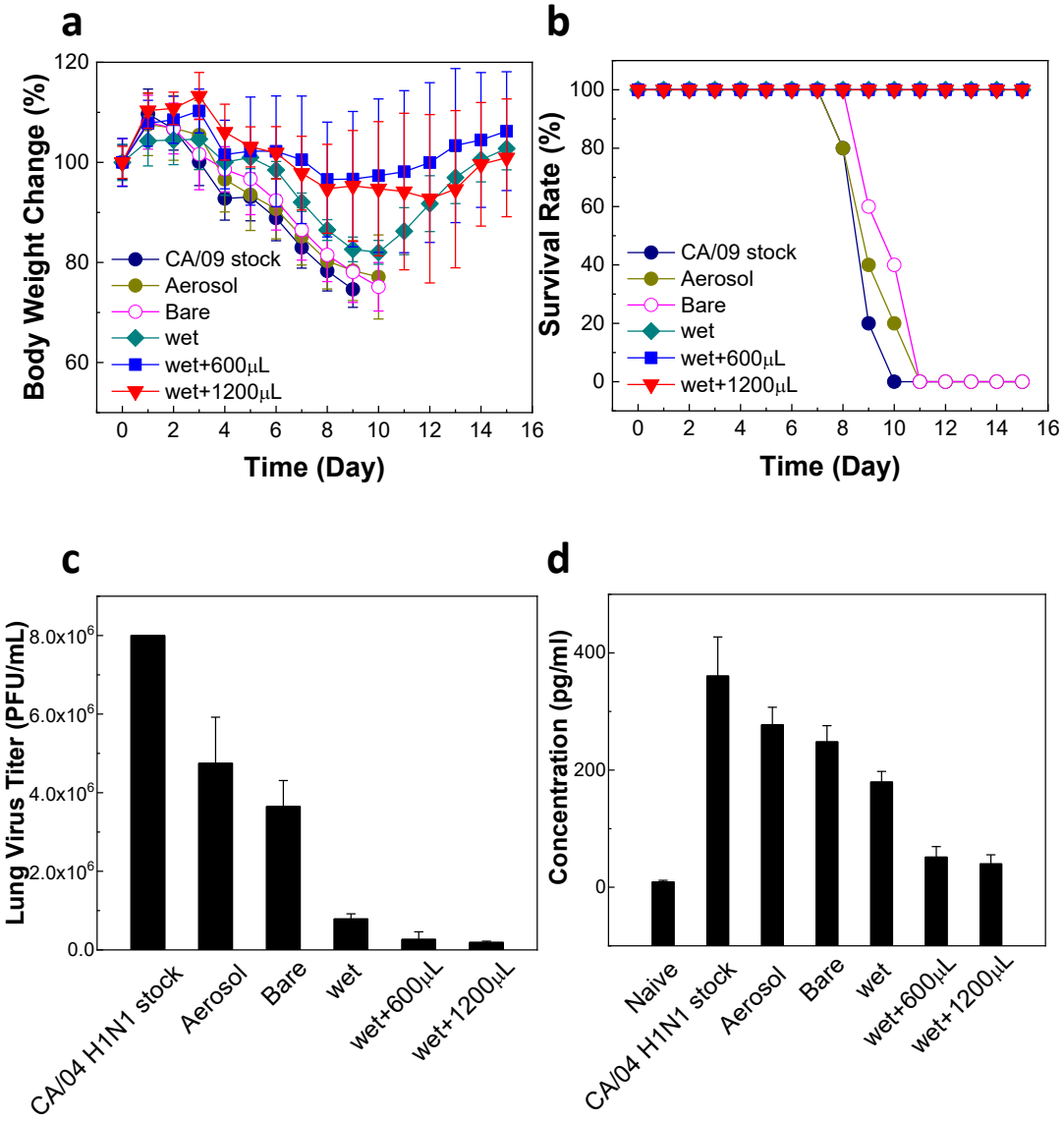

Figure 2.8 Effects of viral filtration efficiency on protective efficacy *in vivo*. **(a-d)** Body weight change of mice after infection with the dosages of penetrated virus (n = 6–12, mean ± SD) **(a)**, survival rates (mean; 100% means that all mice in the group survived as penetrated dosages were lower than lethal dose) **(b)**, lung virus titers (n = 4, mean ± SD) **(c)**, and lung inflammatory cytokine (IFN-γ) assay (n = 11, mean ± SD) **(d)**.

2.3.3 Inactivation of virus on salt-functionalized filters

Influenza virus stability tests were performed to investigate the effects of salt coating. The same amount of recovered viruses from the polypropylene fibers was used, and, in the case of bare filters, viral aerosol exposure was conducted in the absence of pressure due to 100% penetration of viral aerosols. Unlike bare filters (Figure 2.9a(i)), formation of micron-sized NaCl phase represents a typical feature of salt-coated filters due to recrystallization of NaCl salt, following local dissolution upon aerosol exposure (SEM images in Figure 2.9a, ii to iv, and EDX mapping in Figure 2.9b). In contrast to 8% HA activity loss of virus adsorbed onto $Filter_{bare}$, salt-coated filters exhibited almost complete HA activity loss within 5 min of incubation (Figure 2.10a). Such dramatic virus destabilization on salt-coated filters is further supported by negligible levels of viral titers compared to $Filter_{bare}$ with incubation time (t-test, $P < 0.001$) (Figure 2.10b). It is also noted that virus titers exhibited significant decrease with increase of incubation time and amount of coated salt (ANOVA general linear model, $P < 0.001$). Lower levels of native fluorescence and nile red fluorescence from virus recovered from salt-coated filters accounted for more severe conformational change of antigenic proteins and destabilization of viral envelope, respectively (t-test, $P < 0.001$) (Figure 2.10c). Transmission electron microscopy (TEM) analysis showed that influenza virus on $Filter_{bare}$ experiences morphological change into non-spherical shape during aerosol drying compared to control (Figure 2.11). Notably, influenza virus was severely damaged on salt-coated filters even at 5 min of incubation (Figure 2.11). From microscopic analysis, aerosol drying time was about 3 min, indicating that destruction of virus observed at 5 min is associated with drying-induced salt crystallization. Physical damage of virus due to crystallization was similarly reported as a major destabilizing factor of inactivated influenza virus [171,174].

In parallel, we investigated the separate effect of salt concentration increase on virus stability during the aerosol drying process, irrespective of crystal growth. As displayed in Figure 2.12, the materials collected in suspension from $Filter_{wet+600\mu L}$ induced visible morphological transformation of the virus (Figure 2.12b) compared to suspension of $Filter_{bare}$ (Figure 2.12a). This can be attributed to the high salt/surfactant concentration and osmotic pressure, which have been well-known to destabilize proteins and viruses [174-176]. Therefore, the marked virus destabilization on salt-coated polypropylene fibers can be explained by the combined effects of salt concentration increase during drying and evaporation-induced salt crystallization.

To verify *in vitro* virus stability on the filters, an *in vivo* study was performed by infecting mice with virus incubated for 60 min on polypropylene filters. As shown in Figure 2.13a, $Filter_{bare}$ group exhibited 5% body weight loss at day 9 post-infection, reaching a body weight lower than that of salt-coated filter groups by 10–15%. Thus, significantly higher lung virus titers in the negative control group were observed in contrast to no detectable titers in the salt-coated filter groups (Figure 2.13b).

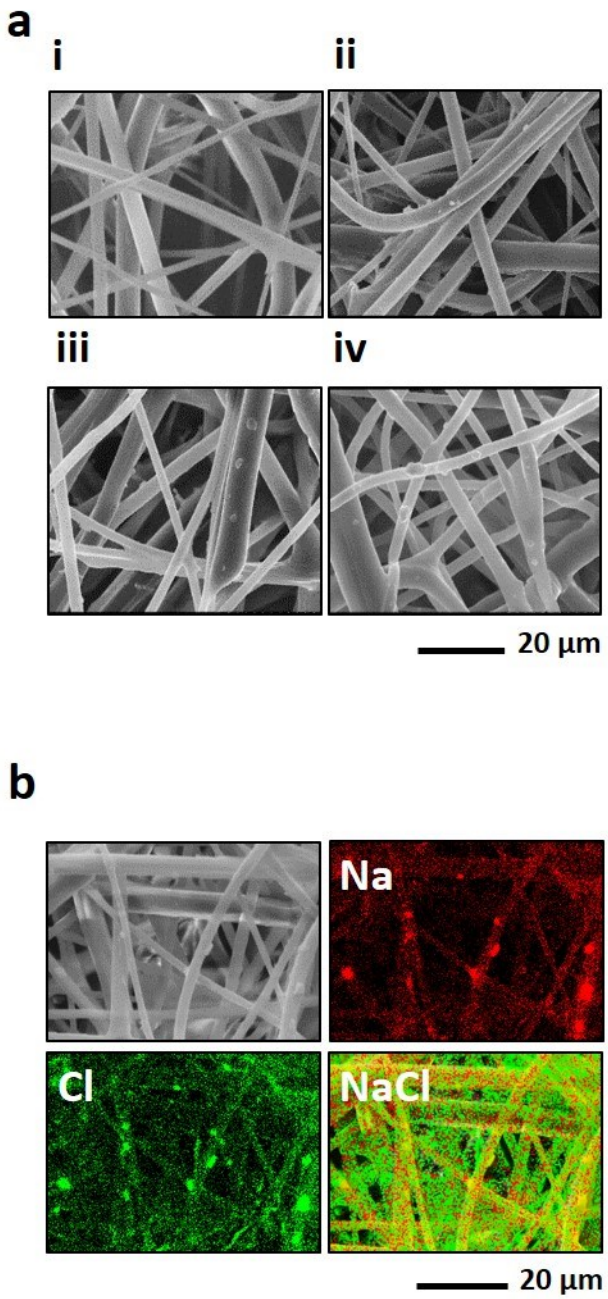

Figure 2.9 Salt recrystallization on filters following aerosol exposure. **(a)** SEM images of filters incubated for 60 min after exposure to influenza virus (i: $Filter_{bare}$, ii: $Filter_{wet}$, iii: $Filter_{wet+600\mu L}$, iv: $Filter_{wet+1200\mu L}$) showing the micron-sized NaCl phase on salt-coated filters upon drying of aerosols. **(b)** SEM/EDX mapping images of $Filter_{wet+600\mu L}$ exposed to aerosols (Na: red, Cl: green). Micron-sized structure on the filter is identified as NaCl phase due to NaCl salt recrystallization.

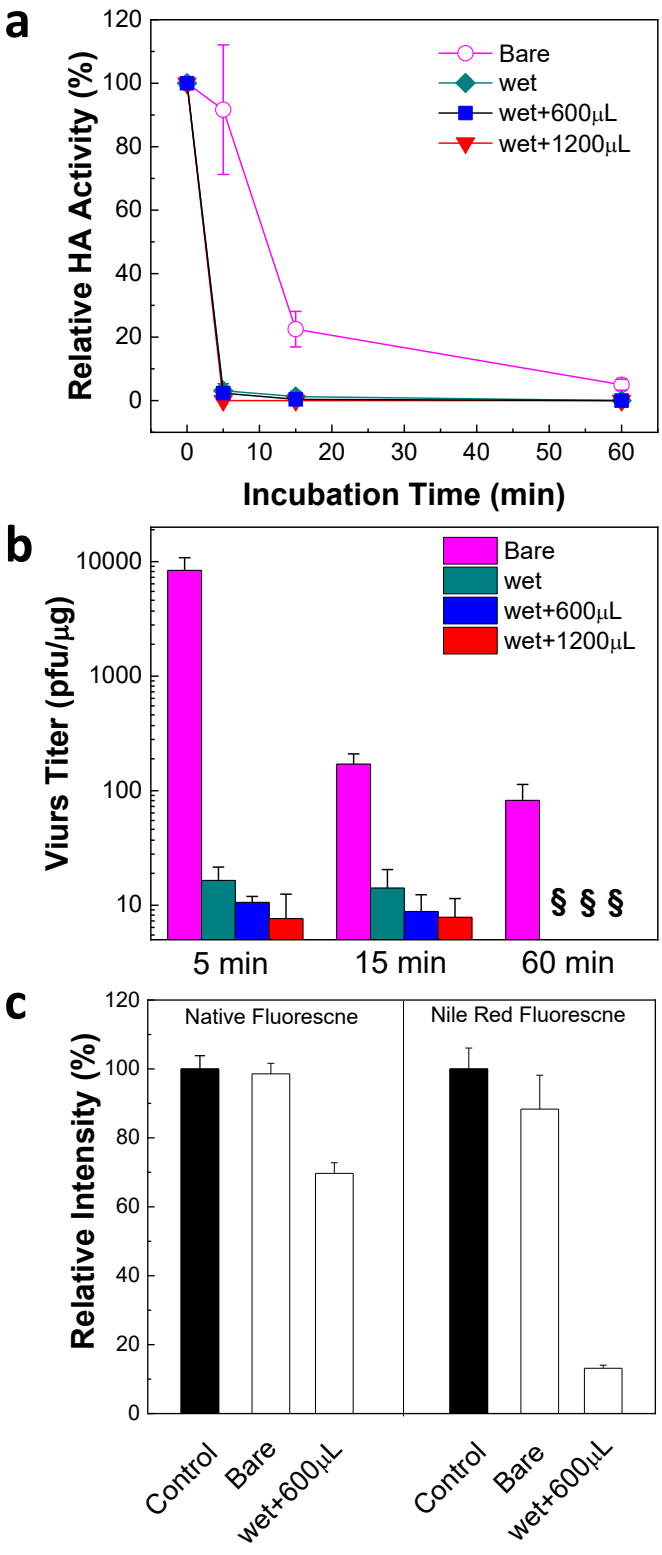

Figure 2.10 Inactivation of virus adsorbed on salt-coated filters. **(a,b)** HA activity **(a)** and virus titer **(b)** displaying the effects of incubation time on the remaining activity of virus (n = 4–8, mean ± SD). **(c)** Native fluorescence and nile red fluorescence of viruses incubated for 60 min (n = 12, mean ± SD). §: below detection limit.

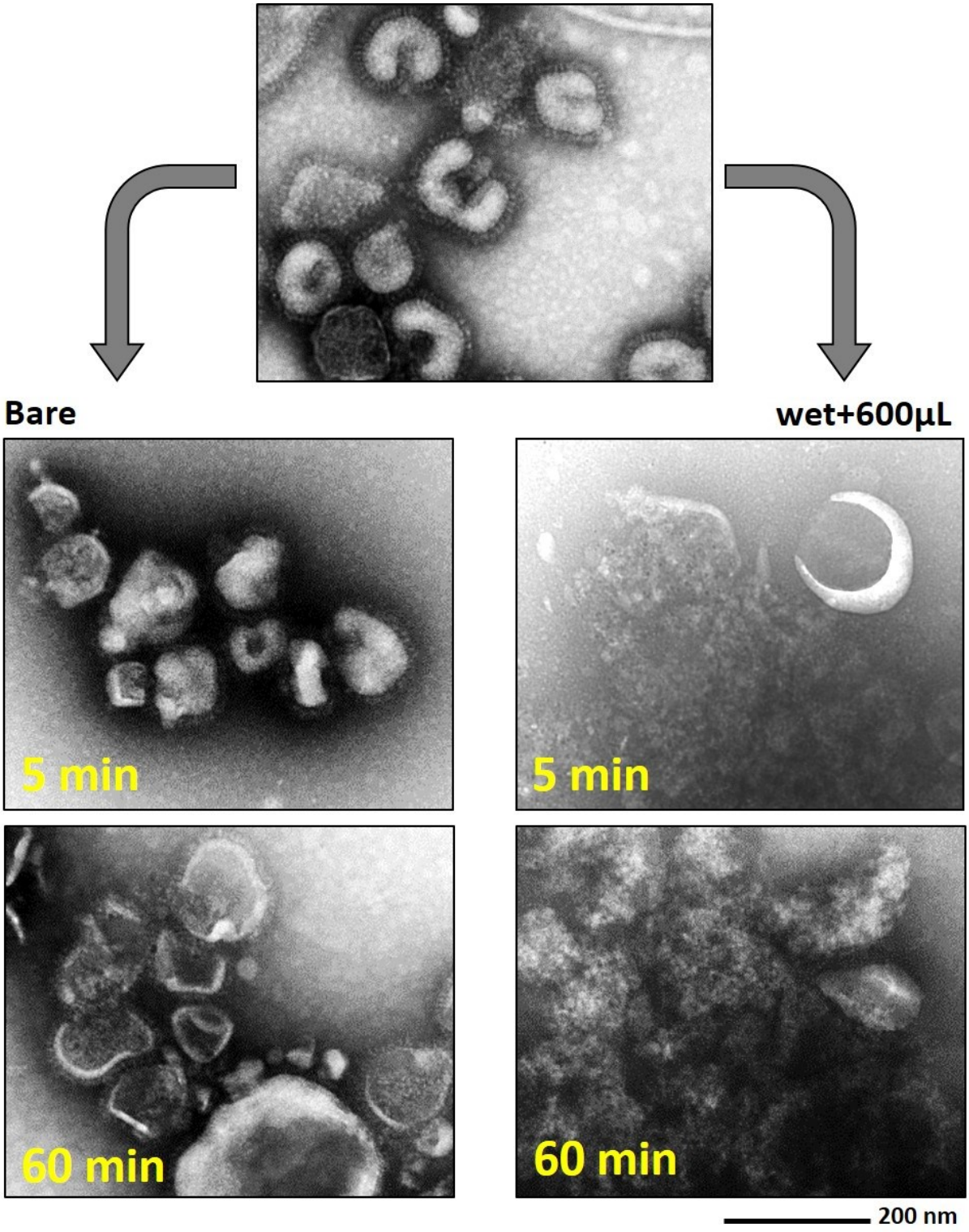

Figure 2.11 TEM images of CA/09 H1N1 influenza virus control (top) and viruses reconstituted from $Filter_{bare}$ (left) and $Filter_{wet+600\mu L}$ (right) after incubation for 5 and 60 min.

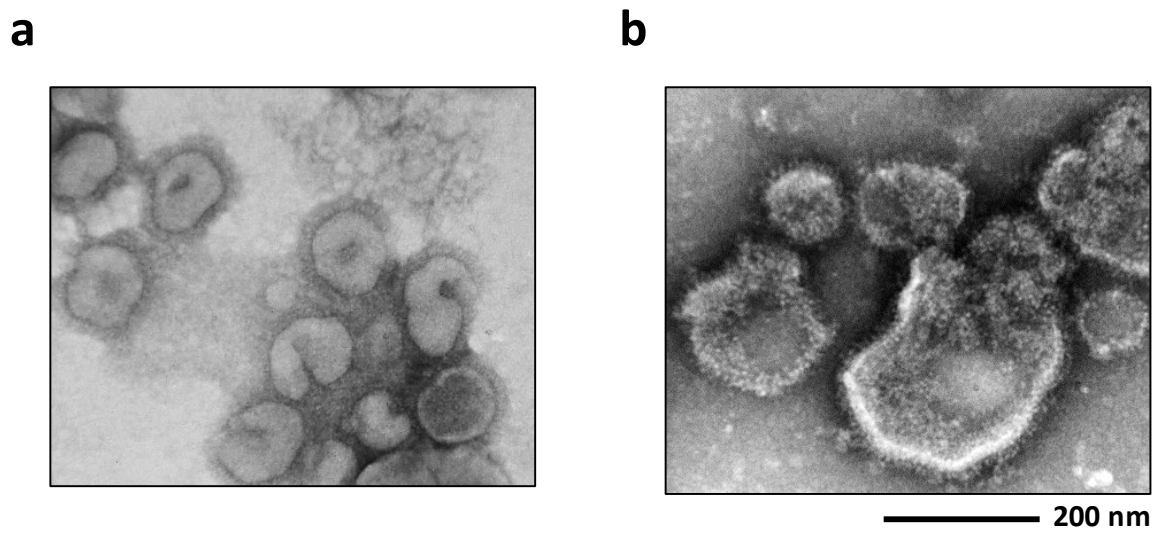

Figure 2.12 TEM images of CA/09 (H1N1) influenza virus incubated for 60 min in solution obtained from suspension of **(a)** $Filter_{bare}$ and **(b)** $Filter_{wet+600\mu L}$ showing the effects of high salt/surfactant concentration and osmotic pressure on virus morphology.

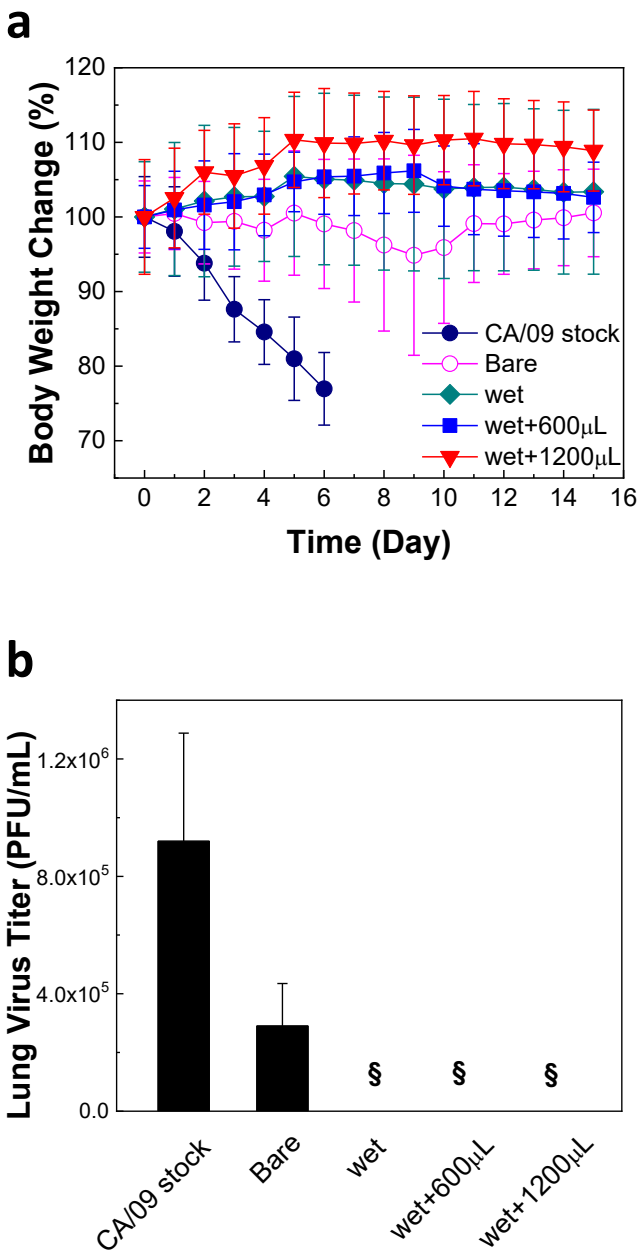

Figure 2.13 *In vivo* test of inactivation of virus adsorbed on salt-coated filters. **(a,b)** Body weight change of mice after infection with virus recovered from filters after incubation for 60 min (n = 6–12, mean ± SD) **(a)**, and lung virus titers (n = 6, mean ± SD) **(b)**. §: below detection limit.

2.3.4 Strain-nonspecific virus inactivation and effects of storage under harsh environmental conditions on salt coating stability

Broad-spectrum protection of salt-coated filters against multiple subtypes of viral aerosols was evaluated by investigating both lethal infectivity by penetrated virus *in vivo* and infectivity by virus collected on filters during filtration *in vitro* using A/Puerto Rico/08/1934 (PR/34 H1N1) and A/Vietnam/1203/2004 (VN/04 H5N1). Similarly to CA/09 H1N1, 100% of mice survived viral infection (PR/34 and VN/04) with no evidence of weight loss, due to higher filtration efficiency of salt-coated filter than that of bare filter (Figure 2.14a). In addition, as shown in Figure 2.14b, salt-coated polypropylene filters destroyed adsorbed influenza viruses irrespective of both subtypes and amount of coated salts. The stability of salt coating on polypropylene fibers was tested under harsh environmental conditions. Incubation at 37 °C and 70% RH for 1 day did not cause any significant difference in filtration efficiency (t-test, P = 0.718) (Figure 2.15a). As a result, all mice infected with dosage of penetrated virus through the filter stored at high temperature and RH displayed 100% survival with 7% of body weight loss (Figure 2.15b,c). Even after 15 days of incubation, salts remained to coat the polypropylene fibers (Figure 2.16), despite change in grain orientation due to recrystallization (Figure 2.17).

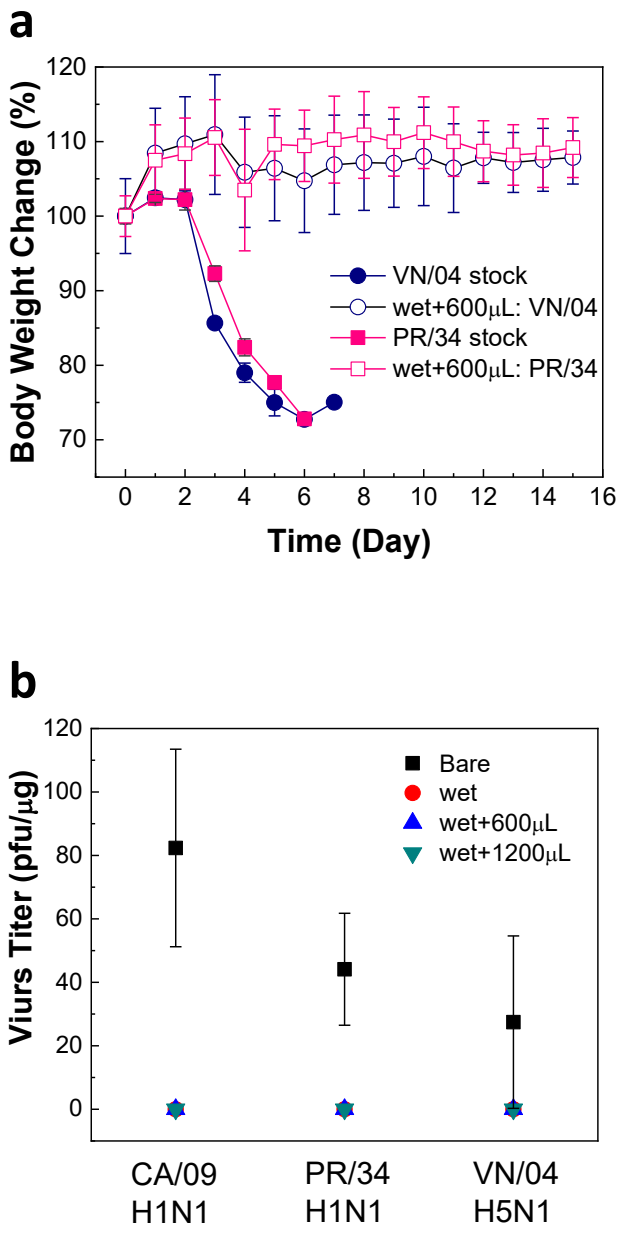

Figure 2.14 Strain-dependent performance of salt-coated filters. **(a)** Body weight change of mice infected with penetrated PR/34 H1N1 and VN/04 H5N1 viruses through $Filter_{wet+600\mu L}$ (n = 12, mean ± SD). **(b)** Virus titers of recovered viruses from bare and salt-coated filters (n = 4, mean ± SD; data for $Filter_{wet}$, $Filter_{wet+600\mu L}$ and $Filter_{wet+1200\mu L}$ are overlapped).

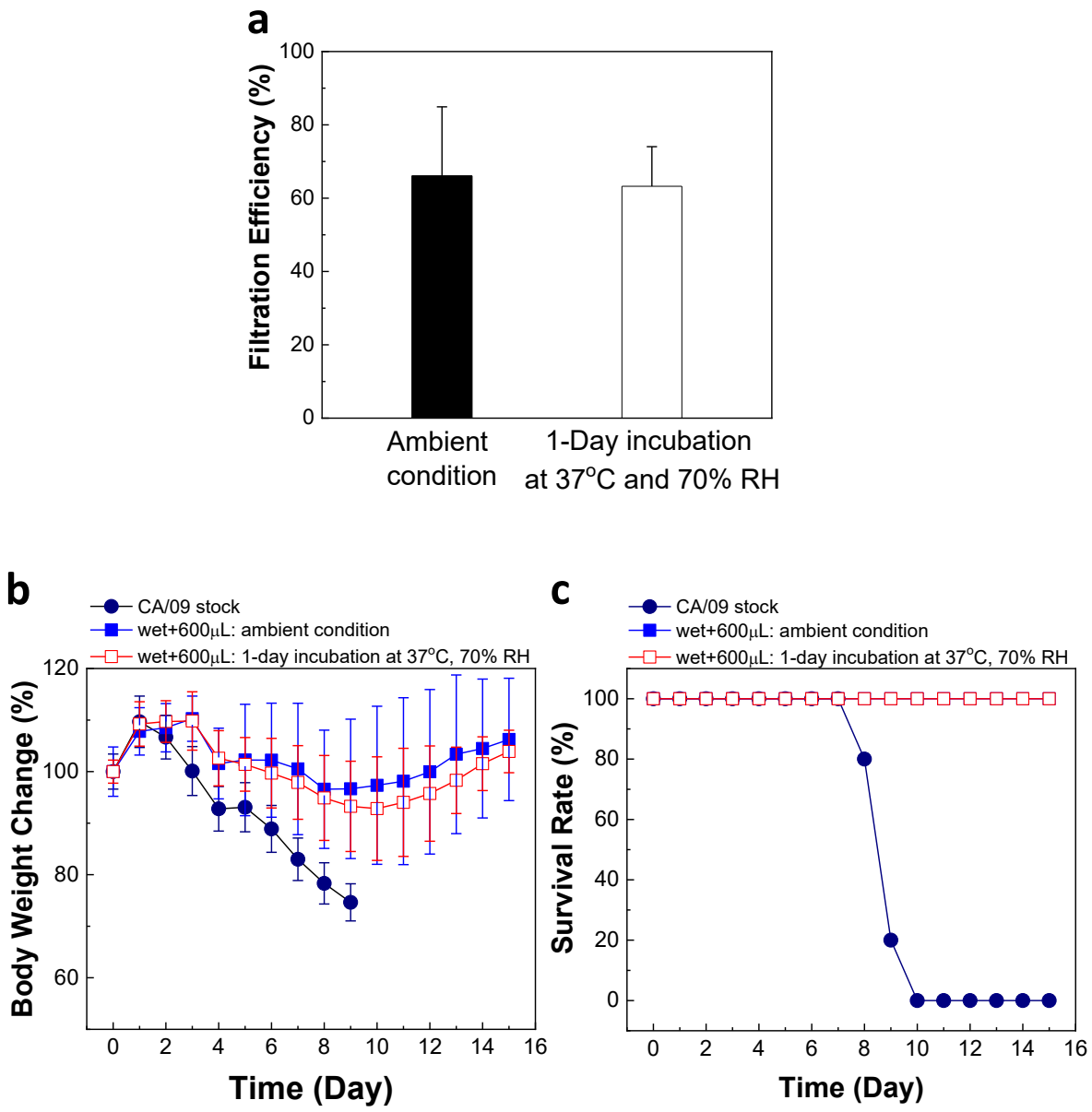

Figure 2.15 Environment-dependent performance of salt-coated filters. **(a)** Filtration efficiency of $Filter_{wet+600\mu L}$ before and after 1 day incubation at 37 °C and 70% RH (n = 12, mean ± SD). **(b,c)** Body weight change **(b)** and survival rate **(c)** of mice infected with dosage of penetrated virus through $Filter_{wet+600\mu L}$ before and after exposure to harsh environmental conditions (37 °C and 70% RH) for 1 day (filled square and open square overlap in (c); n = 6–12 for (b) and n = 6 for (c), mean ± SD).

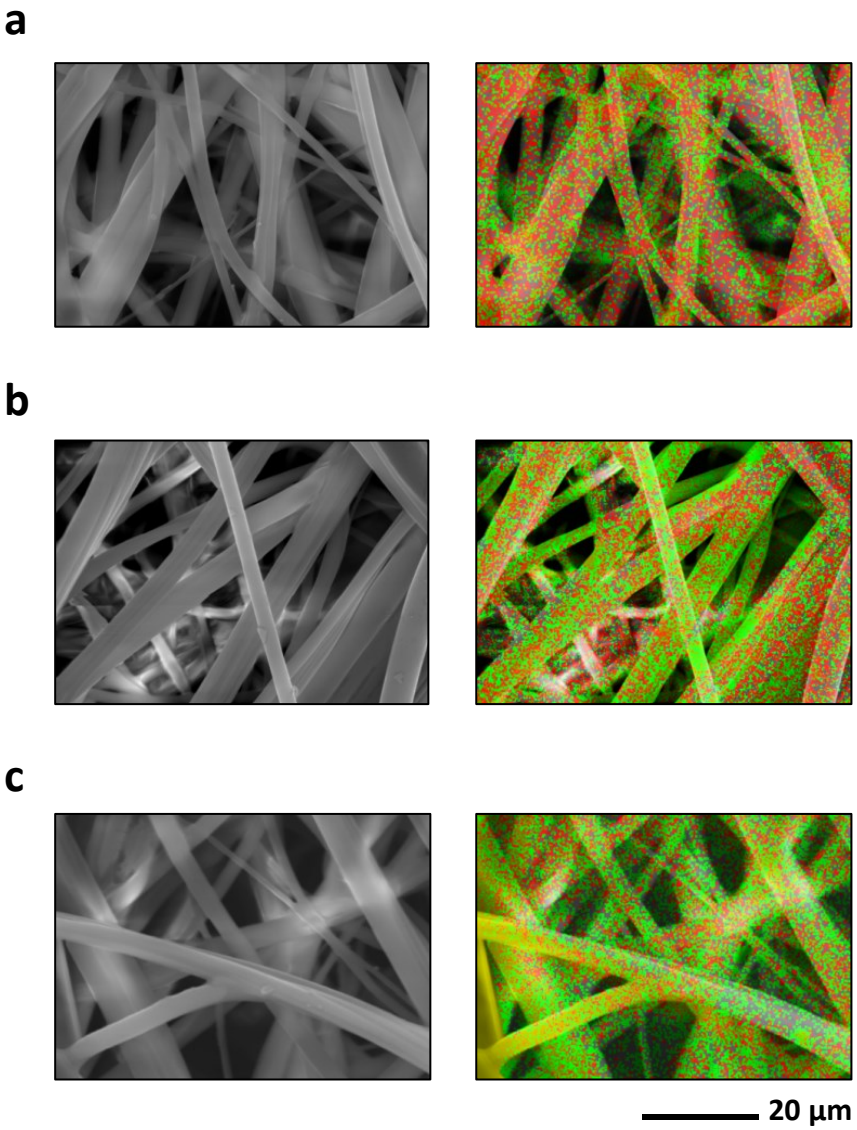

Figure 2.16 SEM images (left) and EDX mapping images (right; combination of Na (red) and Cl (green) mapping images) of NaCl-coated $Filter_{wet}$ **(a)**, $Filter_{wet+600\mu L}$ **(b)**, and $Filter_{wet+1200\mu L}$ **(c)** after incubation for 15 days at 37 °C and 70% RH.

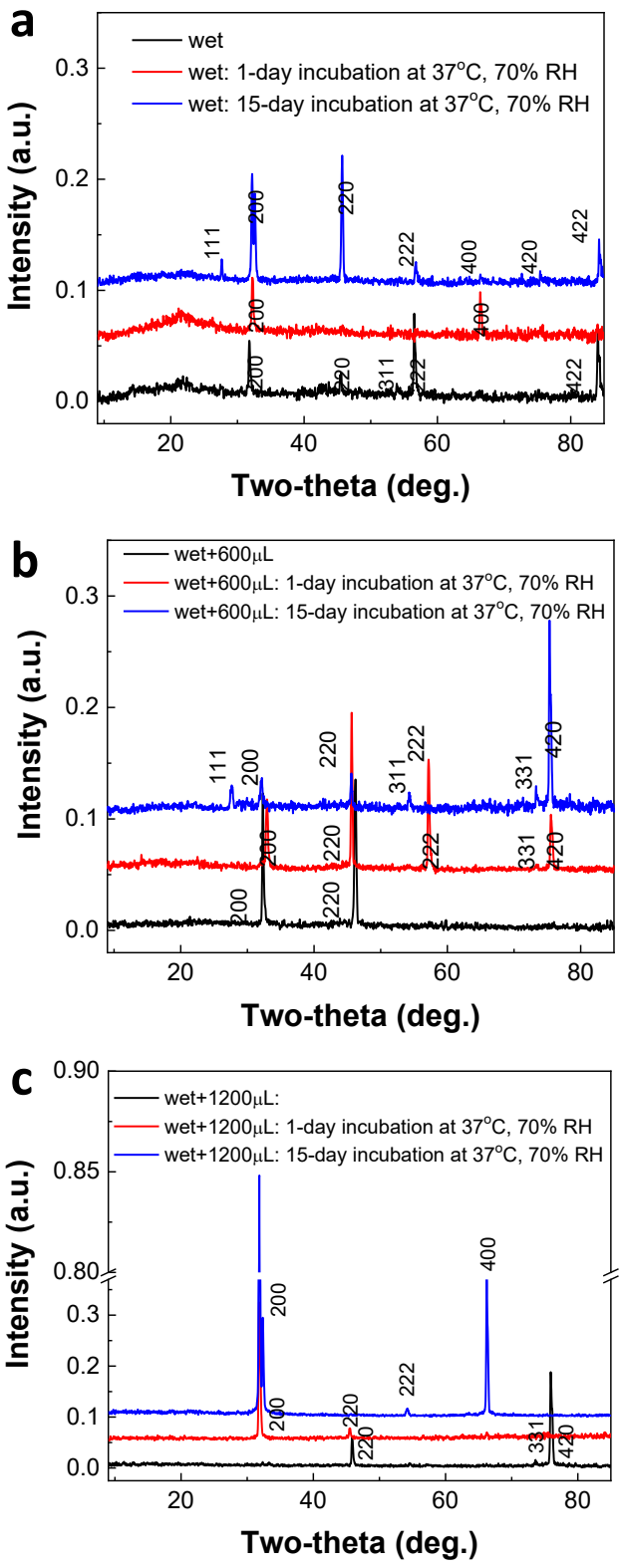

Figure 2.17 XRD spectra of Filter$_{wet}$ **(a)**, Filter$_{wet+600\mu L}$ **(b)**, and Filter$_{wet+1200\mu L}$ **(c)** before and after incubation at 37 °C, 70% for 1 day and 15 days.

2.4 Discussion and conclusion

Development of a universally applicable, low-cost, and efficient mechanism for pathogen negation is regarded as a major challenge in public health against general airborne biological threats. This led us to propose a new concept of personal/public preventive and control measures using salt recrystallization against pathogenic aerosols based on two hypotheses. The salt-coating can enhance adsorption of virus on the filter fibers and inactivate virus by the increase of osmotic pressure followed by the crystallization of salts. As shown in Figure 2.7, salt-coated filters exhibited significantly higher levels of filtration efficiency than bare filters. Notably, the bacterial filtration efficiency (BFE) reported by the mask manufacturer is 99%. The different value of filtration efficiency for bare filters obtained under our experimental conditions may be partially due to the use of aerosols with different biological origins. The FDA-recognized ASTM F2101 – 14/19 standard for evaluation of BFE exposes surgical masks to *Staphylococcus aureus* aerosols, by employing *S. aureus* ATCC 6538 [47,48], which has an average diameter of about 1 μm. In this study, filtration efficiency was calculated following exposure of bare and salt-coated filters to influenza virus, which exhibits a smaller diameter than that of *S. aureus* by one order of magnitude. Additionally, whereas during BFE evaluation all three layers of surgical masks are used, in this work filtration efficiency refers to mask filters (middle layer). It is worth noting that the conditions for BFE standard evaluation (such as flow rate and time of application of flow) do not coincide with the experimental procedure we used for measurement of the filtration efficiency, which may further contribute to the different result. The enhanced filtration efficiency of salt-coated filters against influenza virus aerosols as compared to bare filters can be explained by the observed wetting of aerosols, favoring greater adhesion to salt-coated filters. Furthermore, the significant improvement in filtration efficiency resulted in complete protection of mice

against lethal influenza aerosols, which demonstrates the high level of protection provided by salt-coated filters, outperforming currently used bare filters. Rapid loss of HA activity and viral infectivity on salt-coated filters can be explained by physical destruction of virus during recrystallization of the coated salts. When the salt-coated filter is exposed to virus aerosols, salt crystals below the aerosol droplet dissolve to increase osmotic pressure to virus. Due to evaporation, the salt concentration of the droplet significantly increases and reaches the solubility limit, leading to recrystallization of the salt. As a consequence, virus particles are exposed to increasing osmotic pressure during the drying process and are physically damaged by crystallization. As shown in Figure 2.13, the superior advantage of physically destroying the virus adsorbed to the salt-coated polypropylene filters through the natural salt crystallization process was further confirmed *in vivo*. According to previous reports, hyperosmotic stress (>541 mOsm) and crystallization induce membrane perturbation with irreversible deformation of the viral envelope and structural virus damage, respectively, resulting in infectivity loss of virus [171,174,176]. Therefore, our data support that the extensive level of infectivity loss associated with a salt recrystallization process caused by physical contact between virus aerosols and salt coating can be used in developing virus negation systems that are reusable without reprocessing. Similarly to CA/09 H1N1 aerosols, increased protection *in vivo* due to higher filtration efficiency of salt-coated filters compared to bare filters and inactivation of virus on salt-coated filters were observed following exposure to PR/34 H1N1 and VN/04 H5N1 (Figure 2.14). This suggests that salt-coated filters prevent virus penetration and destroy virus attached to the filter in a non-specific way. Furthermore, the performance of salt-coated filters was not degraded by storage at 37 °C and 70% RH, demonstrating that salt-recrystallization based filters can ensure protection even under harsh environmental conditions. Notably, for demonstration of the

concept of salt-recrystallization based pathogen inactivation system, NaCl salt was used, which has a critical RH of 75% at 30 °C [177]. However, salts with higher critical RH can be easily used, such as potassium chloride and potassium sulfate, which have critical RH of 84% and 96% at 30 °C, respectively [177] (see Chapter 3). This suggests that salt-coated filters may be developed for specific environmental conditions.

In conclusion, we demonstrated that the developed salt-recrystallization based filtration system provides high filtration efficiency and successfully inactivates multiple subtypes of adsorbed viruses. Moreover, we have shown that stability of the salt coating is not compromised by high temperature and humidity, which suggests safe use and long-term storage/reuse at such environmental conditions. Although our tests are based on exposure to different types of influenza virus, the significance of these results for personal and public protective measures may be generally extended to enveloped respiratory viruses where infection and transmission can occur by aerosol, and encouraged further development of the technology (see Chapter 3). Our salt-coated filter unit can promise the development of a long-term stable, versatile airborne pathogen negation system, without safety concerns. In fact, the destruction mechanism of the pathogens solely depends on the simple, yet robust naturally occurring salt recrystallization process, combining the destabilizing effects of salt crystal growth and concentration increase during drying of aerosols. This idea can be easily applied to a wide range of existing technologies to obtain low-cost, universal personal and public means of protection against airborne pathogens, such as masks and air filters in hospitals. Therefore, we believe that the salt-recrystallization based pathogen inactivation system can contribute to global health by providing a more reliable means of preventing transmission and infection of pandemic and epidemic diseases.

3 Salt functionalization system against airborne pathogens

3.1 Salt functionalization of inert membranes into high-performing filters

Respiratory protection is key in infection prevention of airborne diseases. Conventional technologies have several drawbacks (i.e., cross-infection risk, filtration efficiency improvements limited by difficulty in breathing, and no safe reusability), which have yet to be addressed in a single device. Here, we report the development of a filter overcoming the major technical challenges of respiratory protective devices. Large-pore membranes, offering high breathability but low pathogen capture, were functionalized to have a uniform salt layer on the fibers. The membranes functionalized with different salt types achieved high filtration efficiency as opposed to the bare membrane, while maintaining high breathability. The salt-functionalized filters quickly killed Gram-positive and Gram-negative bacteria as well as virus aerosols by causing structural damage due to salt recrystallization. The salt coatings retained the pathogen inactivation capability at harsh environmental conditions. Combination of these properties in one filter will lead to the production of an effective device, comprehensibly mitigating infection transmission globally.

3.1.1 Background

Airborne pathogens, including bacteria and viruses, transmit in the environment in the form of droplets (>5 μm) or aerosols (<5 μm) [2]. Due to long travelling distance and respirability of aerosols, airborne transmission can occur very easily [7]. As such, respiratory protection measures are essential first lines of defense in health care settings, congregate settings (e.g., correctional facilities, military barracks, homeless shelters, refugee camps, dormitories, and nursing homes), households (including family members and caregivers), and in the event of pandemic or epidemic outbreaks. As the WHO and scientific community highlight the urgency in stopping infectious diseases and preparing for the next disease outbreaks [178], and new pandemic strains emerge [179], development of effective, readily available infection control measures is recognized as a primary challenge in health care.

Specifically, in health care facilities, bacteria including *Klebsiella pneumoniae (K. pneumoniae), Staphylococcus aureus* (*S. aureus*), *Pseudomonas aeruginosa (P. aeruginosa), Streptococcus pyogenes* (*S. pyogenes*) and *Escherichia coli (E. coli)* are the major causes of nosocomial infections [29,180]. Bacteria can transmit infections through the air in locations such as operating theatres, corridors, waste containers as well as intensive care, burn and orthopedic units [27-29,181,182]. Nosocomial *K. pneumoniae* infections have mortality rates as high as 50%; additionally, the WHO has reported global resistance to third-generation cephalosporins and carbapenem in 30–60% and up to 50% of cases, respectively [22]. Methicillin-resistant *S. aureus* (MRSA), also transmissible through the air [21], constitutes another major pathogen in nosocomial infections, causing 20% to above 80% of *S. aureus* nosocomial infections worldwide [22].

The most commonly used respiratory protective device in health care is the N95 respirator, which is designed to capture aerosols. Surgical masks, commonly used to block large droplets during surgeries, were historically utilized against bioaerosols. Surgical masks have seen a continued use for this purpose in the general public during more recent outbreaks, in spite of the improper application [14,74,80-82]. This is due to their high availability, affordability and comfort. Although respirators and masks play a critical role in the protection against bioaerosols, they are limited by four major technical issues of the filters: (i) cross-infection, (ii) filtration efficiency, (iii) breathability, and (iv) recyclability [183]. When respirators/masks capture bioaerosols, they become contaminated, since pathogens survive on the surface of the filters. This presents a threat to the wearer and people that they come in contact with. As the devices can easily become a source of infection, commercial respirators and masks are limited to a single use. Additionally, in the traditional technologies, it is well-known that increasing the filtration efficiency leads to filters that cause higher pressure drop across the masks, with consequent difficulty in breathing. Some efforts have been directed towards production of filters that can overcome the burden of decreased breathability [143,144]. However, these methods cannot address the risks arising from the survival of pathogens captured on the filters.

We envisioned the development of a technology that could solve all major technical challenges simultaneously, which cannot be addressed by conventional respiratory protective devices. The mechanism we developed consists of functionalizing the polypropylene fibers of large-pore (~60 μm) membranes with salt. Large-pore membranes have high breathability compared to commercial respirators and masks, but no pathogen filtration activity. We hypothesized that the salt coating would: (i) increase the filtration efficiency of the breathable membranes, turning them into an active filtration unit, and (ii) inactivate pathogens. The latter

hypothesis was based on our previous report that coating filters with sodium chloride salt kills multiple strains of influenza virus [184] (Chapter 2).

In this work, we demonstrate that salt functionalization greatly increases the filtration efficiency of large-pore membranes, while at the same time exhibiting no significant increase in pressure drop. The proposed filtration mechanism is non-mechanical in nature, which is evidenced by the insensitivity of filtration efficiency with respect to increasing layer numbers and the high filtration efficiency of the top layer (the first layer interacting with aerosols) of salt-functionalized filters even with presence of large-pore fiber mesh. Additionally, the salt recrystallization upon exposure of the salt-functionalized filters to infectious aerosols caused the physical damage of the bacteria independent of strain (*K. pneumoniae,* MRSA*, P. aeruginosa, S. pyogenes* and *E. coli*) and influenza virus, leading to their inactivation. As such, we report a diverse respiratory protection system that is manufactured without extensive engineering efforts, and achieves quick universal pathogen inactivation, high filtration efficiency, high breathability, and safe recyclability, all in one platform.

3.1.2 Methods

3.1.2.1 Filter samples preparation

Three-ply surgical masks (Fisherbrand Facemasks; Fisher Scientific, Pittsburgh, PA, USA) were used to obtain the large-pore membranes. The elastic ear loops and metal nose clip were cut and discarded. The three membranes of the mask were separated; the middle membrane (filtration unit) and outer protective membrane were discarded; the innermost polypropylene membrane (typically used against the wearer's face to offer mechanical protection to the middle filter) was used to produce the salt filter samples in the study. As the innermost mask membrane has higher porosity than the middle filter, it was selected for the study; the performance of the salt filter samples was controlled by varying the thickness of the samples by stacking different numbers of layers. Circular samples of the mask innermost large-pore membrane were cut with 3-cm radius (bare membranes, labelled Bare×# where # is the number of stacked layers). The membranes were coated with different salt types to obtain the salt-functionalized filters: sodium chloride (NaCl; Sigma Aldrich, St. Louis, MO, USA), potassium sulfate (K_2SO_4; Sigma Aldrich), and potassium chloride (KCl; Sigma Aldrich). To prepare the coating solutions, the salts were dissolved in filtered (0.22 μm pore size; Corning, Tewksbury, MA, USA) DI water under stirring at 400 rpm and 90 °C for NaCl, and 400 rpm and room temperature (RT) for K_2SO_4 and KCl. The final salt concentrations were 29.03 w/v%, 9.72 w/v% and 26.31 w/v% for NaCl, K_2SO_4 and KCl, respectively. Surfactant (Tween 20, Fisher Scientific) was added at 1 v/v% (5-min stirring at RT) in all salt coating solutions. The salt filters were prepared by first pre-wetting the membrane samples with approximately 350 μL of coating solution of a given salt type; complete wetting was obtained by gently stroking the membrane samples with tweezers while in the coating solution, to remove any dry areas (pre-wet membranes). The amount of

coated salt was controlled by varying the volume of coating solution in which the samples were dried: the specific volume (0, 300, 600, and 1200 µL) of coating solution was added in 60 × 15 mm petri dishes (Fisher Scientific), and then the pre-wet membrane samples were deposited on the petri dishes. More layers of pre-wet membrane samples were added on top, based on the desired total number of layers (1, 3 and 5), to control thickness. Gentle tweezer strokes were used to lay the layers flat and remove any air bubbles at the interfaces layer-layer and layer-petri dish surface. The salt filter samples were dried overnight in an incubator (Thermolyne 42000; Thermolyne, Dubuque, IA, USA) at 45 °C. The salt-coated filter samples thus obtained were labelled as Salt×#$_{vol}$, where Salt is the salt type (NaCl, K_2SO_4, or KCl), # is the number of stacked layers (1, 3 or 5), and $_{vol}$ is the volume of coating solution in which the filters were dried (0, 300, 600, or 1200 µL).

3.1.2.2 Bacteria cultures

Klebsiella pneumoniae (ATCC BAA-1705) was streaked on tryptone soya agar (TSA; Oxoid, Nepean, Canada) plates and incubated at 37 °C for 24 h. Single colonies were inoculated in tryptic soy broth (TSB; BD, Franklin Lakes, NJ, USA) at 37 °C and 200 rpm for 24 h. The *K. pneumoniae* suspension was transferred into fresh TSB 1:500 and incubated at 37 °C and 200 rpm until it entered the exponential growth phase. The *K. pneumoniae* suspension was stored at –80 °C in 20% glycerol (Fisher Scientific). For experiments, *K. pneumoniae* from frozen state was grown at 37 °C and 200 rpm with Mueller Hinton (MH) broth (BD) at 1:500 to OD_{600} of 0.8.

Methicillin-resistant *S. aureus* (ATCC 33593) and *Escherichia coli* (ATCC 25922) were streaked on MH II agar (BD) plates, *Pseudomonas aeruginosa* (ATCC 10145) was streaked on TSA plates, and *Streptococcus pyogenes* (ATCC 19615) was streaked on brain heart infusion (BHI; BD) agar plates. The plates were incubated at 37 °C overnight. Single colonies were

inoculated in MH broth, TSB or BHI medium at 37 °C and 200 rpm overnight. The bacteria suspensions were transferred into fresh media 1:100 and grown at 37 °C and 200 rpm for 4 h. All bacteria cultures were washed 3 times in phosphate buffered saline (PBS) before experiments.

3.1.2.3 Influenza virus and cells preparation

Influenza virus A/Puerto Rico/8/34 (PR/34, H1N1) was grown in 11-day old embryonated chicken eggs and purified from allantoic fluid by cell strainer (70 μm), low-speed centrifugation (2,800 rpm, 4 °C, 15 min), and high-speed centrifugation (30,000 rpm, 4 °C, 1 h). Madin-Darby Canine Kidney (MDCK) cells were grown and maintained in Dulbecco's modified Eagle's medium (DMEM) at 37 °C and 5% CO_2.

3.1.2.4 Filtration efficiency tests

Filtration efficiency tests were designed by adapting the ASTM F2101 – 14/19 standard tests [47,48], recommended by the FDA for evaluation of the bacterial filtration efficiency of surgical masks [39] (see Section 1.2.2). The filtration efficiency test apparatus (Figure 3.1) includes a filter holder which has a top circular aperture to tightly accommodate the nebulizer unit (Aeroneb Lab Nebulizer System; Aerogen, Galway, Ireland), an air inlet open to the atmosphere above the filter samples, and an outlet below the filter samples. The filter samples are clamped in place below the nebulizer, with an area of 4.9 cm^2 exposed to the air flow. For bare membranes, the multiple layers were glued together (at the edge area not exposed to the air flow), to facilitate handling during loading/unloading into the filter holder; salt filters (NaCl, K_2SO_4, KCl) had a thin layer of silicone (Dowsil 732 Multi-Purpose Sealant Silicone; Dow, Midland, MI, USA) at the edge area not exposed to the air flow, to secure sealing when the filters are clamped in place. A vacuum pump (WOB-L Pump 2546; Welch, Niles, IL, USA) was used to generate the air flow and a flowmeter with needle valve (Omega FLD1201; Omega,

Norwalk, CT, USA) was used to control the air flow rate; a bleach trap and a safety filter were placed between the filter holder and the pump.

After loading the filter samples, 60 μL of *K. pneumoniae* DI water suspension (OD_{600} = 10) were added into the nebulizer unit, and the filter samples were exposed to the bacteria aerosols (diameter = 2.5–4 μm) for 30 sec, under an air flow rate of 15 L/min. The air flow was maintained for an additional 1 min following aerosol generation, and then the filter samples were unloaded. Notably, in the case of tests run at air flow rate of 0 L/min, no air flow was generated, and 20 μL of *K. pneumoniae* suspension were aerosolized for 15 sec at 20 sec intervals for three times (total aerosolized volume = 60 μL) to avoid aerosol condensation.

The bacteria were reconstituted from the filter samples as follows. The glue (bare membranes) or the silicone (salt-coated filters) at the sample edge was cut and discarded, and the filter samples were incubated in PBS for 30 sec–1 min. After vortexing, the filters were transferred to a new tube and centrifuged (6,000 rpm, RT, 1 min) to collect any remaining bacteria. The recovered bacteria were centrifuged (14,000 rpm, 15 min, 4 °C) to discard any salt/surfactant dissolved from the filters into the suspension, and then resuspended in 1.2 mL of fresh PBS, eliminating any interference with assays.

To collect all the bacteria in the exposure aerosols upstream (C_t), 60 μL of *K. pneumoniae* suspension were aerosolized without membrane/filter samples and the bacteria concentration was measured. To do this, bacterial aerosols were generated into a 15-mL centrifuge tube, containing 1.5 mL of PBS for 30 sec, followed by 1-min aerosolization of DI water to avoid drying of the bacteria condensed against the tube wall. After vortexing, the bacteria were centrifuged (14,000 rpm, 15 min, 4 °C) and resuspended in 1.2 mL of fresh PBS.

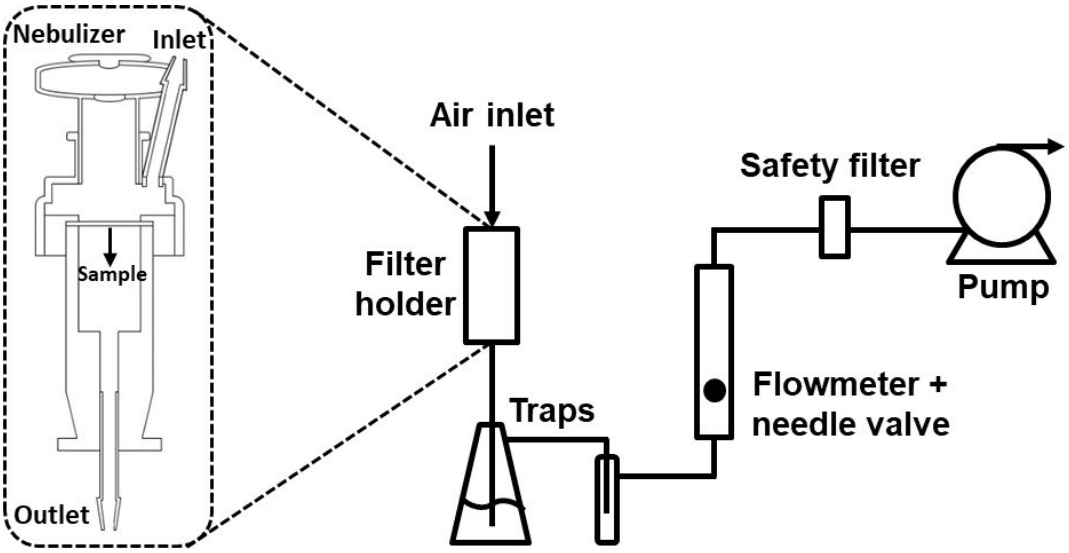

Figure 3.1 Process flow diagram of the filtration efficiency experiment.

The filtration efficiency η_t of each sample was calculated as:

$$\eta_t = \frac{C_f}{C_t} \times 100 \qquad (3.1)$$

where C_f is the amount of bacteria recovered from the filter samples. The amount of bacteria was determined as the protein concentration measured with bicinchoninic acid assay (Micro BCA protein assay kit; Thermo Fischer Scientific, Waltham, IL, USA), with bovine serum albumin (BSA) as a standard.

3.1.2.5 Pressure drop tests

Pressure drop tests were designed by adapting the MIL-M-36945C standard test [49], recommended by the FDA for evaluation of the breathability of surgical masks [39] (see Section 1.2.2). The pressure drop test apparatus (Figure 3.2) includes a filter holder which has (i) an inlet above the filter samples, connected to the flowmeter (model 150 mm Correlated Flowmeter; Cole-Parmer, Vernon Hills, IL, USA), which in turn has an air inlet open to the atmosphere, and (ii) an outlet below the filter samples, connected to the needle valve used to control the air flow

rate and the vacuum pump (WOB-L Pump 2522, Welch) used to generate the air flow. A differential pressure gauge (Traceable Manometer Pressure/Vacuum Gauge model CON3460, Fisher Scientific) is connected in parallel to the filter holder to measure the pressure drop across it. Salt-coated filters (NaCl, K_2SO_4, KCl) had a thin layer of silicone at the edge area not exposed to the air flow, to secure sealing when the filters are clamped in place.

Differential pressure measurements were conducted at an air flow rate of 8 L/min (breathing condition [185], recommended by the standard), both with (P_1) and without (P_0) loaded filter samples, and the final pressure drop ΔP was calculated as:

$$\Delta P = \frac{P_1 - P_0}{A} \qquad (3.2)$$

where A is the area of filter sample exposed to the air flow (6.6 cm^2).

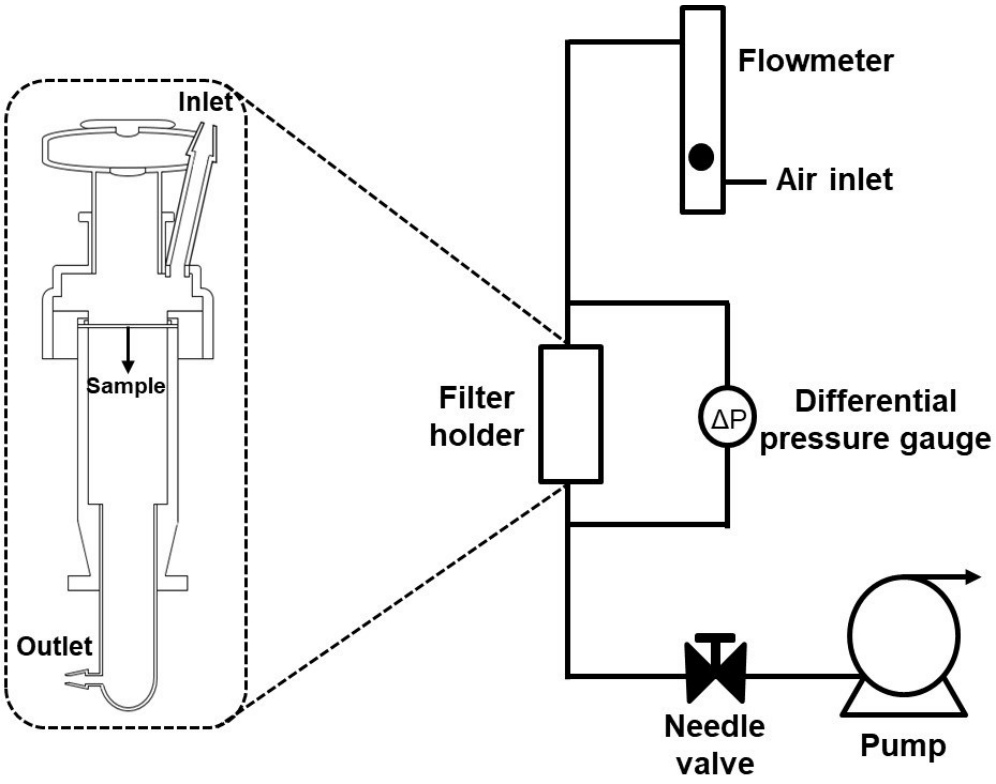

Figure 3.2 Process flow diagram of the pressure drop experiment.

To quantify the overall filter performance, the quality factors (*QF*) of the bare membranes and salt-coated filters were calculated at 15 L/min. The *QF* is defined as:

$$QF = -\frac{\ln(1-F)}{P_1 - P_0} \quad (3.3)$$

where *F* is the fraction of captured bacteria ($F = C_f / C_i$) [2].

3.1.2.6 Test of bacteria stability change on filters *in vitro*

To measure the time-dependent inactivation, aerosols of multiple bacteria were exposed to the bare membranes (3 layers) and salt-functionalized filters (3 layers; NaCl, K_2SO_4, KCl). After washing, the bacteria were resuspended in DI water to an OD_{600} of 12.5 (*K. pneumoniae, P. aeruginosa* and *E. coli*) or 100 (MRSA and *S. pyogenes*). The nebulizer unit was placed on top of the filter samples (radius = 1.2 cm), which were loaded on a porous support, and 20 μL of bacteria suspension were aerosolized for 30 sec (Figure 3.3). The bacteria aerosols were incubated on top of the filter samples at ambient condition for a specific time point (3, 5, 15 or 30 min), and then the bacteria were reconstituted from the filters as described above. Finally, after removing the supernatant containing salt/surfactant, the bacteria were resuspended in 100 μL of fresh PBS. To collect all the bacteria in the exposure aerosols (at 0 min incubation on the filters), the *K. pneumoniae* suspension was aerosolized without membrane/filter samples. To do this, bacterial aerosols were generated into a 15-mL centrifuge tube, containing 1.5 mL of PBS for 30 sec, followed by 1-min aerosolization of DI water. After vortexing, the bacteria were centrifuged (14,000 rpm, 15 min, 4 °C) and resuspended in 100 μL of fresh PBS.

To investigate the bacteria survival, colony forming unit (CFU) measurements were obtained by incubating 5 μL of 10× dilutions onto MH II agar plates (*K. pneumoniae,* MRSA and *E. coli*), TSA plates (*P. aeruginosa*) or BHI agar plates (*S. pyogenes*) at 37 °C overnight. CFU

were divided by the amount of bacteria recovered from the filters (determined as protein concentration measured by BCA assay with BSA standard). The measurements were expressed as relative to the CFU of bacteria contained in the exposure aerosols, i.e. at 0 min incubation on the filters (Relative CFU = CFU_{sample} / $CFU_{0\ min}$). To determine the integrity of the bacteria membrane, green fluorescence (bacteria with intact membrane) was measured with LIVE/DEAD *Bac*Light Bacterial Viability Kit (Thermo Fischer Scientific) following the manufacturer's protocol. Green fluorescence was expressed per amount of bacteria recovered from the filters.

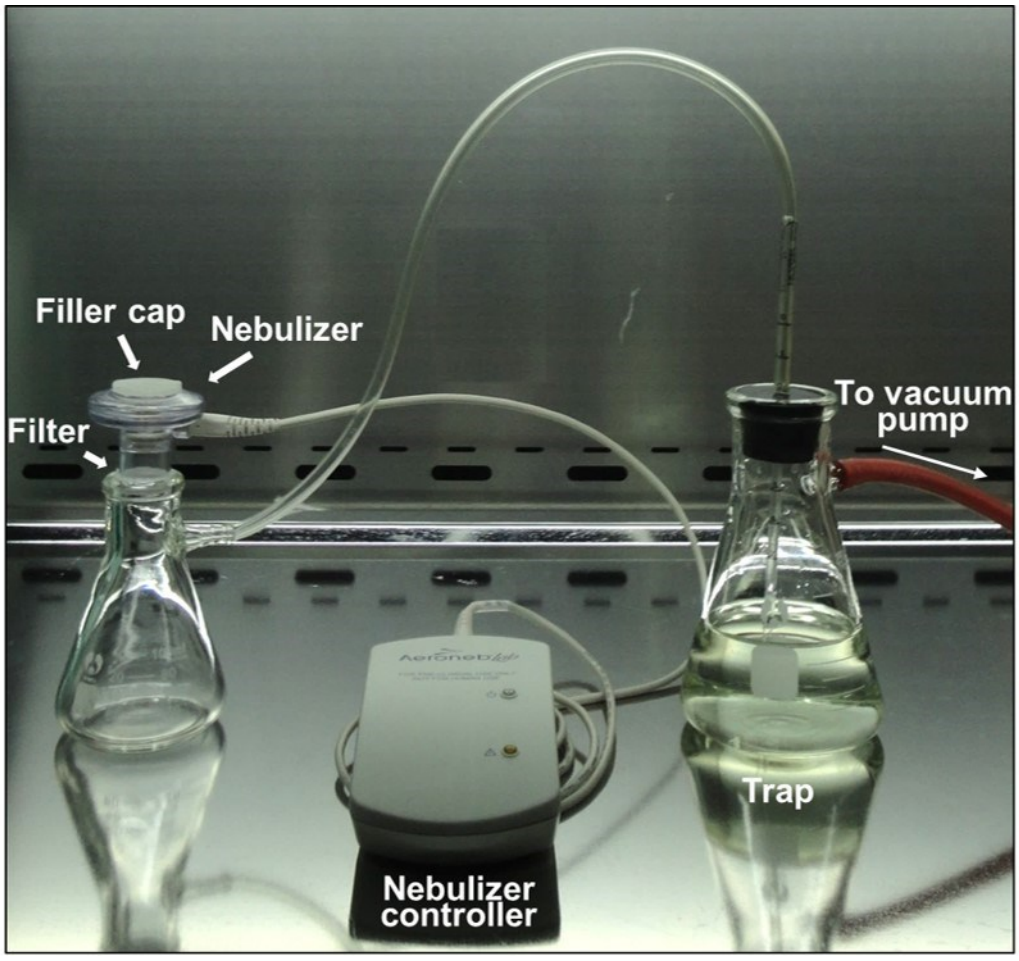

Figure 3.3 Experimental set-up for aerosol exposure.

3.1.2.7 Test of bacteria stability change on filters *in vivo*

To confirm the findings on bacteria inactivation *in vivo*, 20 μL of *K. pneumoniae* DI water suspension (OD_{600} = 10.5) were aerosolized on the filter samples and incubated for 5, 15 and 30 min. A lethal dose of bacteria reconstituted from the filters was used to infect 8 7-week old BALB/c mice (KOATECH, Pyeongtaek, Republic of Korea) per group by the intranasal route. As negative controls, two mice groups were infected with the bacteria before and after aerosolization, respectively, to consider infectivity change due to the aerosolization process. The body weight change was measured daily for 10 days. The mice were euthanized if the body weight reached below 75% of the starting weight. Kyung Hee University (KHU) Institutional Animal Care and Use Committee (IACUC), which operates under National Veterinary Research and Quarantine Service (NVRQS) and animal welfare law and regulations of the WOAH-OIE (World organization for animal health), provided approval for all animal protocols (KHUASP(SE)-18-085). The approved protocols and guidelines of KHU IACUC were followed for all animal experiments and husbandry related to this study. At day 3 post-infection, 4 mice per group were sacrificed to collect the lung tissues. The lung supernatants from the homogenizing process was used to measure OD_{600} (NanoDrop One C; Thermo Fisher Scientific). For body weight measurements n = 8 before sacrifice and n = 4 after sacrifice, for lung tissue assays n = 4; off-trend measurements were not considered, and n is reported for each figure.

3.1.2.8 Test of viral stability change on filters

To measure the time-dependent inactivation, aerosols of influenza virus were exposed to the bare membranes (Bare×3) and salt-functionalized filters ($NaCl \times 3_{600}$, $K_2SO_4 \times 3_{600}$, $KCl \times 3_{600}$). The virus was resuspended in DI water; the viral aerosols were exposed to the samples for 3, 5, 15, 30 and 60 min, and reconstituted, as described above. After removing the

supernatant containing salt/surfactant (by centrifugation at 14,800 rpm and 4 °C for 15 min), the virus was resuspended in fresh PBS. To collect all the virus in the exposure aerosols (at 0 min incubation on the filters), 20 μL of virus suspension were aerosolized without membrane/filter samples. To do this, viral aerosols were generated into a 15-mL centrifuge tube, containing 1.5 mL of PBS for 30 sec, followed by 1-min aerosolization of DI water. After vortexing, the virus was centrifuged (14,800 rpm, 15 min, 4 °C) and resuspended in fresh PBS. Stability of virus was characterized by measuring hemagglutinin activity (HA) with chicken red blood cells and virus titers on confluent MDCK monolayers. The plaque forming units (PFU) were divided by the amount of virus used to infect the cells (determined as protein concentration measured by BCA assay with BSA standard). The HA titer and PFU measurements were expressed as relative to the measurements at 0 min incubation on the filters.

To test the effect of osmotic pressure, the filters (NaCl, K_2SO_4, KCl) and Bare membranes as a control were dissolved in PBS in a 15-mL tube. The virus suspension (20 μL) was aerosolized into the tube for 30 sec, followed by 1-min aerosolization of DI water and vortexing, at a time. The virus was incubated in the dissolved filter solutions for 60 min, and then centrifuged (14,800 rpm, 15 min, 4 °C) to interrupt the incubation and resuspend in fresh PBS. HA and virus titers were conducted as described above.

3.1.2.9 Performance of salt-functionalized filters at different environmental conditions

To investigate the environmental stability of the salt coatings on the filters, bare membranes (Bare×3) and salt-functionalized filters (NaCl×3_{600}, K2SO4×3_{600}, KCl×3_{600}) were stored in an environmental chamber (Memmert HPP260; Memmert, Buchenbach, Germany) at 37 °C, and 70%, 80% and 90% RH. The bacteria stability change on filters *in vitro* was tested

against *K. pneumoniae* aerosols at day 1, 3 and 5 of storage, by measuring the CFU after 30 min incubation of the bacteria on the filters, as described above.

3.1.2.10 Electron microscopy analysis

Scanning electron microscopy (SEM) and energy dispersive X-ray (EDX) analysis of the salt-coated filters (NaCl, K_2SO_4, KCl) was conducted to observe the morphology and distribution of the salt coatings. SEM analysis (secondary electron mode at 20 kV, Hitachi S-3000N; Hitachi, Toronto, Canada) was performed on the salt filters coated with a gold layer (thickness = 10 nm), and an EDX detector (Oxford Instruments, Concord, MA, USA) was used for the EDX analysis. The pore size of bare membranes was determined from SEM images.

To observe the bacteria structural changes, transmission electron microscopy (TEM) analysis (200 kV, JEOL JEM 2100; JEOL, Peabody, MA, USA) was performed on *K. pneumoniae* reconstituted after 5 and 30-min incubation on the bare membranes and salt-functionalized filters, as described above. For this purpose, the reconstituted bacteria suspended in PBS were deposited on copper grids (Electron Microscopy Sciences, Hatfield, PA, USA) and negatively stained with tungsten using a solution of 1.5 w/v% phosphotungstic acid hydrate at pH = 7.0 (Sigma Aldrich).

3.1.2.11 Statistical analysis

Pearson correlation coefficients basis of correlations was conducted between levels of salt weight and volume of salt coating solution. The statistical analysis was performed by using one-way ANOVA, two-way ANOVA, General Linear Model, t-test, and chi-square analysis for multiple comparisons. All statistical analyses were performed using SPSS ver. 21 (IBM, Armonk, NY, USA) and Minitab (Minitab, State College, PA). The significance of multiple comparisons was considered by *P* value; *P* value of less than 0.05 was considered significant.

3.1.3 Results and discussion

3.1.3.1 Production and characterization of salt-coated filters

Development of environment-resistant filters is key to their universal application. Thus, when designing the salt-functionalized filters, fine tuning of the properties of the mask to satisfy different temperature/humidity conditions during use and storage was considered. To this end, safe and inexpensive salt types with different critical RH were selected. At a given temperature, if a salt is exposed to an RH above its critical RH, it will take up water from the atmosphere. NaCl, KCl and K_2SO_4 have critical RH of 74.7%, 81.2% and 95.7% at 40 ℃, respectively [177], and were investigated in this study. The salt coatings were applied onto the polypropylene microfibers of large-pore membranes, which were not designed to capture aerosols. The membranes (bare membranes) were dried in different volumes of coating solution (V_{salt}; NaCl, K_2SO_4 or KCl), to produce filters coated with different amounts of salts per unit area (W_{salt}). The linear relationship between W_{salt} and V_{salt} for each salt type at different thicknesses can be found in Figure 3.4 (Pearson test, *P* values on graphs).

By stacking different numbers of membrane layers during drying, the overall thickness was varied. This allows for control over the final design of the salt-functionalized filters based on application needs. The formation of NaCl, K_2SO_4 or KCl salt coatings was analyzed by scanning electron microscopy (SEM) and energy dispersive X-ray (EDX) mapping. Homogenous coating formation on the surface of the fibers and throughout the cross section of multi-layer filters was observed (Figure 3.5). These results show the successful fabrication of filters uniformly functionalized with NaCl, K_2SO_4 or KCl salts at controlled thicknesses.

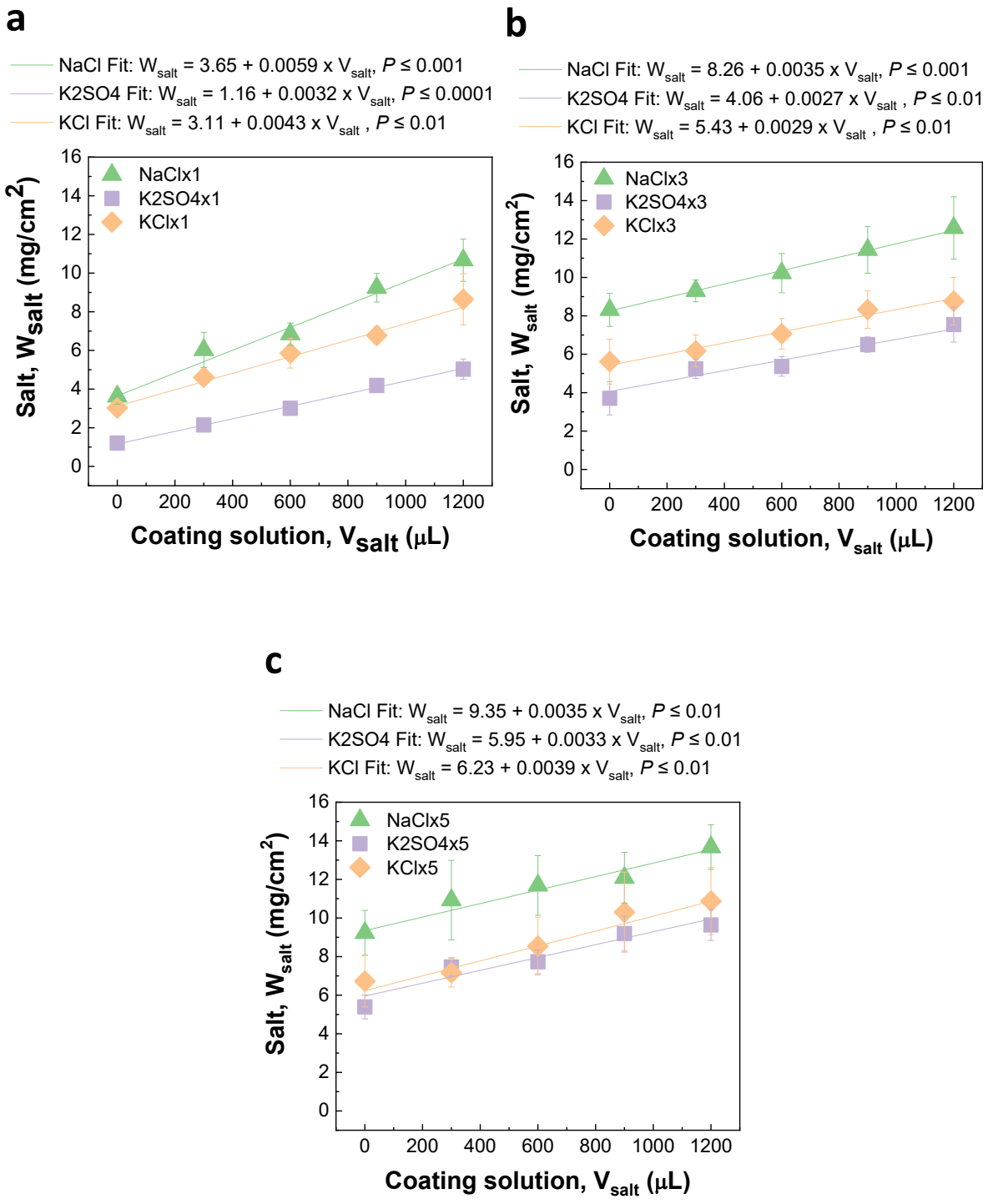

Figure 3.4 Relationship between volume of salt coating solution in which the filters were dried (V_{salt}) and amount of salt coated on the filters (W_{salt}) for 1 **(a)**, 3 **(b)**, and 5 **(c)** stacked layers (n = 5, mean ± SD). Linear fit equations are shown.

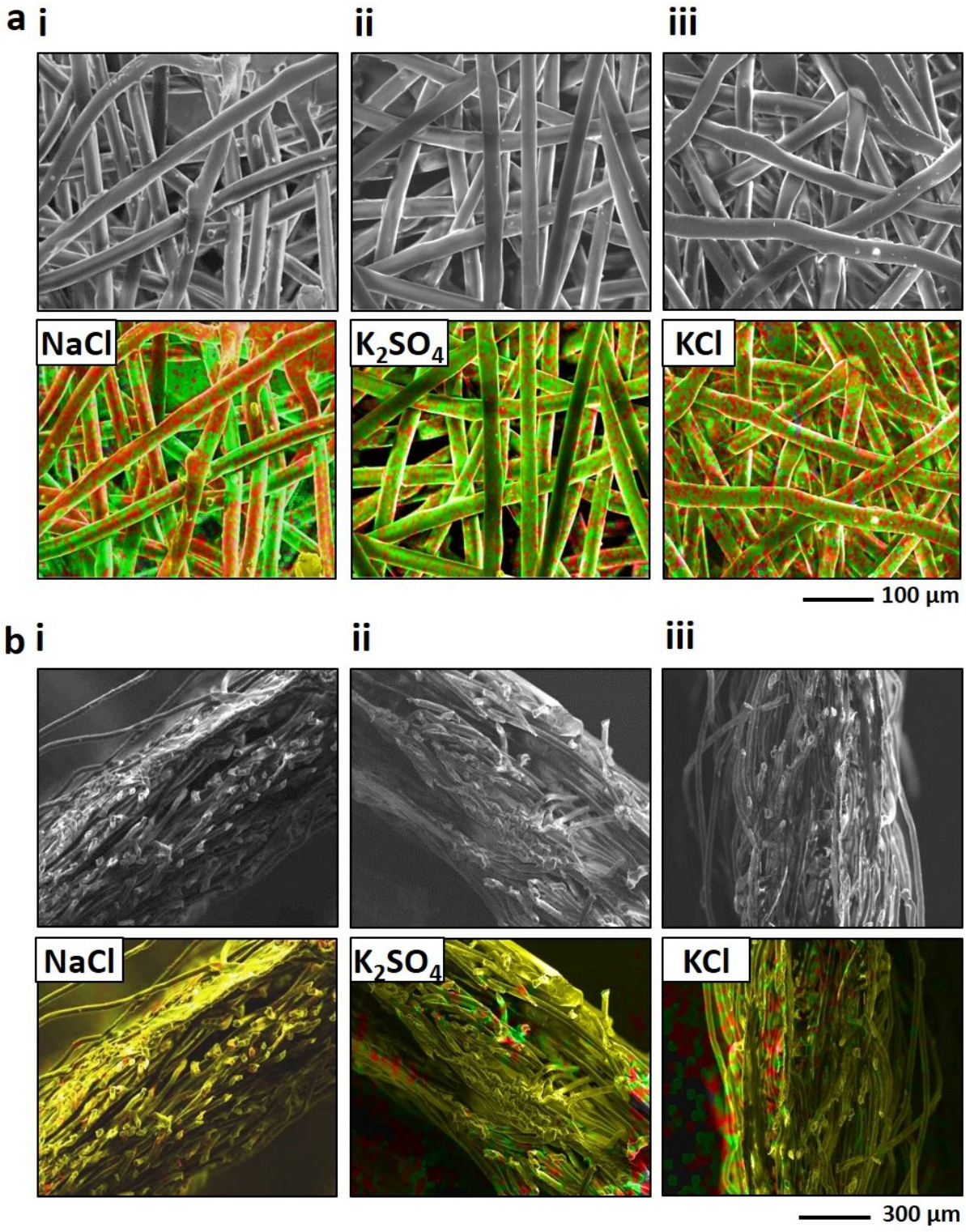

Figure 3.5 Characterization of salt-coated filters. **(a,b)** Plain view **(a)** and cross-sectional view **(b)** SEM (top) and EDX mapping (bottom) images of (i) NaCl (combination of Na (red) and Cl (green) mapping images), (ii) K_2SO_4 (combination of K (red) and S (green)), and (iii) KCl (combination of K (red) and Cl (green)) filters, showing formation of NaCl, K_2SO_4, and KCl coatings, respectively.

3.1.3.2 Filtration efficiency against pathogenic aerosols

The filtration performance of the salt-coated filters was probed against *K. pneumoniae* aerosols at 0 and 15 L/min air flow rates. Overall, at 0 L/min air flow, salt-coated filters showed significantly higher filtration efficiency than bare membranes at all conditions of salt type (NaCl, K_2SO_4 and KCl), thickness (1, 3 or 5 layers), and salt amount (3, 6 or 7 mg/cm^2) (two-way ANOVA, *P* values on graphs) (Figure 3.6a,b). In particular, the NaCl, K_2SO_4 and KCl filters exhibited an increase in filtration efficiency from 50% to 79%, 98% and 81%, respectively, as compared to bare membranes (Figure 3.6a). Even when the *K. pneumoniae* aerosols were passed through the filters at 15 L/min, NaCl and KCl salt filters still captured significantly more bacteria than the bare membranes; 5-layered K_2SO_4 filters showed a significant increase in filtration efficiency compared to bare membranes as well (two-way ANOVA, *P* values on graphs) (Figure 3.6c). Interestingly, with the sole exception of K_2SO_4 filters tested at 15 L/min air flow, the filtration efficiency of the salt-coated filters did not depend on the filter thickness (two-way ANOVA, $P > 0.05$) (Figure 3.6a,c). This led us to hypothesize that the top layer (first layer to interact with the aerosols) is mainly responsible for the increased filtration efficiency observed in salt-coated filters. Considering the relatively large size of pores against aerosols, the collection of aerosols possibly occurs via the absorption mechanisms of coated dry-salt agents (mainly those applied on the top layer), as opposed to the conventional filtration mechanism where the collection efficiency is governed by the fine mesh size and the number of added layers.

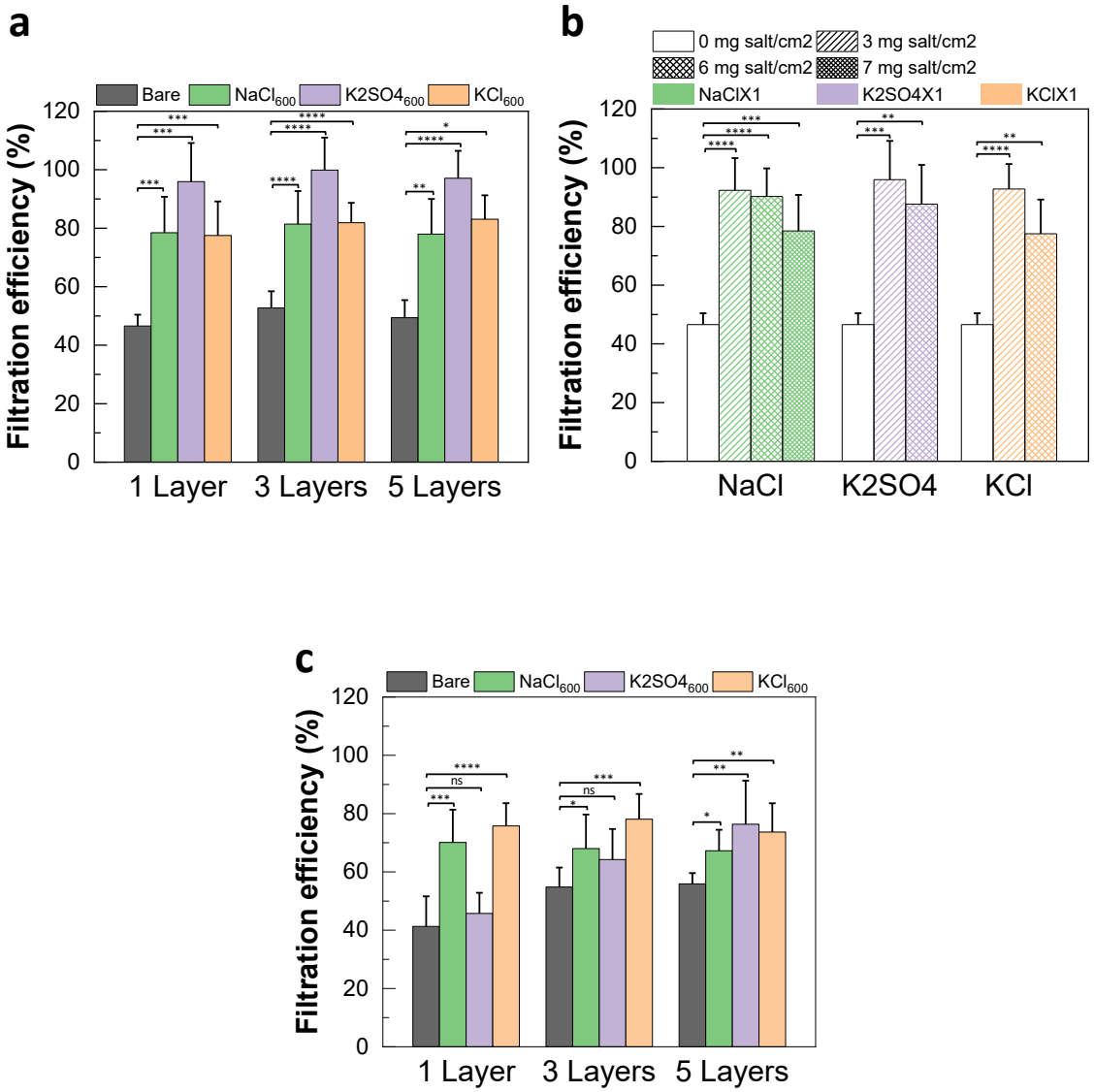

Figure 3.6 Filtration efficiency of salt-coated filters. **(a)** Filtration efficiency of Bare, $NaCl_{600}$, $K2SO4_{600}$, and KCl_{600} with 1, 3 and 5 stacked layers with no air flow (n = 7–20, mean ± SD). **(b)** Filtration efficiency of Bare×1, and NaCl×1, K2SO4×1, and KCl×1 coated with 3, 6 and 7 mg salt/cm^2 with no air flow (n = 7–15, mean ± SD). **(c)** Filtration efficiency of Bare, $NaCl_{600}$, $K2SO4_{600}$, and KCl_{600} with 1, 3 and 5 stacked layers at an air flow rate of 15 L/min (n = 10, mean ± SD). $^{**}P < 0.01$; $^{***}P < 0.001$; $^{****}P < 0.0001$, by ANOVA.

3.1.3.3 Pressure drop across the salt-coated filters

Since traditional technologies that enhance capture of pathogens/particles negatively affect the filter breathability, the pressure drop of the salt-coated filters at an air flow rate of 8 L/min was measured. Pressure drop levels evaluate the perceived resistance breathing through the filters. Notably, the pressure drop across NaCl, K_2SO_4 and KCl filters did not significantly change as compared to bare membranes, irrespective of the amount of coated salt (one-way ANOVA, $P > 0.05$) (Figure 3.7a) and thickness of the filters (two-way ANOVA, $P > 0.05$) (Figure 3.7b). Since the pore size of the fiber mesh remains sufficiently large after salt coating treatment (Figure 3.8), the above results further suggest that the proposed filtration mechanism is non-mechanical in nature, ensuring maximum filtration efficiency with high breathability.

To represent the overall filter performance, the quality factors (QF) of the salt-coated filters were compared with those of the bare membranes at 15 L/min. The QF represents the ratio between the filtration efficiency and the pressure drop of a filter [2]. The QF of NaCl, K_2SO_4 and KCl filters increased by 107%, 26% and 103%, respectively, compared with bare membranes at 1-layer thickness, 16%, 23% and 57% for 3 layers and 23%, 66% and 51% for 5 layers. The increase in QF of the salt-functionalized filters compared to bare membranes indicates an overall enhancement in performance. It is also important to note that, in theory, the QF is independent of the filter thickness. However, NaCl and KCl filters show differences in QF at different thicknesses. This is related to the fact that the top layer constitutes the main capture medium responsible for increased filtration efficiency of the salt-coated filters compared to bare membranes, as mentioned. Overall, these performance test results indicate that functionalizing large-pore membranes with salts leads to a substantial increase of the amount of captured pathogens, without increasing the resistance to air flow, yielding improved filter quality.

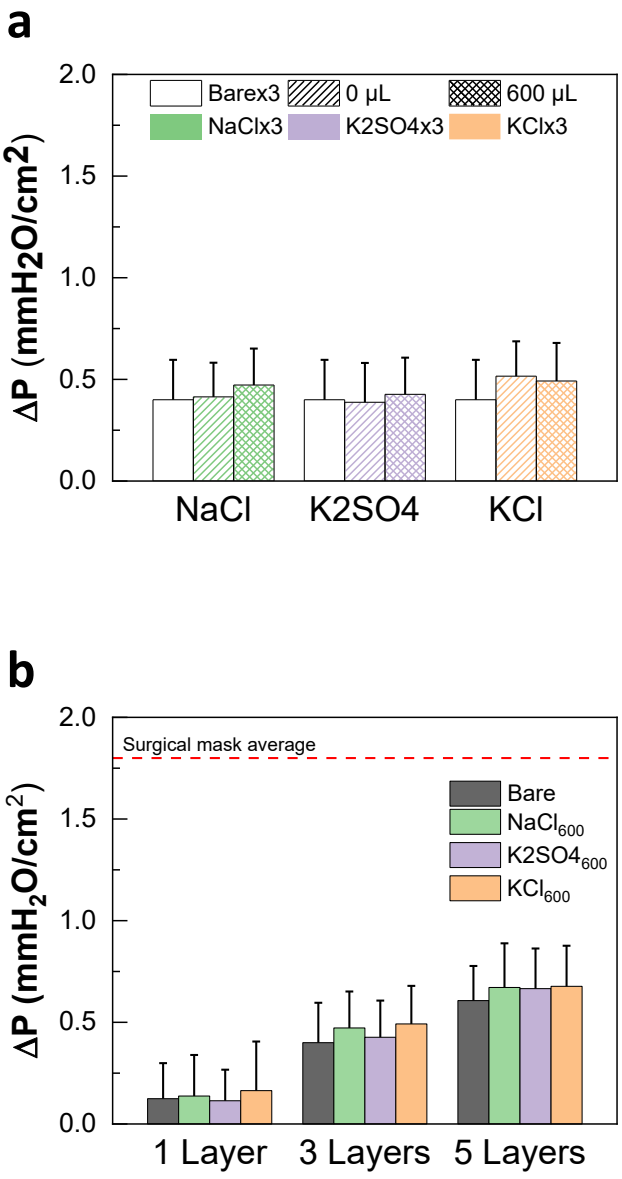

Figure 3.7 Pressure drop of salt-coated filters. **(a)** Pressure drop of Bare×3, and NaCl×3, K2SO4×3, and KCl×3 coated with different amount of salt (n = 26–45, mean ± SD). **(b)** Pressure drop of Bare, $NaCl_{600}$, $K2SO4_{600}$, and KCl_{600} with 1, 3 and 5 stacked layers (n = 27–65, mean ± SD). Dotted line: average pressure drop of commercial surgical mask (measured as purchased), as reference. For all panels: no stars means not significant ($P > 0.05$).

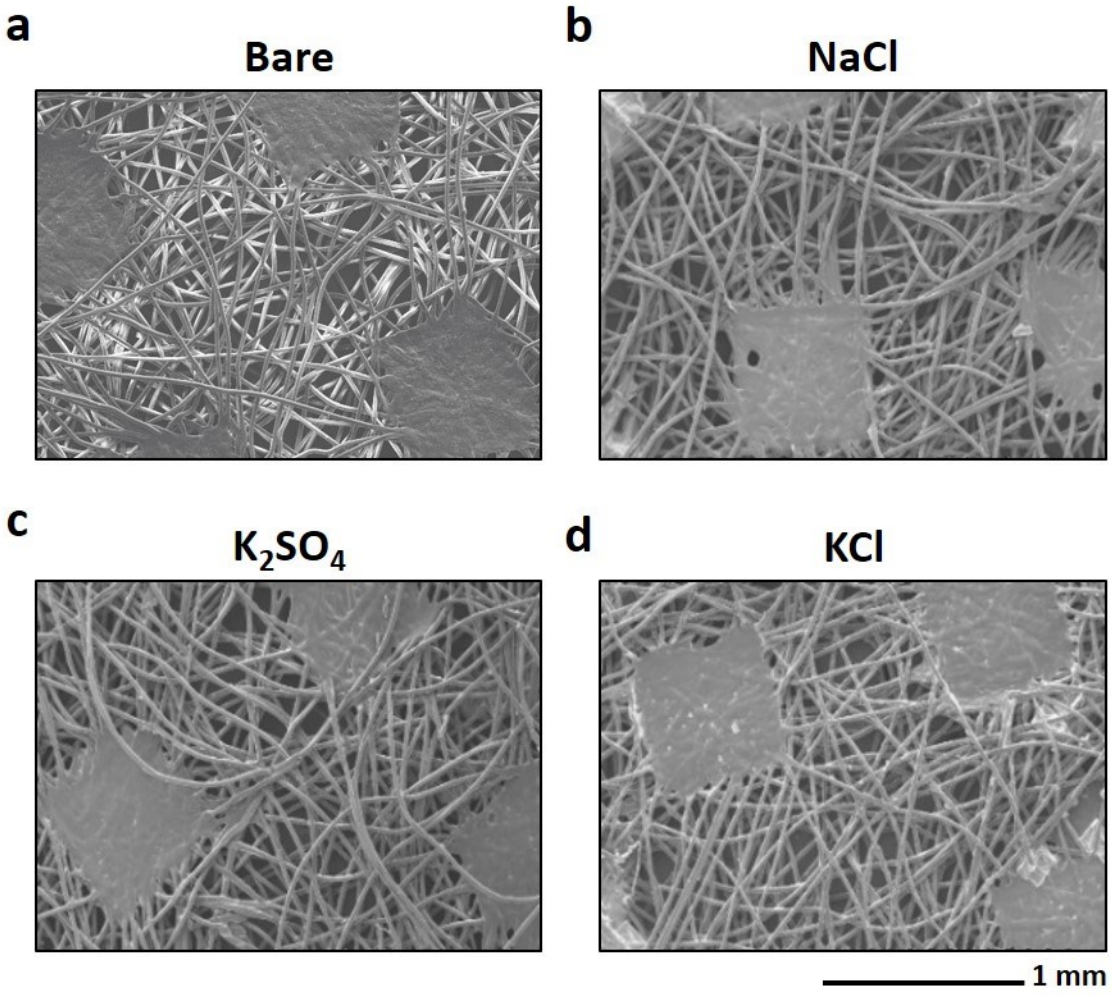

Figure 3.8 SEM images of Bare×1 **(a)**, NaCl×1_{600} **(b)**, K2SO4×1_{600} **(c)**, and KCl×1_{600} **(d)**.

3.1.3.4 Inactivation of *K. pneumoniae* on the salt-coated filters and protective efficacy *in vivo*

The pathogen inactivation on NaCl, K_2SO_4 and KCl filters was investigated by exposing them to *K. pneumoniae* bacterial aerosols. Time-dependent inactivation of bacteria incubated on filters coated with all salt types was observed (General Linear Model, $P < 0.001$) (Figure 3.9a). In particular, the KCl-coated filters exhibited significant colony forming units (CFU) reduction compared to bare membranes even within 5 min from aerosol exposure (two-way ANOVA, $P \leq 0.0001$). The decrease in survival of the bacteria on the salt-functionalized filters compared to the bare membranes was also confirmed by detecting a significant decrease in green fluorescence following propidium iodide/Syto 9 staining (General Linear Model, $P < 0.001$ for NaCl and KCl, $P < 0.05$ for K_2SO_4) (Figure 3.9b). As shown in the transmission electron microscopy (TEM) images in Figure 3.10, in contrast to intact bacteria in the control and on bare membranes, bacteria recovered from the salt-coated filters were found to be severely damaged due to the salt growth during the evaporation process. This explains the measured destabilization and viability loss of the bacteria.

Furthermore, the effect of different amounts of NaCl coated on the filters on the stability of *K. pneumoniae* aerosols was investigated. NaCl-coated filters showed rapid time-dependent bacteria inactivation (General Linear Model, $P < 0.001$) (Figure 3.11a). Notably, $NaCl{\times}3_{1200}$ caused a 4 log CFU reduction within 30 min from aerosol exposure. The decrease in bacteria survival on filters with different amounts of coated salt compared to the bare membranes was also confirmed by a significant decrease in green fluorescence (General Linear Model, $P < 0.001$) (Figure 3.11b). The TEM analysis revealed the rapture, structural damage and morphological changes incurred by the bacteria due to the salt recrystallization (Figure 3.12).

Similarly, when *K. pneumoniae* aerosols were exposed to the K_2SO_4 and KCl filters prepared to contain a lower amount of salt (K2SO4×3_0 and KCl×3_0), quick time-dependent CFU reduction was still measured (General Linear Model, $P < 0.001$) (Figure 3.13). The bacteria inactivation on K2SO4×3_0 and KCl×3_0 was also confirmed by the significant decrease of green fluorescence levels compared to bare membranes (General Linear Model, $P < 0.001$) (Figure 3.14), and TEM analysis (Figure 3.15). Overall, the bacteria stability results indicate that the NaCl, K_2SO_4 and KCl coatings rapidly neutralize bacteria by physical damage induced during the salt recrystallization process.

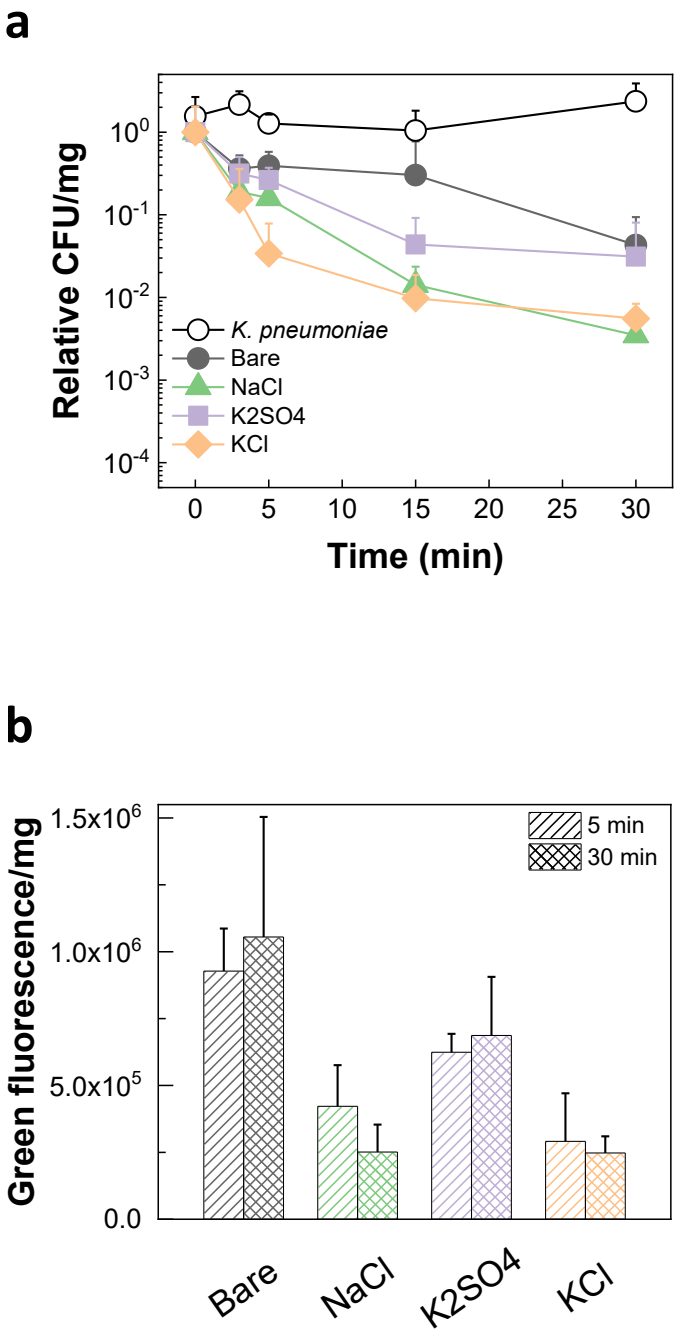

Figure 3.9 Pathogen inactivation on salt-coated filters due to salt recrystallization. **(a)** CFU change showing the effect of incubation time on *K. pneumoniae* exposed to Bare×3, NaCl×3_{600}, K2SO4×3_{600}, and KCl×3_{600} showing the effect of the salt coatings on the bacteria viability (n = 5–38, mean ± SD). **(b)** Green fluorescence following propidium iodide/Syto 9 staining of *K. pneumoniae* recovered from Bare×3, NaCl×3_{600}, K2SO4×3_{600}, and KCl×3_{600} showing the effect of the salt coatings on the bacteria membrane integrity (n = 3–10, mean ± SD).

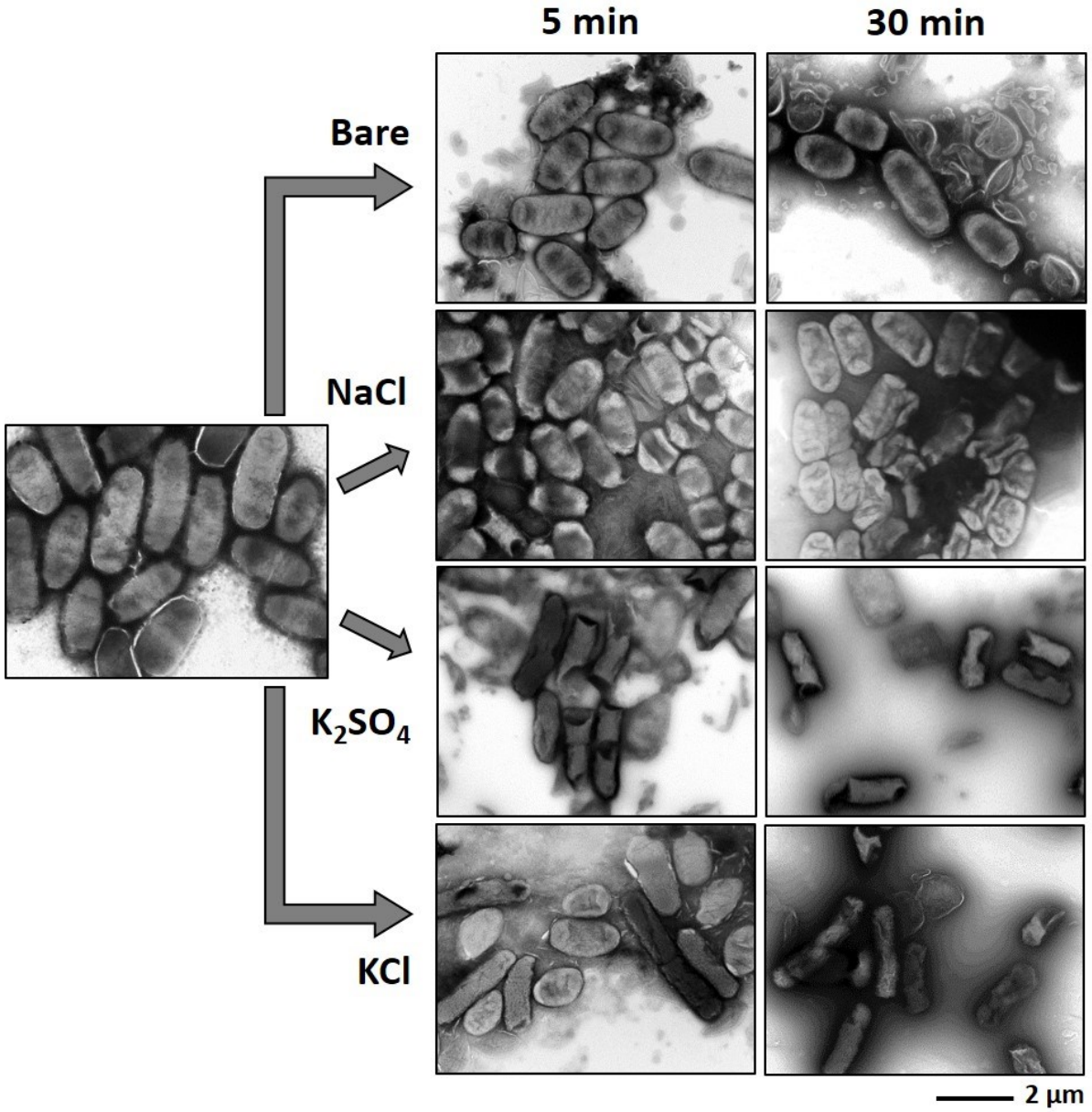

Figure 3.10 TEM images of *K. pneumoniae* incubated on Bare×3, NaCl×3_{600}, K2SO4×3_{600}, and KCl×3_{600} for 5 (center) and 30 min (right), and of *K. pneumoniae* suspension as control (left).

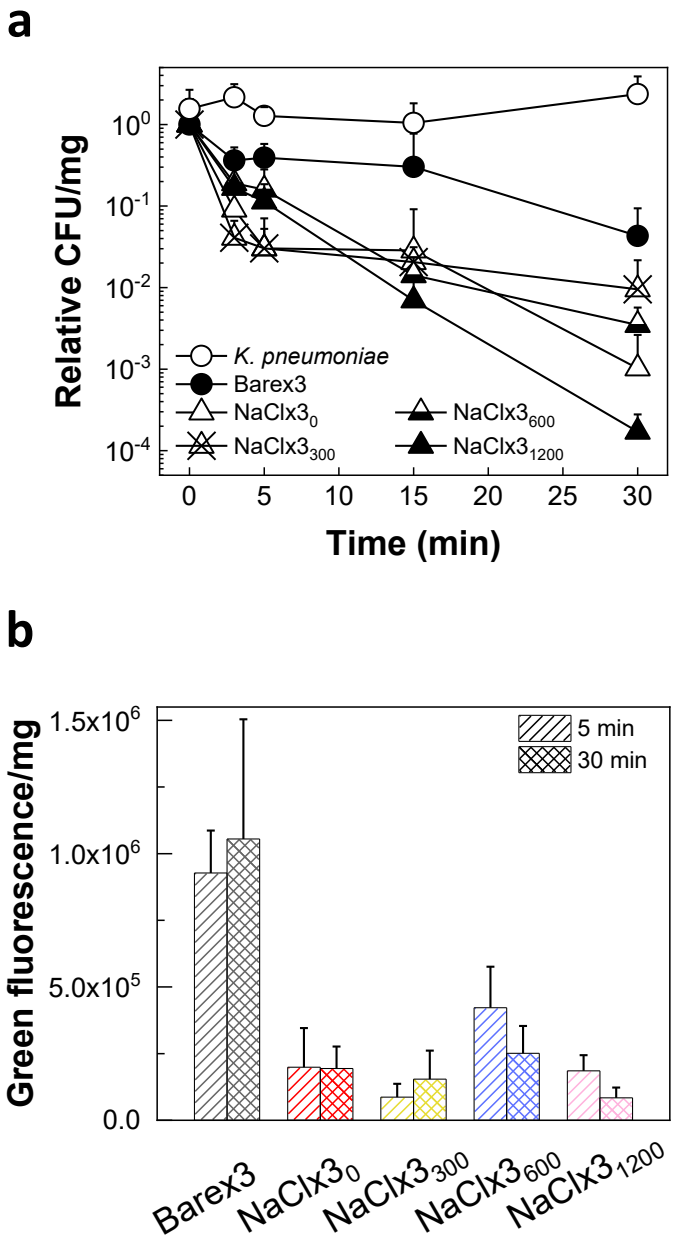

Figure 3.11 Effect of *K. pneumoniae* incubation on NaCl filters coated with different amount of salt. **(a)** CFU change showing the effect of incubation time on *K. pneumoniae* exposed to Bare×3, NaCl×3_0, NaCl×3_{300}, NaCl×3_{600}, and NaCl×3_{1200} (n = 5–38, mean ± SD). **(b)** Green fluorescence following propidium iodide/Syto 9 staining of *K. pneumoniae* recovered from Bare×3, NaCl×3_0, NaCl×3_{300}, NaCl×3_{600}, and NaCl×3_{1200} showing the effect of the NaCl coatings on the bacteria membrane integrity (n = 4–10, mean ± SD).

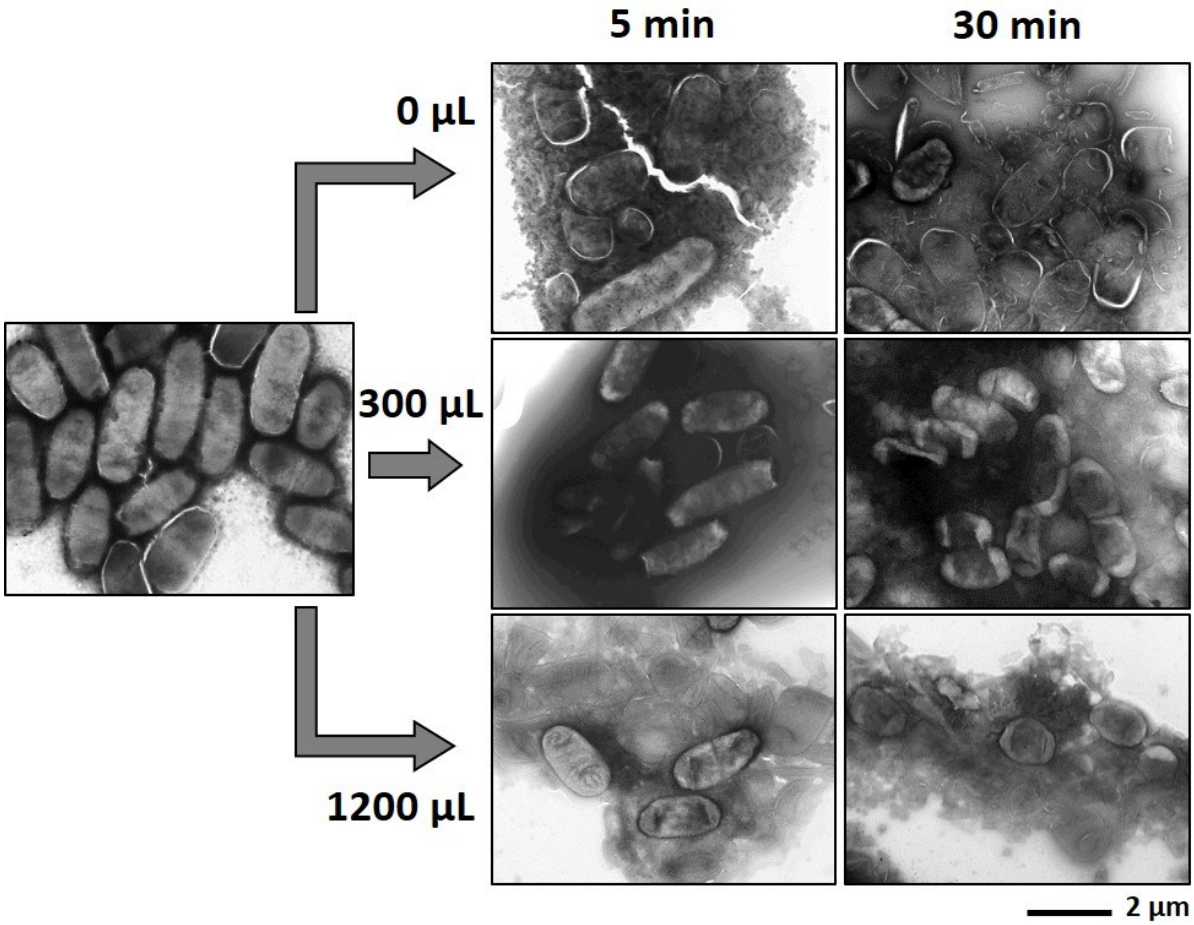

Figure 3.12 TEM images of *K. pneumoniae* incubated on NaCl×3_0, NaCl×3_{300}, and NaCl×3_{1200} for 5 (center) and 30 min (right), and of *K. pneumoniae* suspension as control (left).

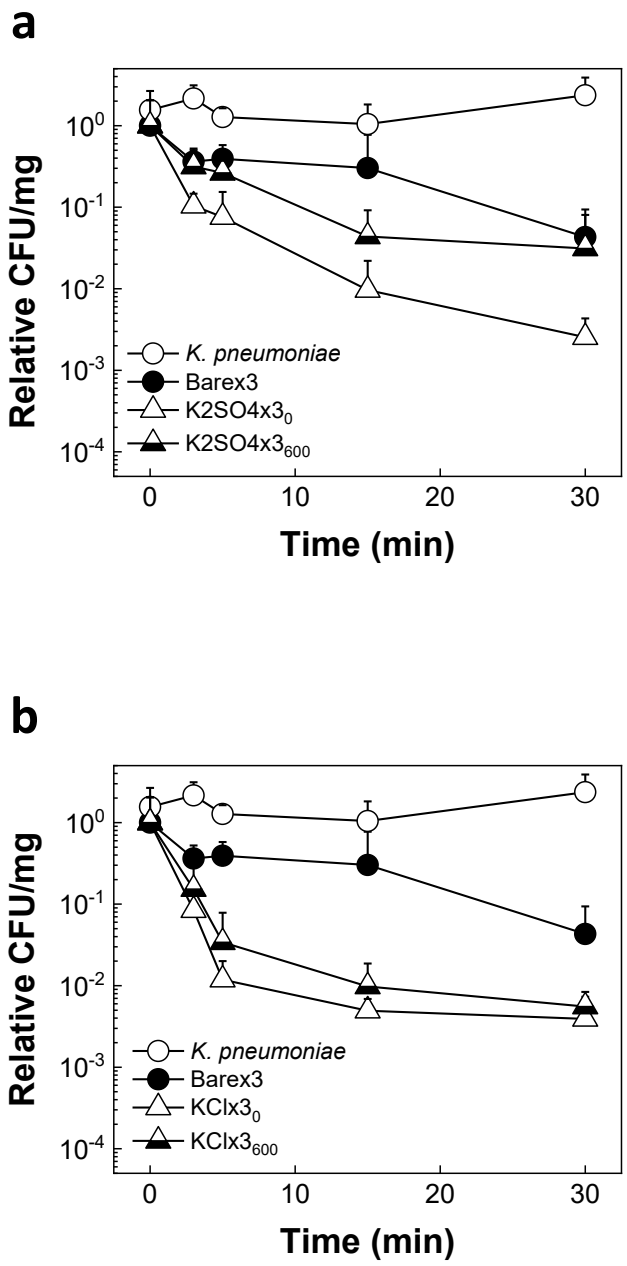

Figure 3.13 Effect of *K. pneumoniae* incubation on K_2SO_4 and KCl filters coated with different amount of salt. **(a,b)** CFU change showing the effect of incubation time on *K. pneumoniae* exposed to K2SO4×3_0 and K2SO4×3_{600} **(a),** and KCl×3_0 and KCl×3_{600} **(b)** filters (n = 5–38, mean ± SD).

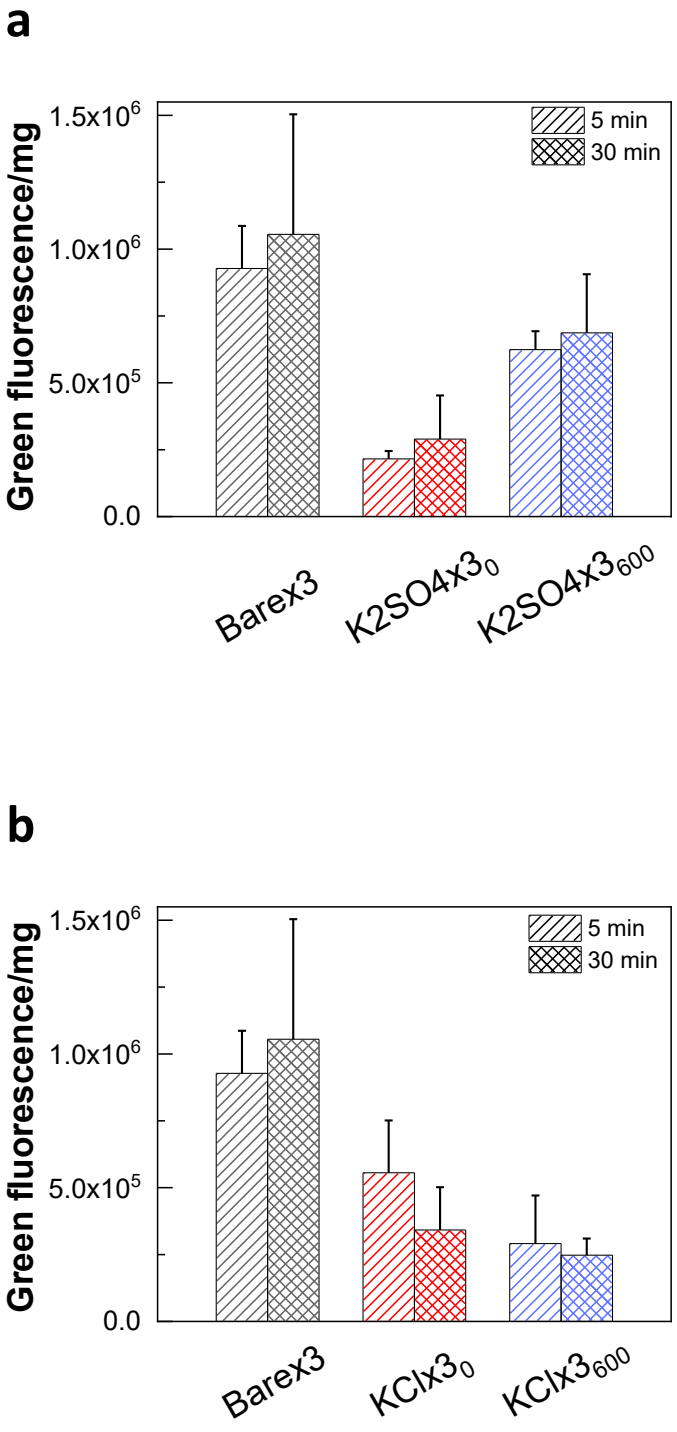

Figure 3.14 Green fluorescence following propidium iodide/Syto 9 staining of *K. pneumoniae* recovered from Bare×3, and K2SO4×3_0 and K2SO4×3_{600} **(a)**, and KCl×3_0 and KCl×3_{600} **(b)** (n = 3–10, mean ± SD).

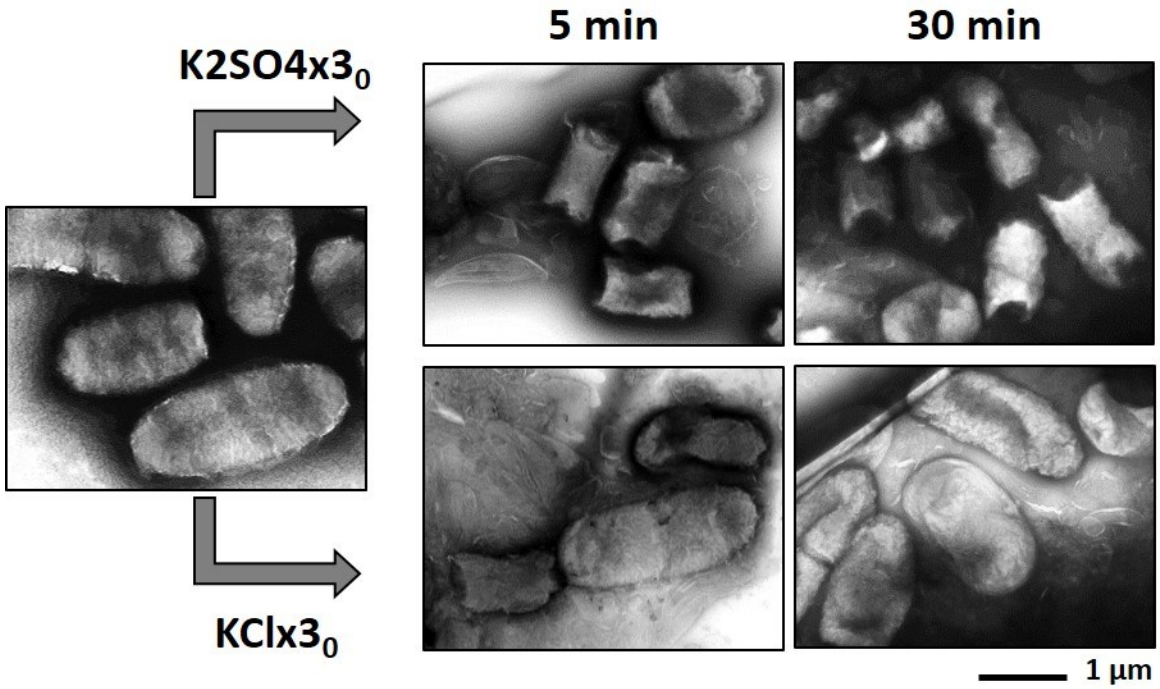

Figure 3.15 TEM images of *K. pneumoniae* incubated on K2SO4×3$_0$ (top) and KCl×3$_0$ (bottom) filters for 5 (center) and 30 (right) min, and of *K. pneumoniae* suspension as control (left).

The bacteria inactivation findings were confirmed *in vivo*. Mice were infected with *K. pneumoniae* recovered from NaCl×3_{600}, K2SO4×3_{600} and KCl×3_{600} at 5 and 30 min incubation. At 30-min incubation, the bare membrane group reached a body weight loss that was significantly higher than that of NaCl, K_2SO_4 and KCl filter groups by 10% (Figure 3.16a-c) (two-way ANOVA, $P \leq 0.05$). As shown in Figure 3.16d, OD_{600} measured from the lungs of salt filter group mice were significantly lower than those of the control groups (bare membranes) (one-way ANOVA, *P* values on graph). Furthermore, the OD_{600} levels decreased with incubation time (General Linear Model, $P < 0.001$). After 2–4 days, all salt filter mice groups showed a significant rapid recovery in body weight as opposed to the bacteria aerosol control group (two-way ANOVA, $P \leq 0.05$), unlike bare membrane groups (Figure 3.16a-c).

Additionally, the *in vivo* response to *K. pneumoniae* was investigated after incubation on NaCl×3_0 and K2SO4×3_0 for 5, 15 and 30 min. At day 2 post-infection, the salt filter groups exhibited a significantly lower body weight loss than the bacteria aerosol control group (two-way ANOVA, $P \leq 0.05$), unlike the bare membrane group (Figure 3.17a-c). The lung OD_{600} measurements further supported these results by showing significantly lower levels in NaCl×3_0 and K2SO4×3_0 mice groups than bare membrane groups (one-way ANOVA, $P \leq 0.0001$) (Figure 3.17d). In general, a decrease in lung OD_{600} was also observed with the increase in incubation time on the filters (General Linear Model, $P < 0.001$). Thus, these studies support the *in vitro* results, indicating that protection of the mice was obtained by the NaCl, K_2SO_4 and KCl salt coatings due to inactivation of the aerosolized pathogens.

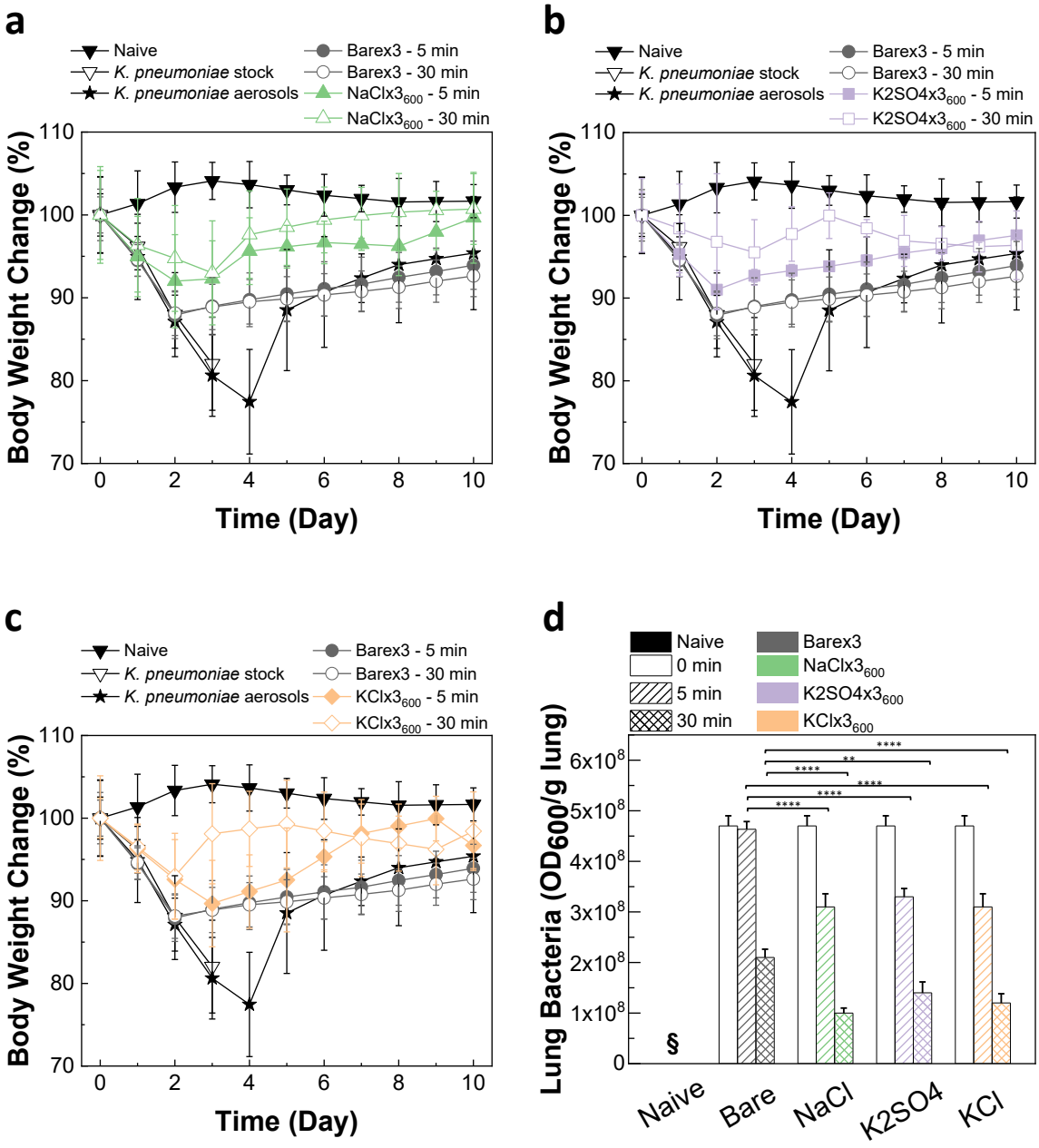

Figure 3.16 Protective efficacy *in vivo* of NaCl×3_{600}, K2SO4×3_{600}, and KCl×3_{600}. **(a-d)** Mice body weight change after infection with bacteria incubated on bare membranes, and NaCl×3_{600} **(a)**, K2SO4×3_{600} **(b)**, and KCl×3_{600} **(c)** for 5 and 30 min (n = 3–8, mean ± SD), and OD_{600} of lungs (n = 3–4 mean ± SD; §: below detection limit) **(d).** $^{**}P < 0.01$; $^{****}P < 0.0001$, by one-way ANOVA.

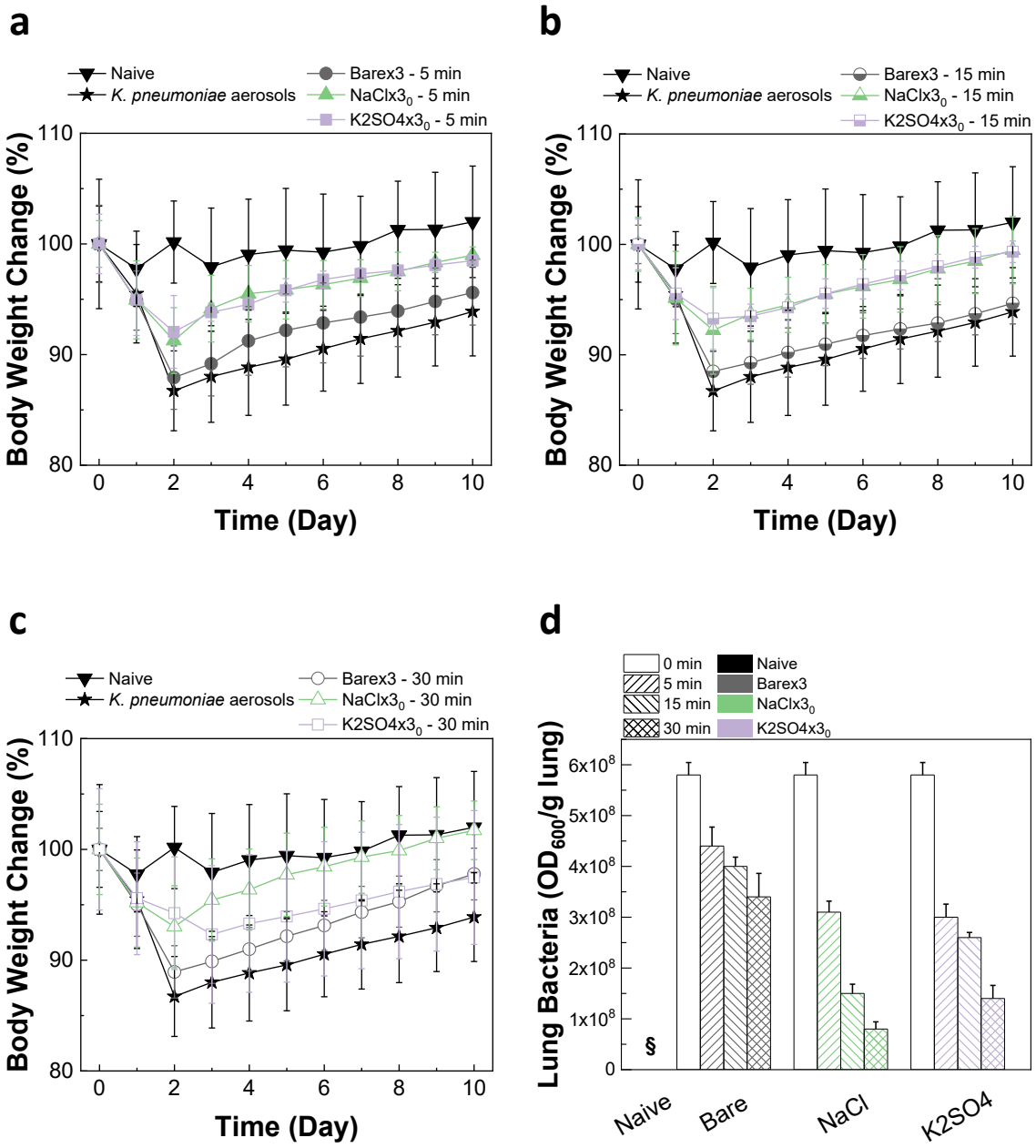

Figure 3.17 Protective efficacy *in vivo* of NaCl×3$_0$ and K2SO4×3$_0$. **(a-b)** Mice body weight change after infection with bacteria incubated on bare membranes, NaCl×3$_0$, and K2SO4×3$_0$ for 5 min **(a)**, 15 min **(b)**, and 30 min **(c)** (n = 4–8, mean ± SD), and OD$_{600}$ of lungs (n = 3–4, mean ± SD; §: below detection limit) **(d)**.

3.1.3.5 Universal pathogen inactivation on salt-coated filters

Strain-nonspecific bacteria inactivation on NaCl, K_2SO_4 and KCl coated filters was tested by exposure to four further bacteria strains (MRSA*, P. aeruginosa, S. pyogenes* and *E. coli*). Similar to *K. pneumoniae*, the salt filters exhibited inactivation capabilities irrespective of pathogen strain (Figure 3.18). In particular, in the case of *E. coli, P. aeruginosa* and *S. pyogenes,* the bacteria showed significant decrease in CFU on all salt filters compared to bare membranes, even within 5 min (General Linear Model, $P < 0.001$ for *E. Coli*, $P < 0.001$ for *P. aeruginosa*, $P < 0.05$ for *S. pyogenes*) (Figure 3.18a-c). NaCl-coated filters showed effective time-dependent MRSA inactivation (General Linear Model, $P < 0.001$) (Figure 3.18d).

Virus inactivation on NaCl, K_2SO_4 and KCl coated filters was tested by exposure to aerosolized influenza H1N1. Similar to bacteria, all salt filters exhibited inactivation capabilities. In particular, bare membranes showed no HA activity loss within 5 min, in contrast to >50% loss on NaCl and KCl filters; K_2SO_4 filters caused a substantial HA activity loss of >70% within 15 min (Figure 3.19a). Additionally, the HA titer of the virus recovered from the salt-coated filters exhibited significant decrease with increase of incubation time (General Linear Model, $P < 0.001$). Furthermore, the virus titer levels on all salt-coated filters was significantly lower compared to the bare membranes within 5 min, and negligible within 30–60 min (one-way ANOVA, $P < 0.001$) (Figure 3.19b). The virus titer also showed to significantly decrease on the salt-coated filters with time (General Linear Model, $P < 0.001$). Therefore, these results indicated dramatic virus destabilization and infectivity loss on all salt-coated filters due to the recrystallization of the salts.

In parallel, the virus stability during salt concentration increase due to aerosol drying was investigated without the salt crystallization effect. As influenza is an enveloped virus, osmotic

pressure may also have a destabilizing effect on the proteins/virus [174-176]. However, after 60-min incubation, no change in the HA titer was detected (Figure 3.19c) and the virus titer level decreased by ~1 log (Figure 3.19d) (one-way ANOVA, $P < 0.001$). As such, it was concluded that salt recrystallization constitutes the main mechanism of virus inactivation observed on the filters, although high salt concentration generated during aerosol drying caused minor pathogen infectivity loss.

Overall, these data indicate that, due to exploitation of a physical mechanism to inactivate the pathogens (i.e., evaporation-induced salt-recrystallization), the salt-coated filters offer a universal infection prevention unit.

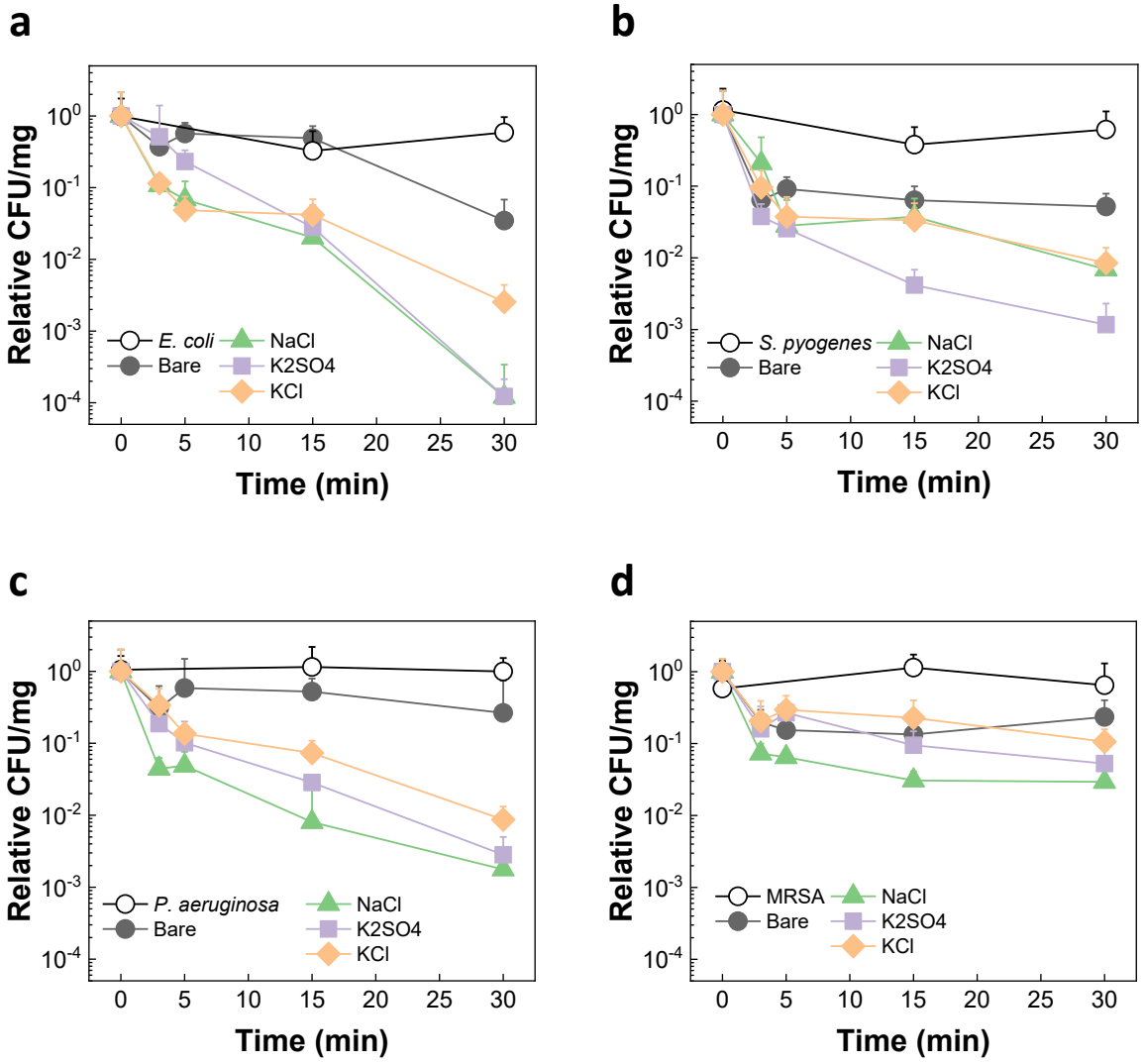

Figure 3.18 Strain-nonspecific protective efficacy. **(a-d)** CFU change showing the effect of incubation time on *E. coli* **(a)**, *S. pyogenes* **(b)**, *P. aeruginosa* **(c)**, and MRSA **(d)** exposed to Bare×3, NaCl×3_{600}, K2SO4×3_{600}, and KCl×3_{600} (n = 4–19 for (a), n = 3–19 for (b), n = 3–25 for (c), n = 2–10 for (d), mean ± SD).

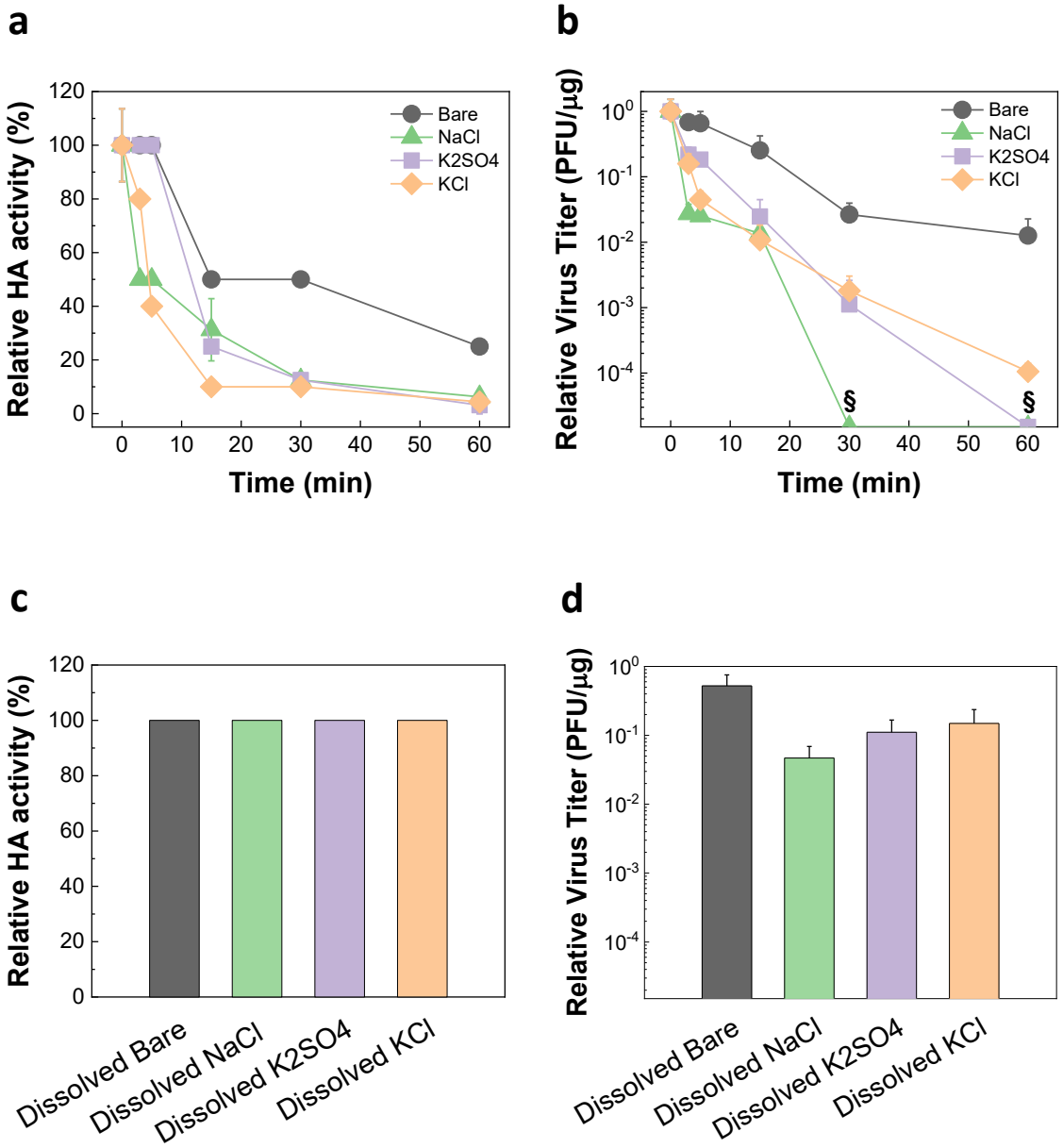

Figure 3.19 Virus inactivation on salt-coated filters. **(a,b)** HA titer **(a)** and virus titer **(b)** showing the effect of incubation time on PR/34 H1N1 virus exposed to Bare×3, NaCl×3_{600}, K2SO4×3_{600}, and KCl×3_{600} (n = 8–53 for (a), n = 4–33 for (b), mean ± SD). **(c,d)** HA titer **(c)** and virus titer **(d)** showing the effect of osmotic pressure on PR/34 H1N1 virus exposed to dissolved Bare×3, NaCl×3_{600}, K2SO4×3_{600}, and KCl×3_{600} for 60 min (n = 8–53 for (c), n = 5–33 for (d), mean ± SD). Relative: with respect to 0 min. §: below detection limit.

3.1.3.6 Exposure of salt coatings to harsh environmental conditions

Next, the environmental stability of the salt-functionalized filters was investigated. The filters were stored at 37 ℃ and 70%, 80% and 90% RH for 1, 3 and 5 days. The SEM analysis showed that all salt types remained coated on the surface of the filter fibers (Figure 3.20, Figure 3.21, and Figure 3.22). Additionally, the salt coatings showed morphological changes and increased roughness due to recrystallization at the conditions above the respective critical RH (i.e., at 80% and 90% RH for NaCl, and at 90% RH for KCl). The salt-functionalized filters retained their ability to inactivate *K. pneumoniae* (Figure 3.23). Interestingly, the salt-coated filters showed a significant increase in inactivation properties after exposure to the humid environment, and no bacteria were detected from filters after 5-days storage at 90% RH (t-test, *P* values on graphs). This phenomenon is due to the morphological change of the salt coatings after storage, leading to increased surface roughness which affects viability of bacteria [186]. Additionally, bare membranes showed the opposite trend, where the bacteria recovered from filters stored at higher RH levels yielded significantly higher CFU counts as compared to the ambient condition (t-test, *P* values on graphs). This is due to remaining humidity trapped in the membranes, protecting the bacteria. Altogether, these findings indicate that prolonged exposure of the salt-coated filters to harsh environmental conditions does not compromise the stability of the coating, while inducing further antimicrobial activity.

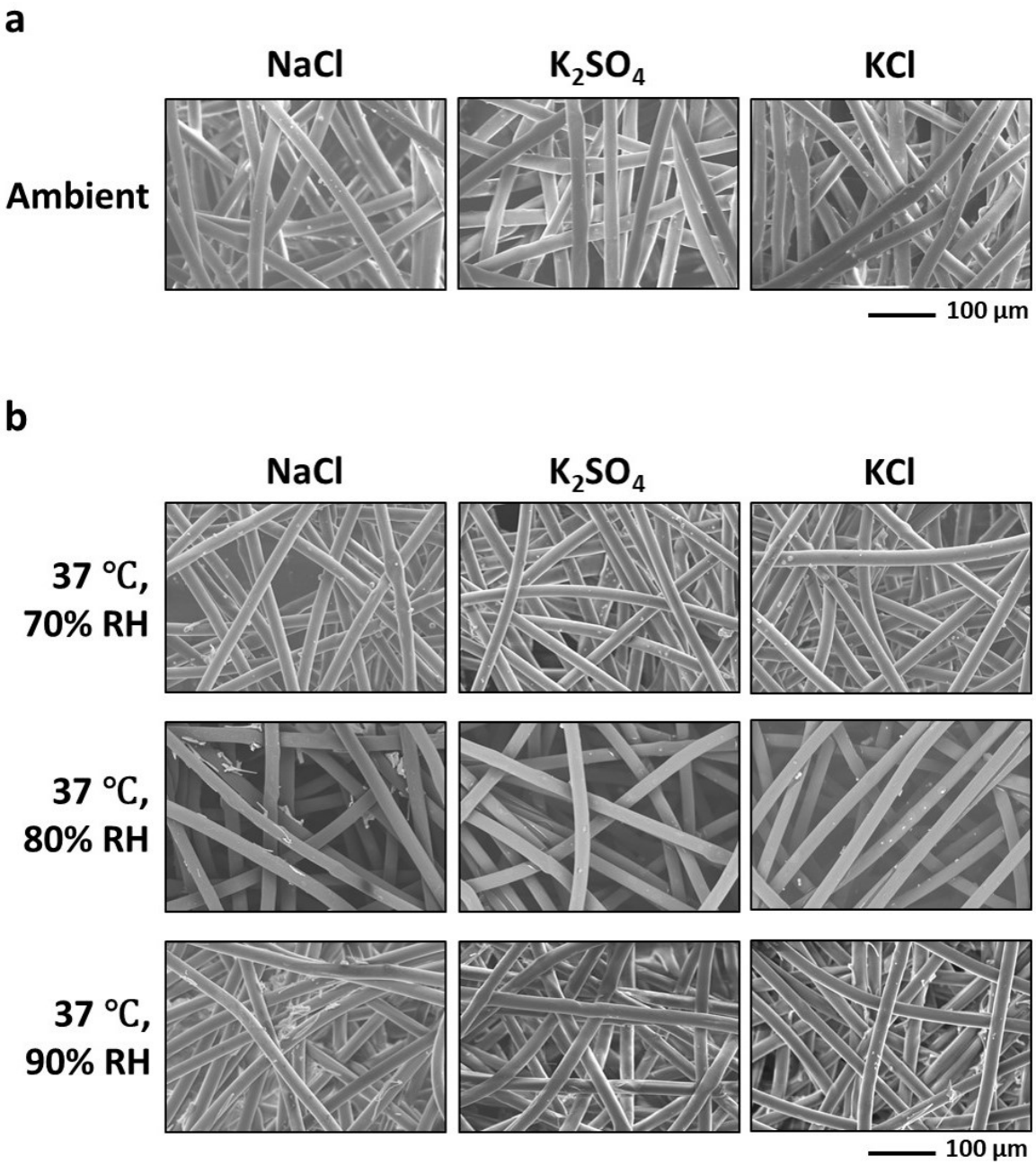

Figure 3.20 SEM images of NaCl×3_{600}, K2SO4×3_{600}, and KCl×3_{600} at ambient condition (controls) **(a)**, and following 1-day storage at 37 °C and 70, 80 and 90% RH **(b)**.

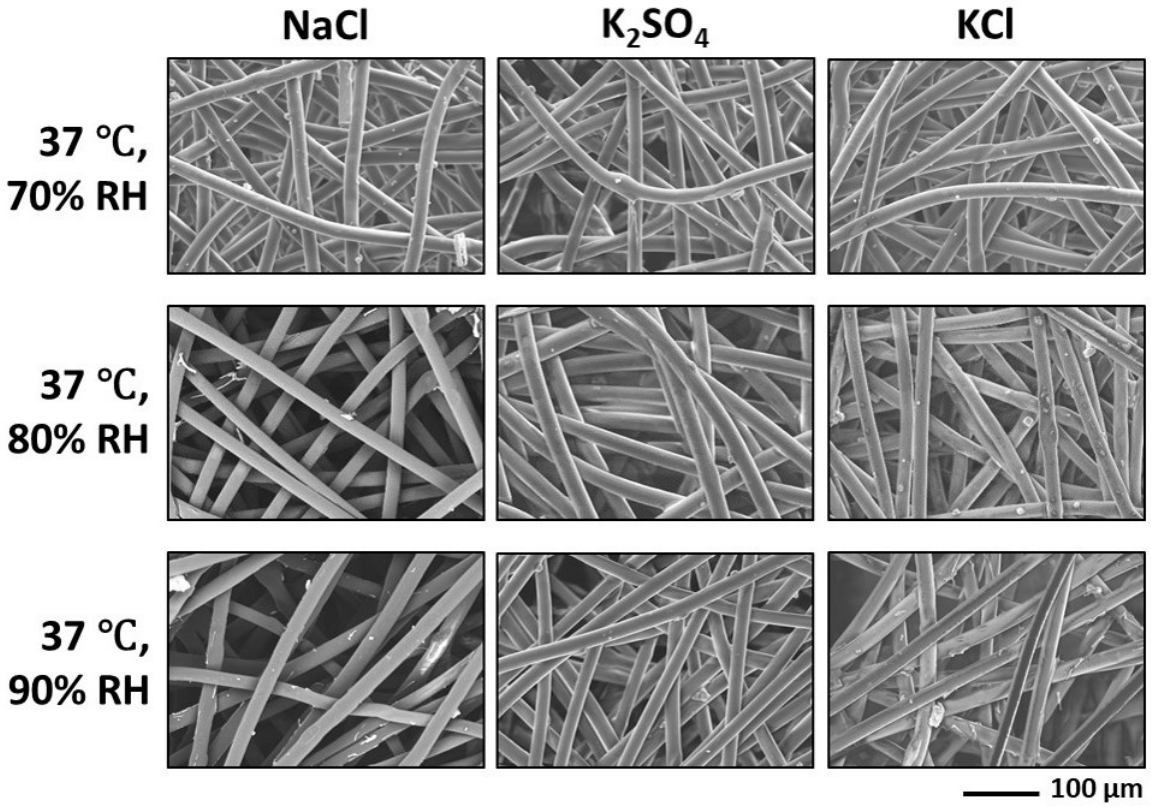

Figure 3.21 SEM images of NaCl×3_{600}, K2SO4×3_{600}, and KCl×3_{600} following 3-days storage at 37 ℃ and 70, 80 and 90% RH.

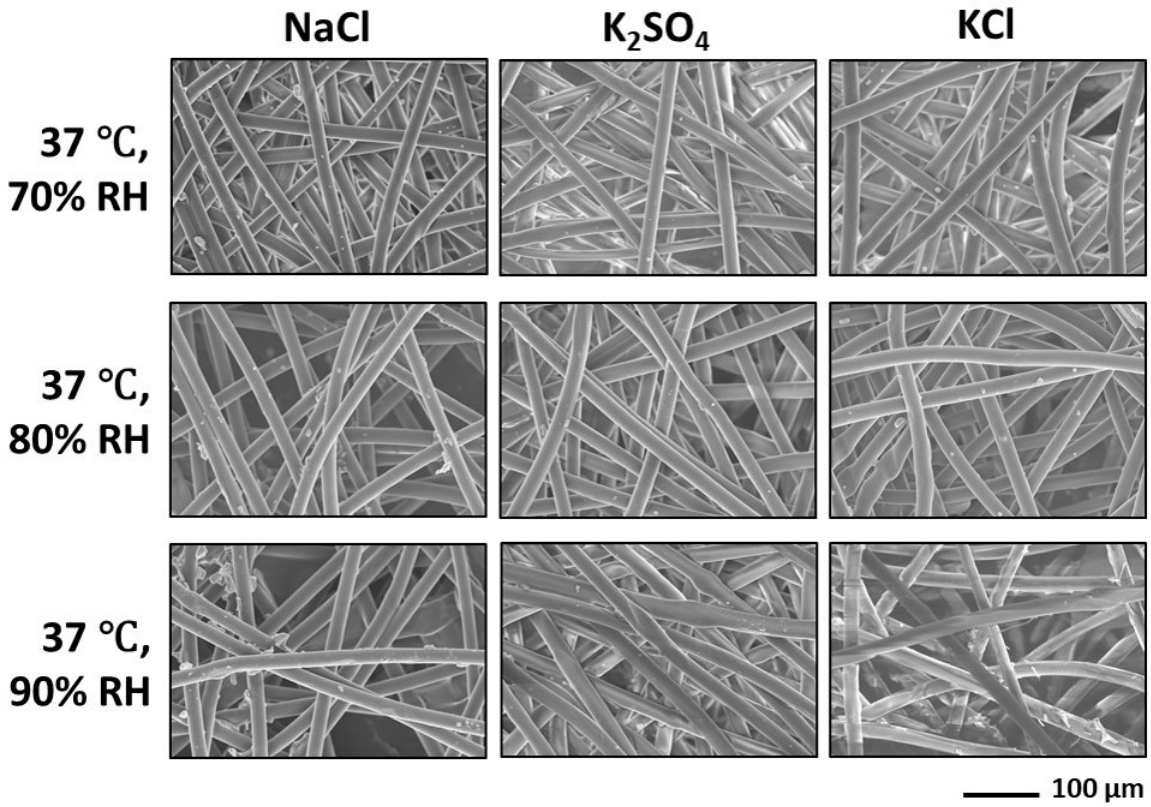

Figure 3.22 SEM images of NaCl×3_{600}, K2SO4×3_{600}, and KCl×3_{600} following 5-days storage at 37 ℃ and 70, 80 and 90% RH.

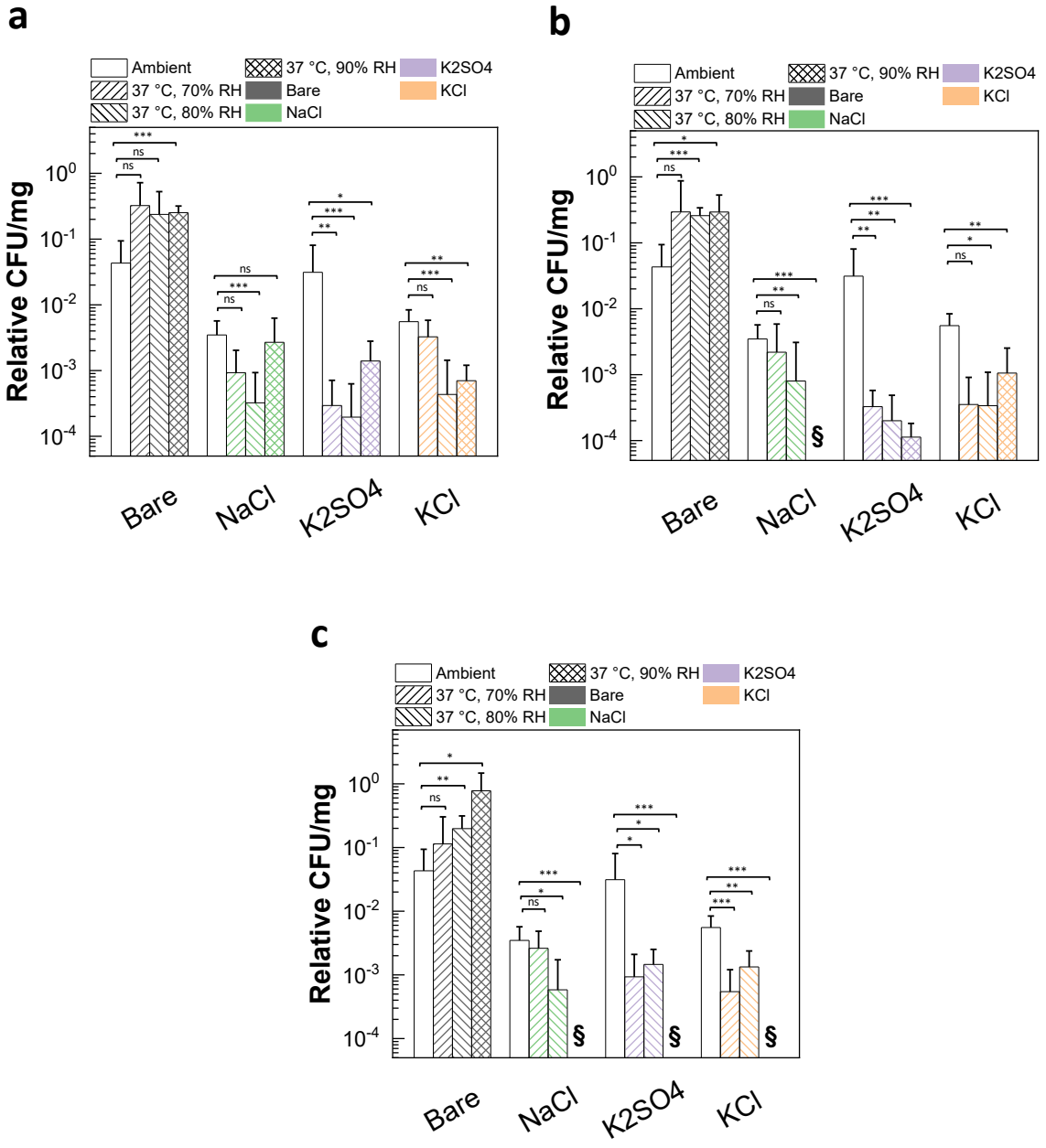

Figure 3.23 Environmental stability. **(a-c)** CFU change showing the effect of temperature and humidity (1 day **(a)**, 3 days **(b)**, and 5 days **(c)** storage) on bare membranes and NaCl, K_2SO_4, and KCl filters in inactivating *K. pneumoniae* after 30-min incubation (n = 4–19 for (a), n = 4–10 for (b), n = 3–10 for (c), mean ± SD). §: below detection limit. ns: $P > 0.05$; *$P < 0.05$; **$P < 0.01$; ***$P < 0.001$, by t-test.

3.1.4 Conclusion

In summary, we developed an antimicrobial respiratory protective system with high filtering performance and improved breathability levels compared to regular masks, based on the salt functionalization technology of large-pore membranes. The filters coated with different salt types are able to capture more pathogens than the bare membranes, converting a non-functional system into an active respiratory protection unit. Simultaneously, the enhancement in filtration efficiency does not cause any decrease in the breathability of the large-pore membranes, which is not achievable in traditional technologies. Due to the natural salt-recrystallization process physically neutralizing both Gram-positive and Gram-negative bacteria as well as virus within a short time, the salt-coated filters offer broad-spectrum protection. This results in no risk of cross infection, safe reusability of the device without further processing, reduced amounts of biohazardous waste and no risk of shortage of respirators during outbreaks. Additionally, the salt coatings remained stable on the filters following prolonged exposure to high temperature and humidity. This offers complete protection at varying environmental conditions of use and storage as well as ensures recyclability of the filters. Overall, the results indicate that our technology can be used to fabricate respiratory protective devices with high filtration and breathability performance, which achieve strain-nonspecific protective efficacy. Notably, the simple and cost-effective functionalization process with salt addresses all major technical challenges of respiratory protection devices in a single system, and could be readily applied to other devices that are already in use, such as filters in buildings and hospitals. This comprehensive technology could lead to an enhanced and timely response to epidemics and pandemics, and provides a safe and effective solution to prevent diseases globally.

3.2 Pathogen inactivation behavior

3.2.1 Background

In Section 3.1, large-pore membranes were coated with different types of salt candidates (NaCl, K_2SO_4, and KCl) to identify salt-coated filters that meet different application needs. The salt candidates cover a wide range of critical RH values, ideal for production of environment-resistant respiratory protection devices and filters. Concurrently, it can be observed in Figure 3.9a, Figure 3.11a, Figure 3.13, and Figure 3.19a,b that different salt types exhibit different pathogen inactivation kinetics. In this Section, the pathogen inactivation properties are investigated in terms of recrystallization behavior of the salts. Crystallization has two components, nucleation and crystal growth [187]. During nucleation, the atoms in the liquid matrix need to form solid phase particles bigger in size than a critical radius in order to be stable, originating nuclei. Stable nuclei increase in size (crystal growth) as the liquid to solid transformation proceeds. The driving force is supersaturation Δc, defined as:

$$\Delta c = c - c_s \tag{3.4}$$

where c is the solute concentration and c_s is the saturation concentration. Supersaturation is achieved by either lowering the temperature or increasing the solute concentration (such as in the case of evaporation). The crystallization kinetics can be described by the rate of nucleation R_n and the rate of crystal growth R_g:

$$R_n = k_n(\Delta c)^n \tag{3.5}$$

$$R_g = k_g(\Delta c)^g \tag{3.6}$$

where k_n is the nucleation rate constant, n is the nucleation order, k_g is the crystal growth constant, and g is the crystal growth order [188]. The comparison between crystallization kinetics of the different salt types is discussed in this Section.

Finally, the contribution of osmotic pressure to the destabilization of pathogens aerosolized on salts was evaluated. If osmolarity differences are present across the semipermeable membranes of biological systems, osmotic pressure is generated, which can lead to morphological changes [189]. Under hyperosmotic and hypoosmotic stresses, water is transported through the membranes, causing shrinking and swelling, respectively, which can be responsible for loss of functionality or rapture of the biological system [190]. As the pathogens are exposed to high salt concentrations during the aerosol drying process, the effect of hyperosmotic stress on bacteria viability was included in the investigation.

3.2.2 Methods

3.2.2.1 XRD analysis

To monitor the formation of crystalline NaCl, K_2SO_4, and KCl over time during aerosol drying, filters (NaCl×3_{600}, K2SO4×3_{600}, KCl×3_{600}; sample size = 2.5 × 2.5 cm) and powders were mounted on glass slides for XRD analysis (Bruker D8 Discover; Billerica, MA, USA); Bare×3 samples were analyzed as controls. XRD spectra were obtained in θ–2θ mode using a CuKα radiation before and right after DI water aerosol exposure (20 μL), and at 5, 15, and 30 min. Miller indices corresponding to NaCl, K_2SO_4, and KCl crystals, respectively, were identified based on the standard spectra cards from the literature [191-193].

3.2.2.2 Microscopy analysis

To characterize the salt recrystallization, NaCl, K_2SO_4, and KCl powders were monitored over time during aerosol drying under an optical microscope (Omax G223A-CA; Kent, WA, USA). The powders (300 mg) were each uniformly deposited in a well (diameter = 22 mm) of a 12-well plate, which allows for tight fitting of the nebulizer unit (Aeroneb Lab Nebulizer System; Aerogen, Galway, Ireland). Images (Moticam; Motic, Hong Kong) were obtained before DI water aerosol exposure (20 μL), and at 3, 5, 15, 30, and 60 min after exposure. To observe the morphological changes of the salts due to recrystallization, the salt powders were analyzed by SEM (Hitachi S-3000N; Hitachi, Toronto, Canada) in secondary electron mode at 20 kV before and after aerosol exposure. The samples were coated with a 10-nm layer of gold; after aerosol exposure, samples were allowed to fully dry before applying the gold coating.

3.2.2.3 Test of bacteria stability change on salt powders

The NaCl, K_2SO_4 and KCl powders (300 mg) were each uniformly deposited in a well of a 12-well plate. *K. pneumoniae* was cultured and washed as described in Section 3.1.2.2, and resuspended in DI water to an OD_{600} of 12.5. The nebulizer unit was placed in the well with a tight seal and 20 μL of bacteria suspension were aerosolized for 30 sec. The bacteria aerosols were incubated on top of the powders at ambient condition for a specific time point (3, 5, 15, 30 or 60 min). Then, the bacteria were reconstituted by adding 2 mL (NaCl and KCl powders) or 4 mL (K_2SO_4 powder) of PBS and mixing with pipette to completely dissolve the salt powder. The recovered bacteria were centrifuged (14,000 rpm, 15 min, 4 °C) to discard the dissolved salt, and then resuspended in 100 μL of fresh PBS. The amount of bacteria contained in the exposure aerosols (at 0 min incubation on the powders) and the CFU measurements were determined as described in Section 3.1.2.6.

3.2.2.4 Test of bacteria stability change due to osmotic pressure

To test the effect of osmotic pressure during the experimental procedure, 300 mg of each powder was dissolved in 1.5 mL (NaCl and KCl powders) or 3.5 mL (K_2SO_4 powder) of PBS in a 15-mL tube. The *K. pneumoniae* suspension (20 μL) was aerosolized into the tube for 30 sec, followed by 1-min aerosolization of DI water and vortexing (final volume: 2 mL for NaCl and KCl and 4 mL for K_2SO_4). The final condition corresponds to hyperosmotic differences ΔC (ΔC = osmolarity of solution – cell internal osmolarity) of 5,250 mOsm/L, 1,370 mOsm/L, and 4,080 mOsm/L for NaCl, K_2SO_4 and KCl, respectively; the cell internal osmolarity is considered to be 300 mOsm/L and the osmolarity of the solution is calculated by considering the number of dissociated ions in PBS solution for each salt [189] (notably, this is an estimation as the calculation of the osmolarity of the solution is valid under the assumption of ideal and dilute

solutions). The bacteria were incubated in the dissolved salt powder for a specific time point (15, 30 or 60 min), and then centrifuged (14,000 rpm, 15 min, 4 °C) to interrupt the incubation and resuspend in 100 µL of fresh PBS. CFU tests were conducted as described above.

To test the effect of osmotic pressure due to salt concentration increase during aerosol drying, 20 µL of *K. pneumoniae* suspension were aerosolized into a 15-mL tube containing 2 mL of salt solution for 30 sec, followed by vortexing. The bacteria were incubated in the salt solution for a specific time point (15, 30 or 60 min), and then centrifuged (14,000 rpm, 15 min, 4 °C) to interrupt the incubation and resuspend in 100 µL of fresh PBS. CFU tests were conducted as described above. The aqueous salt solution conditions tested are summarized in Table 3.1; the respective estimated hyperosmotic differences ΔC are reported.

Table 3.1 Salt solutions conditions tested for osmotic pressure effect on bacteria during aerosol drying. *Saturated condition.

NaCl		**K_2SO_4**		**KCl**	
Concentration (w/v%)	**ΔC (mOsm/L)**	**Concentration (w/v%)**	**ΔC (mOsm/L)**	**Concentration (w/v%)**	**ΔC (mOsm/L)**
29*	9,700	10*	1,420	26*	6,630
26	8,670	7	910	18	4,500
18	5,910	4	390	10	2,370
10	3,150				

3.2.2.5 Statistical analysis

The statistical analysis was performed by using General Linear Model using Minitab (Minitab, State College, PA). The significance of multiple comparisons was considered by *P* value; *P* value of less than 0.05 was considered significant.

3.2.3 Results and discussion

3.2.3.1 Characterization of the salt recrystallization

The recrystallization of bare membranes (control) and NaCl, K_2SO_4, and KCl coated-filters after DI water aerosols exposure was monitored over time by XRD (Figure 3.24). For the NaCl coating (Figure 3.24b), the intensity of the (200) peak decreases right after aerosol exposure, as the aerosols dissolve the NaCl salt; within 5 min, the (200) peak intensity is increasing with time. The (220) peak intensity shows a similar pattern. For the K_2SO_4 coating (Figure 3.24c), the (022) peak, not present in the spectrum right after aerosol exposure, starts growing in intensity after 15 min; after 30 min, the (022) peak intensity becomes relatively higher than that of the (040) peak, as opposed to the spectrum before aerosol exposure. Additionally, the (031), (002), and (132) peaks grow in intensity after 15 min from aerosol exposure. For the KCl coating (Figure 3.24d), similarly to the NaCl coating, the intensity of the (200) peak decreases right after aerosol exposure, and within 5 min the intensity is increasing with time. Overall, the XRD spectra indicate that the NaCl and KCl coatings start to recrystallize within 5 min, and the onset of the K_2SO_4 coating recrystallization is within 15 min. These results match the time-dependent pathogen inactivation patterns observed for bacteria (Figure 3.9a, Figure 3.11a, and Figure 3.13) and virus (Figure 3.19a,b), where NaCl and KCl coated filters cause pathogen inactivation initiation earlier than K_2SO_4 filters.

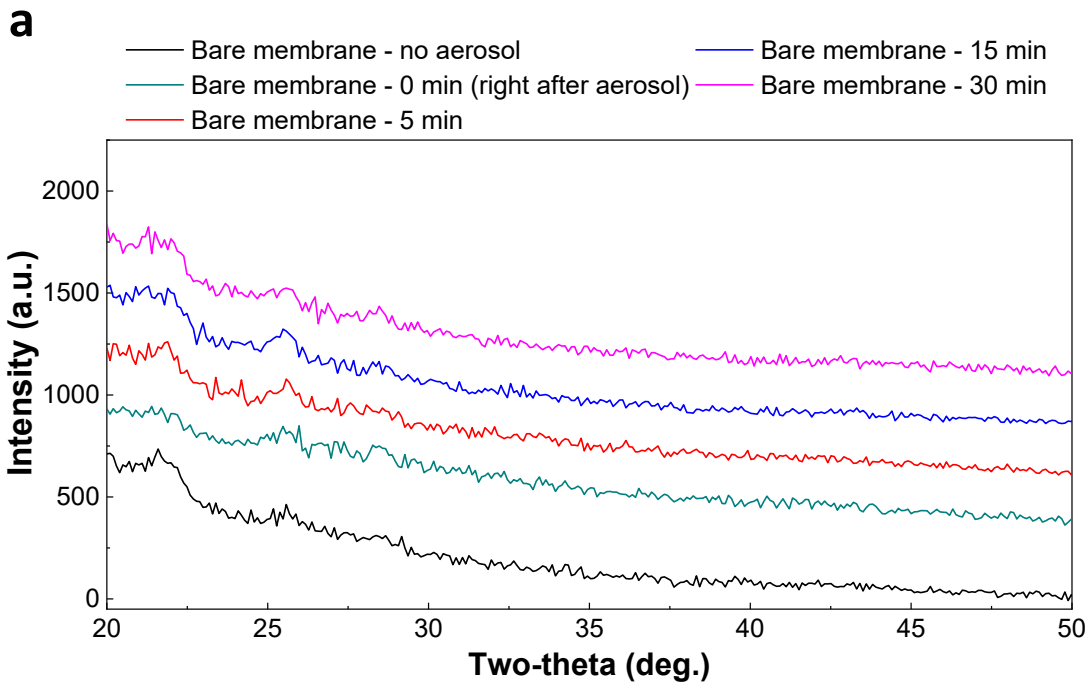
a
Bare membrane - no aerosol
Bare membrane - 0 min (right after aerosol)
Bare membrane - 5 min
Bare membrane - 15 min
Bare membrane - 30 min
Intensity (a.u.)
Two-theta (deg.)

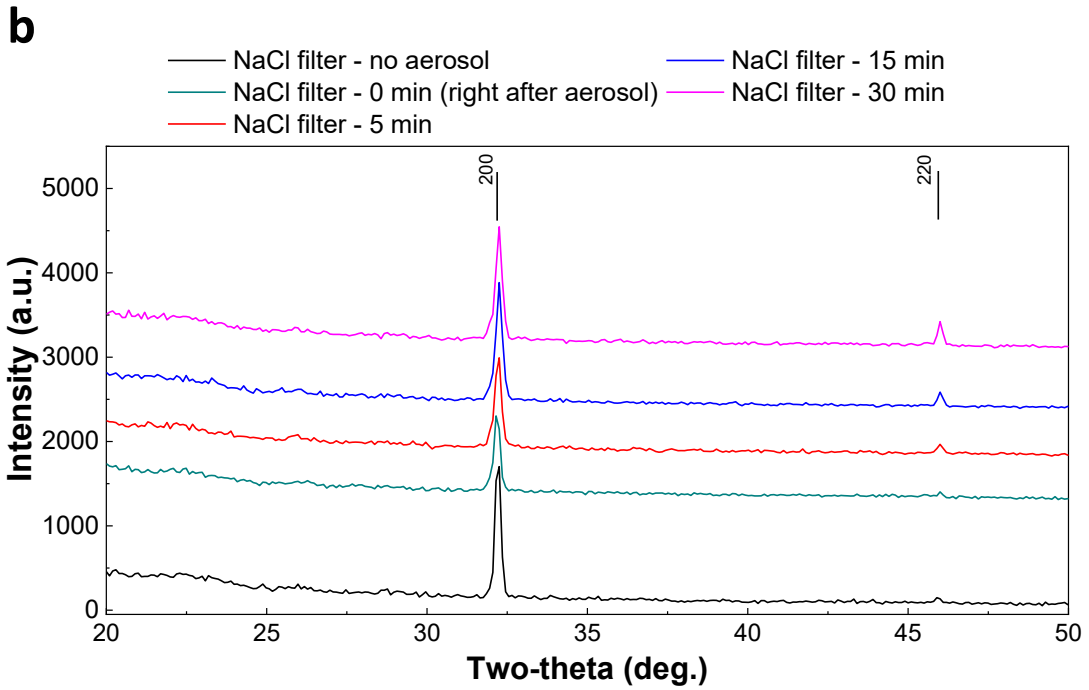
b
NaCl filter - no aerosol
NaCl filter - 0 min (right after aerosol)
NaCl filter - 5 min
NaCl filter - 15 min
NaCl filter - 30 min
200
220
Intensity (a.u.)
Two-theta (deg.)

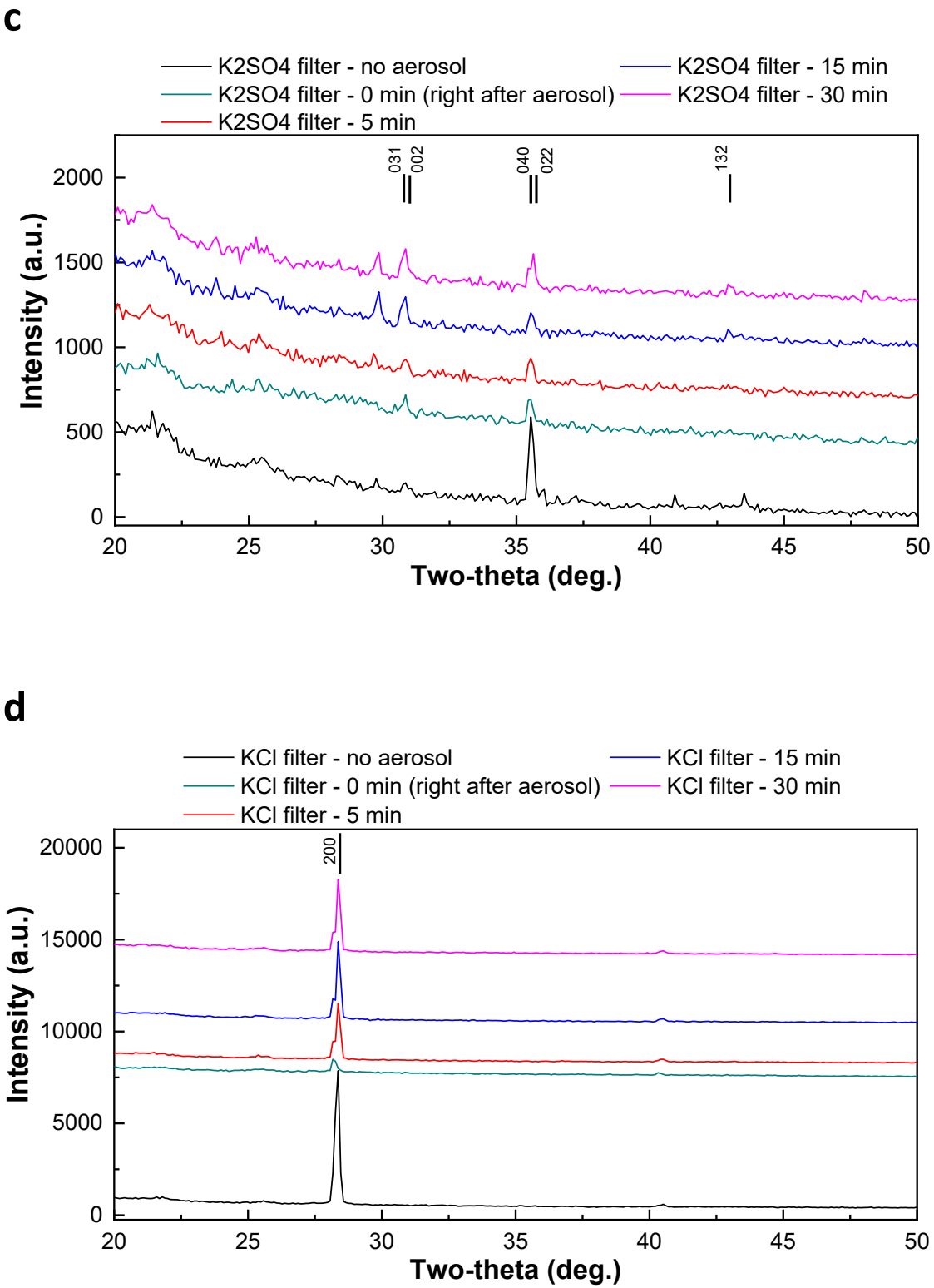

Figure 3.24 Characterization of the salt recrystallization on the coated filters. **(a-d)** XRD spectra of Bare×3 **(a)**, NaCl×3_{600} **(b)**, K2SO4×3_{600} **(c)**, and KCl×3_{600} **(d)** before aerosol exposure, right after, and at 5, 15, and 30 min. Miller indices of relevant peaks corresponding to NaCl, K_2SO_4, and KCl crystals, respectively, are shown at the top of XRD spectra for each position.

To focus the analysis of the pathogen inactivation mechanism on the interaction with salt crystals, the salt-based pathogen inactivation was investigated directly on salt powders. The recrystallization of NaCl, K_2SO_4, and KCl powders after DI water aerosol exposure was monitored over time by XRD (Figure 3.25). For the NaCl powder (Figure 3.25a), the intensity of the (200) peak shows an initial increase right after aerosol exposure; within 5 min, the (200) peak intensity further increases. In the case of the K_2SO_4 powder (Figure 3.25b), the (220) peak, not present in the spectrum right after aerosol exposure, starts growing in intensity after 15 min. The (031) peak starts to decrease in intensity after 15 min. Right after aerosol exposure, the (211) peak intensity becomes higher than that of the (002) peak, as opposed to the K_2SO_4 powder before aerosol exposure; at 15 min, the (211) peak intensity starts to decrease and at 30 min it is once again lower than that of the (002) peak. For the KCl powder (Figure 3.25c), the intensity of the (200) peak decreases with time after aerosol exposure. Altogether, similarly to the XRD spectra obtained for the salt-coated filters, recrystallization of the NaCl and KCl powders begins within 5 min, and recrystallization of the K_2SO_4 powder begins within 15 min.

The effect of DI water aerosol exposure and drying on the salt powders was monitored under the optical microscope (Figure 3.26). At 3 min, the salt powder surfaces are dissolved. At 5 min, NaCl and KCl powders start to recrystallize, as observed by increased surface roughness, formation of aggregates of salt crystals, and sharp edges. Formation of regular, geometric crystals and aggregates for K_2SO_4 is first observed at 15 min. The morphological changes of the salt powders during recrystallization over time are consistent with the XRD results. Additionally, the SEM images show formation of sharp edges on the NaCl and KCl powders after aerosol exposure; the K_2SO_4 powder exhibits a transformation from randomly shaped crystals (before aerosol exposure) to regular, geometric crystals (after aerosol exposure) (Figure 3.27).

a

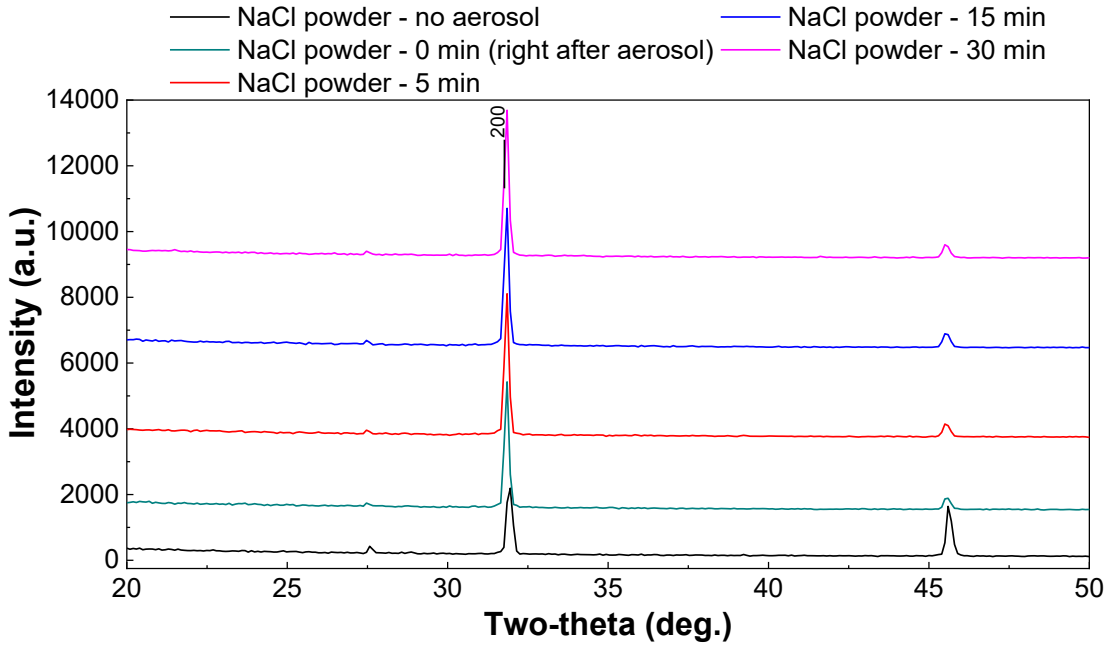
NaCl powder - no aerosol
NaCl powder - 0 min (right after aerosol)
NaCl powder - 5 min
NaCl powder - 15 min
NaCl powder - 30 min
200
Intensity (a.u.)
Two-theta (deg.)

b

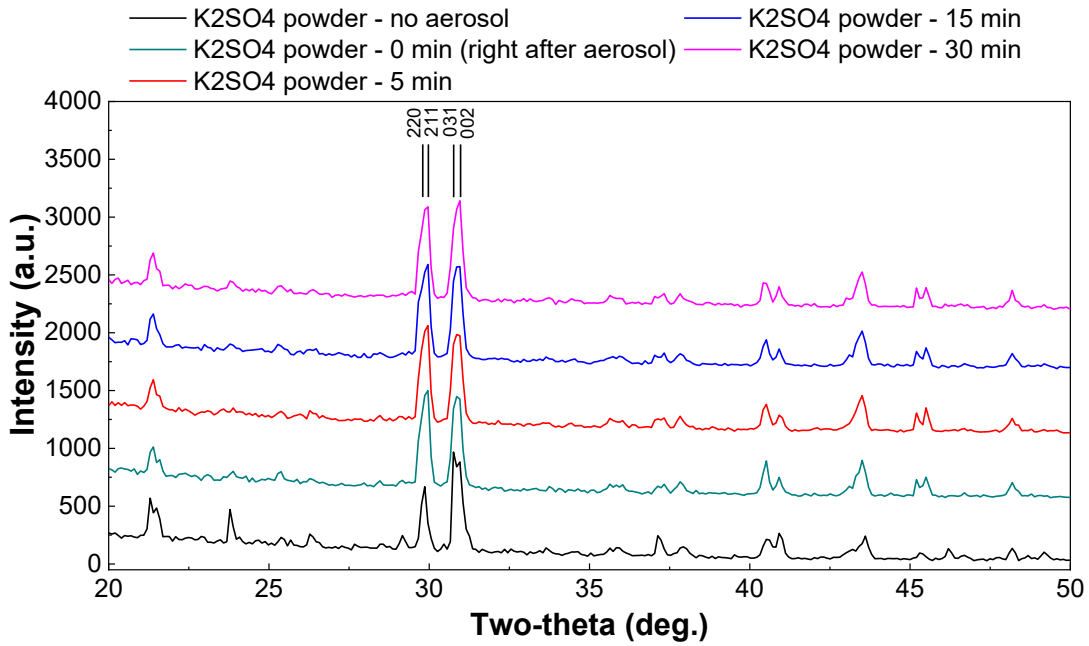
K2SO4 powder - no aerosol
K2SO4 powder - 0 min (right after aerosol)
K2SO4 powder - 5 min
K2SO4 powder - 15 min
K2SO4 powder - 30 min
220
211
031
002
Intensity (a.u.)
Two-theta (deg.)

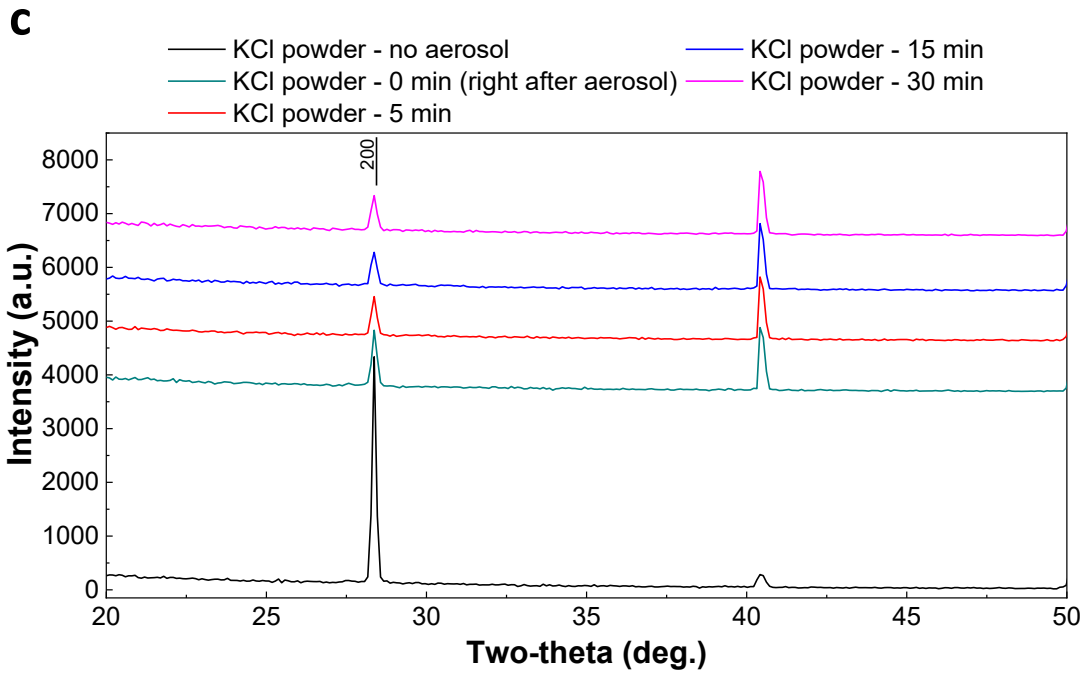

Figure 3.25 Characterization of the salt powder recrystallization. **(a-c)** XRD spectra of NaCl **(a)**, K_2SO_4 **(b)**, and KCl **(c)** powders before aerosol exposure, right after, and at 5, 15, and 30 min. Miller indices of relevant peaks corresponding to NaCl, K_2SO_4, and KCl crystals, respectively, are shown at the top of XRD spectra for each position.

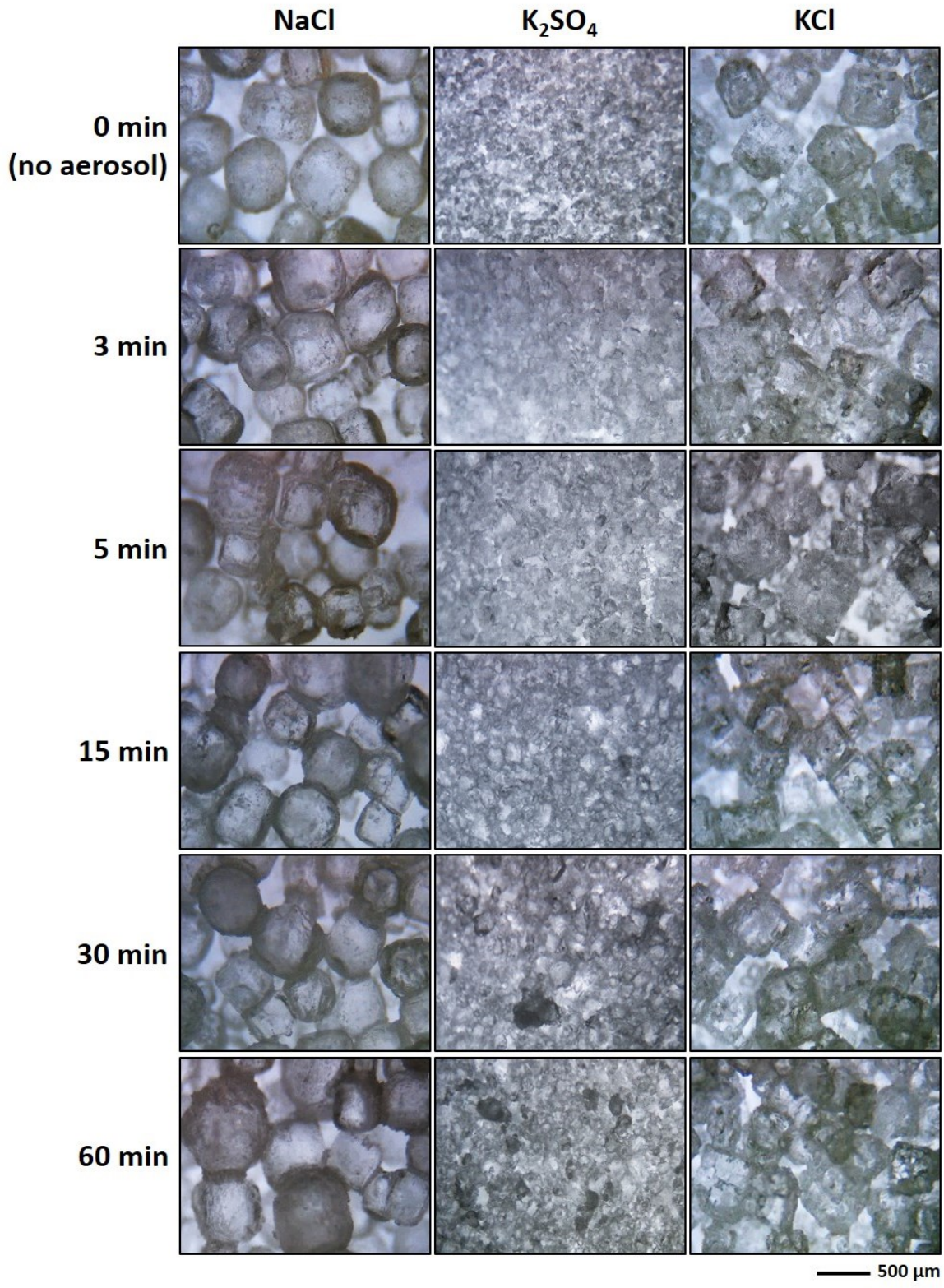

Figure 3.26 Salt powder recrystallization. Optical microscope images of NaCl (left), K_2SO_4 (center), and KCl (right) powders before aerosol exposure, and at 3, 5, 15, 30 and 60 min after exposure, showing the morphological changes during the evaporation-induced salt recrystallization.

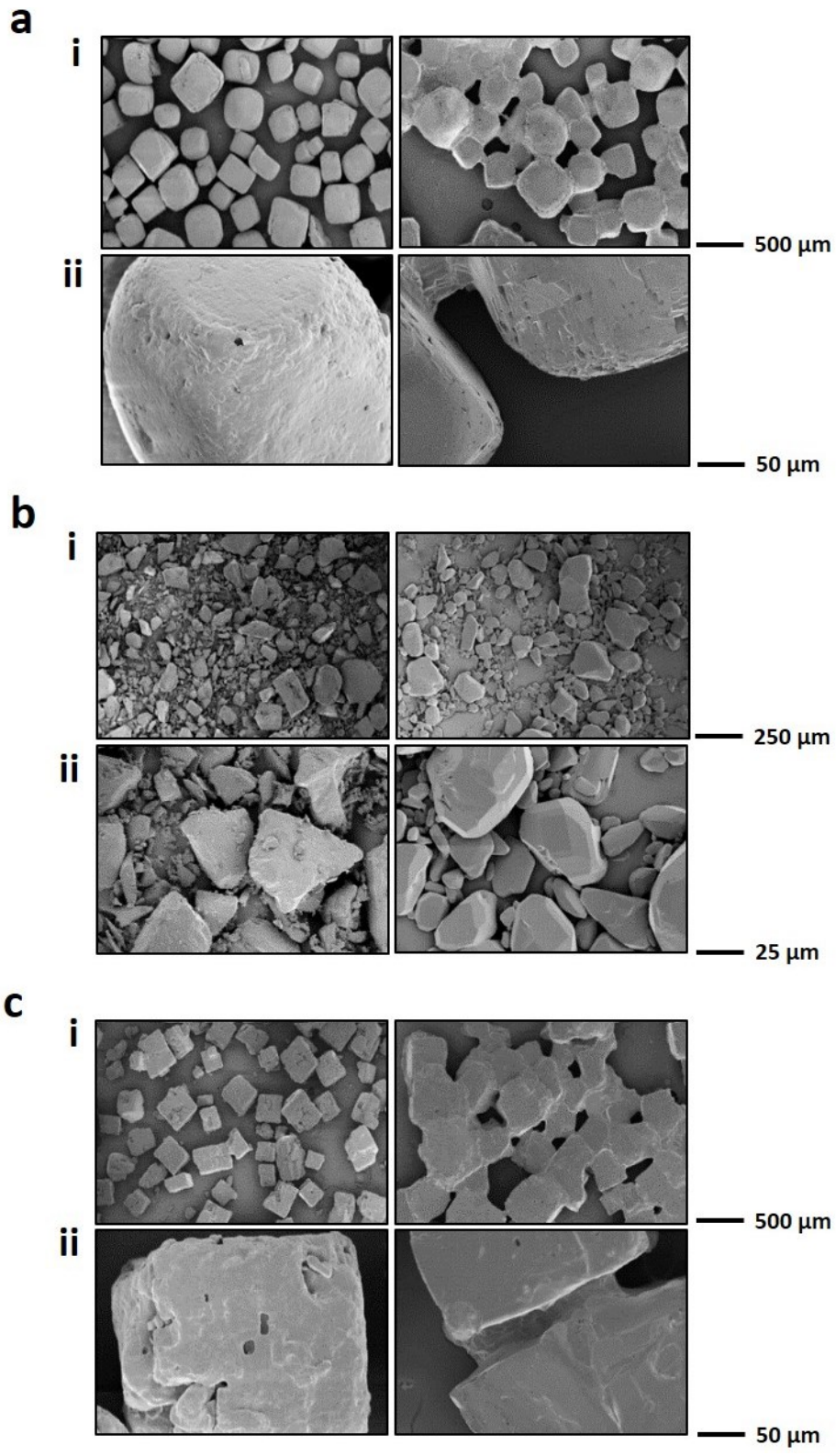

Figure 3.27 Morphological changes due to salt powder recrystallization. **(a-c)** SEM images of NaCl **(a)**, K_2SO_4 **(b)**, and KCl **(c)** powders before (left) and after (right) aerosol exposure ((i): low magnification, (ii): high magnification), showing the morphological changes due to the evaporation-induced salt recrystallization.

3.2.3.2 Pathogen inactivation on the salt powders

To investigate the pathogen inactivation mechanisms, *K. pneumoniae* was aerosolized and incubated on the salt powders. As shown in Figure 3.28a, all salt powders caused time-dependent bacteria inactivation (General Linear Model, $P < 0.001$). NaCl and KCl cause rapid inactivation within 5 min, and K_2SO_4 causes drastic 4-log CFU reduction within 15 min (one-way ANOVA, $P < 0.001$). Notably, this is consistent with the pathogen inactivation patterns previously observed on salt-coated filters. It was confirmed that the osmotic pressure due to the experimental procedure (i.e., dissolving the salts in PBS to recover the pathogens after incubation) has close to no effect on the bacteria viability (Figure 3.28b). In parallel, the effect of different levels of osmotic pressure for each salt type was tested (Figure 3.28c). Only the higher osmotic pressure levels of NaCl and KCl solutions (~saturated conditions) had an effect on bacteria viability, although only up to 1-log CFU reduction (General Linear Model, $P < 0.001$ for NaCl 26, 29 w/v% and KCl 26 w/v%, $P > 0.05$ for all other conditions). Based on the XRD and microscopy analysis over time, it was concluded that the salt recrystallization process is mainly responsible for the pathogen inactivation, although the high salt concentration during aerosol drying caused minor cell viability loss.

Additionally, the different pathogen inactivation kinetics on each salt type are in good agreement with the differences in recrystallization behaviors over time (where NaCl and KCl powders exhibit more rapid recrystallization as compared to K_2SO_4). This is explained by the crystallization kinetics of the salts. NaCl, K_2SO_4, and KCl have similar crystal growth rates R_g, in the order of 10^{-8}–10^{-7} m/s [188,194-201]. Since nucleation time can be significant for drying salt aerosols (in the order of a few minutes) [202], differing nucleation kinetics are hypothesized to be responsible for the different pathogen inactivation behaviors. Substances with higher

molecular weight show a lower nucleation order *n* [203]. The molecular weights of NaCl, K_2SO_4, and KCl are 58, 174, and 75 g/mol, respectively. Therefore:

$$n_{NaCl} > n_{KCl} \gg n_{K_2SO_4}$$

which well matches the pathogen inactivation behavior. In summary, NaCl and KCl exhibit quicker nucleation than K_2SO_4, leading to quicker overall crystallization and the earlier onset of pathogen inactivation (within 3–5 min). Within 15 min, K_2SO_4 overall crystallization is also effectively causing pathogen inactivation.

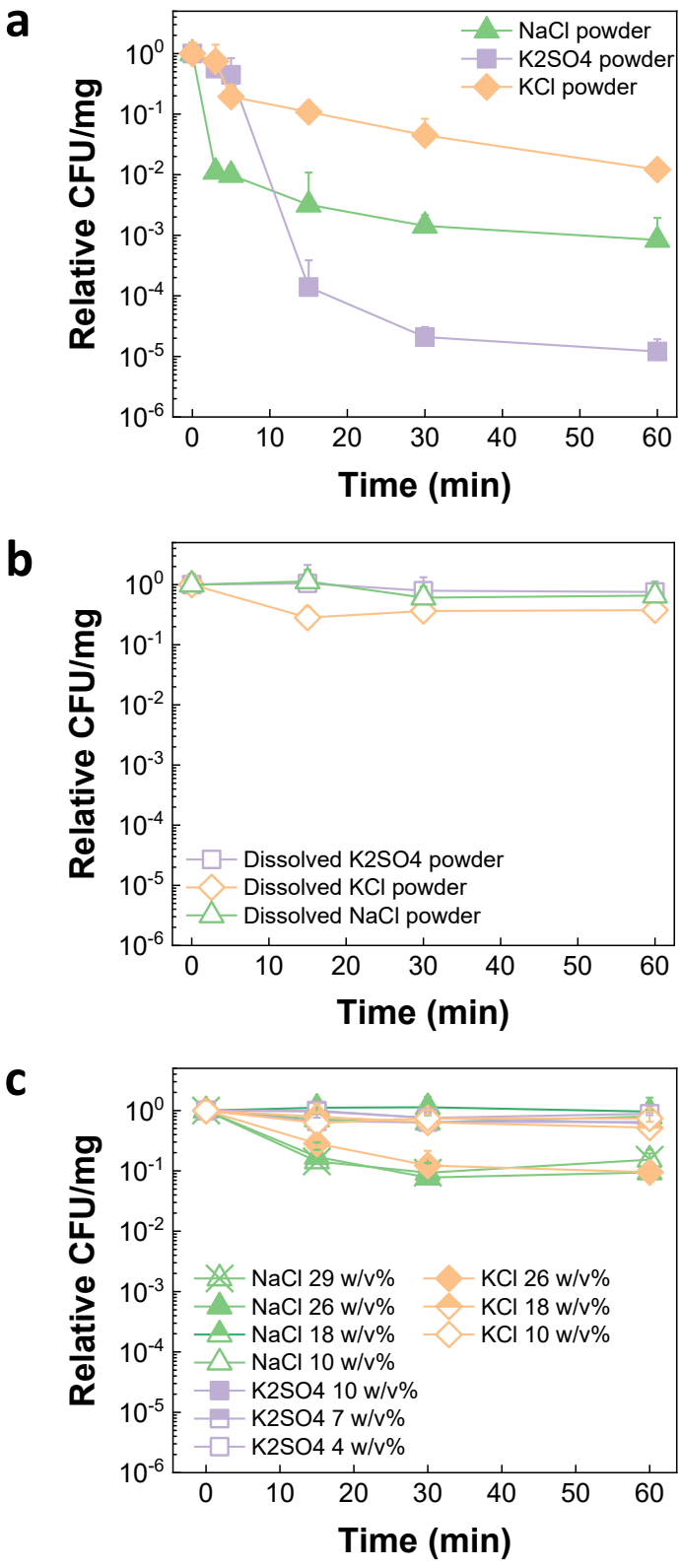

Figure 3.28 Pathogen inactivation on salt powders. **(a-c)** CFU change showing the effect of incubation time on *K. pneumoniae* exposed to NaCl, K_2SO_4, and KCl powders **(a)**, dissolved powders **(b)**, and varying osmotic pressure levels **(c)**. n = 4–20 for (a,b), and n = 3–30 for (c). For all panels: mean ± SD.

3.2.4 Conclusion

In summary, this investigation showed that the salt type-dependent pathogen inactivation rates observed on the functionalized filters are due to the different crystallization behaviors. In particular, it was found that the recrystallization of the different salt coatings over times well matches the pathogen inactivation patterns on the functionalized filters. As such, the pathogen inactivation was studied directly on the salt powders, which revealed that (i) NaCl and KCl cause pathogen inactivation earlier than K_2SO_4 (3–5 min vs. 15 min), and (ii) the differing recrystallization kinetics of the salt powders over time can explain this pathogen inactivation behavior. These differences are due to the differing nucleation rates of each salt, which are consistent with the observed results. Additionally, it was determined that the salt recrystallization constitutes the main destabilizing mechanism, although the increasing osmotic pressure experienced by the pathogens during aerosol evaporation contributes in small part to the pathogen inactivation.

4 Conclusions and future work

4.1 Conclusions

This thesis developed, produced and characterized a pathogen negation system with one-of-its-kind properties. Creating low-cost, highly effective methods for protection against infectious aerosols is a major challenge in public health. Proper respiratory protection is hampered by risk of cross infection, low filtration, low breathability, and no safe recyclability. These gaps lead to ineffective infection prevention due to contamination, shortages, and improper device use. To overcome these challenges, we hypothesized that a salt functionalization system applied to polymeric fibrous meshes would (i) yield high filtration efficiency against airborne pathogens while simultaneously not reducing breathability, and (ii) cause universal, rapid pathogen inactivation due to the salt recrystallization process induced during aerosol evaporation. In this work, salt-based coatings were developed that lead to the production of a high-performing infection prevention system. The salt coatings quickly inactivate aerosol-transported viruses and bacteria on a filter. They yielded high filtration efficiency levels, without disrupting breathability (as measured by no increase in pressure drop following application of the salt films on the surface of the fibers). The system is easily applicable to several already existing devices, such as facemasks and air filters in hospitals, congregate settings and households, and provides inexpensive, broad public and personal protection means against airborne pathogens.

In Chapter 2, the proof-of-concept system was obtained by sodium chloride coating of surgical mask filter layers and probed against aerosols of influenza virus strains. The formulation to functionalize the filter fibers was developed and has two components: surfactant and salt.

Considering the high hydrophobicity of the polypropylene fibers, the surfactant increased wetting, allowing uniform formation of continuous coating film. The salt-coated filters were demonstrated to cause destruction of influenza virus aerosols within 5 min and complete inactivation within 30 min *in vitro* due to the salt recrystallization process. The inactivation results were corroborated by the *in vivo* studies. The NaCl crystals dissolve upon exposure to aerosols; then, crystal regrowth physically disrupted the virus structure, causing infectivity loss. As this is a mechanical inactivation method, it successfully inactivated multiple influenza strains. The NaCl coating was also found to increase the filtration efficiency of the surgical mask filters, leading to complete protection in mice, and be stable after incubation at 37 °C and 70% RH.

In Chapter 3, different salt coatings were employed to functionalize inert membranes into high-performing filters against infectious respiratory diseases. Breathable large-pore membranes without functionality were turned into active filters by applying coatings of salts with different responses to environmental conditions. The salt-coated filters exhibited high filtration efficiency and breathability levels due to absorption of the aerosol particles on the coatings. They caused quick inactivation of multiple types of bacteria and influenza virus aerosols by inducing structural damage, effectively providing universal protection against airborne diseases. The exposure to high humidity levels did not compromise the salt coatings, which exhibited a further increase in pathogen inactivation due to increased surface roughness. Additionally, the pathogen inactivation mechanism was investigated by exposing bacteria aerosols to salt powders and solutions. The combination of salt recrystallization and, to a lesser extent, osmotic pressure induced by aerosol evaporation was found to cause the bacteria viability loss, as indicated by the XRD, microscopy and CFU analysis. NaCl and KCl induced the bacteria inactivation faster than K_2SO_4, which was ascribed to their faster nucleation rates.

4.2 Future work

The salt coatings developed in this work will provide an effective means for production of safe, highly effective respiratory protective devices and air filters for a number of applications. Additional parameters can be investigated to further characterize the system in regards to the scientific implications as well as the real-life conditions of use, and address outstanding challenges. Future studies will include performance evaluation under mimicked real environments using an electronically controlled continuous breathing system. This will further describe the overall response of the system when exposed to different application modes/users. Additionally, the final product will be controlled based on the performance results of different layer-to-layer designs and application considerations, such as self-decontamination, environmental conditions and overall functionality and comfort needs. From the perspective of transmission mode, the effect of pathogen-carrying droplet size will be investigated. This will allow to fully characterize the behavior of the salt-functionalization system in terms of aerosol and droplet-based disease transmission modes. A further potential venue of future research is to combine the salt coating with chemical modifications of the fibers for joint effects on the filter performance.

References

1 Riley, R. L. Airborne contagion. Historical background. *Ann. N. Y. Acad. Sci.* **353**, 3-9 (1980).

2 Hinds, W. C. *Aerosol Technology: Properties, Behavior, and Measurement of Airborne Particles* (Wiley & Sons, 1999).

3 Coia, J. E. *et al.* Guidance on the use of respiratory and facial protection equipment. *J. Hosp. Infect.* **85**, 170-182 (2013).

4 Tellier, R. Aerosol transmission of influenza A virus: a review of new studies. *J. R. Soc. Interface* **6**, S783-790 (2009).

5 CCOHS. *How Do Particulates Enter the Respiratory System?*, <https://www.ccohs.ca/oshanswers/chemicals/how_do.html> (2012).

6 Sattar, S. A. & Ijaz, M. K. Spread of viral-infections by aerosols. *Crit. Rev. Environ. Sci. Technol.* **17**, 89-131 (1987).

7 Weber, T. P. & Stilianakis, N. I. Inactivation of influenza A viruses in the environment and modes of transmission: a critical review. *J. Infect.* **57**, 361-373 (2008).

8 Xie, X., Li, Y., Chwang, A. T., Ho, P. L. & Seto, W. H. How far droplets can move in indoor environments–revisiting the Wells evaporation-falling curve. *Indoor Air* **17**, 211-225 (2007).

9 Weber, A. *et al.* Aerosol penetration and leakage characteristics of masks used in the health care industry. *Am. J. Infect. Control* **21**, 167-173 (1993).

10 Derrick, J. L. & Gomersall, C. D. Protecting healthcare staff from severe acute respiratory syndrome: filtration capacity of multiple surgical masks. *J. Hosp. Infect.* **59**, 365-368 (2005).

11 van Doremalen, N. *et al.* Aerosol and surface stability of SARS-CoV-2 as compared with SARS-CoV-1. *N. Engl. J. Med.* (2020).

12 Zhen-Dong, G. *et al.* Aerosol and surface distribution of severe acute respiratory syndrome coronavirus 2 in hospital wards, Wuhan, China, 2020. *Emerging Infect. Dis.* **26** (2020).

13 Alford, R. H., Kasel, J. A., Gerone, P. J. & Knight, V. Human influenza resulting from aerosol inhalation. *Proc. Soc. Exp. Biol. Med.* **122**, 800-804 (1966).

14 Bunyan, D., Ritchie, L., Jenkins, D. & Coia, J. E. Respiratory and facial protection: a critical review of recent literature. *J. Hosp. Infect.* **85**, 165-169 (2013).

15 Grinn-Gofron, A., Strzelczak, A. & Wolski, T. The relationships between air pollutants, meteorological parameters and concentration of airborne fungal spores. *Environ. Pollut.* **159**, 602-608 (2011).

16 Tang, J. W. The effect of environmental parameters on the survival of airborne infectious agents. *J. R. Soc. Interface* **6**, S737-746 (2009).

17 Wu, Y. & Yao, M. S. Inactivation of bacteria and fungus aerosols using microwave irradiation. *J. Aerosol Sci.* **41**, 682-693 (2010).

18 Hemmes, J. H., Winkler, K. C. & Kool, S. M. Virus survival as a seasonal factor in influenza and poliomyelitis. *Nature* **188**, 430-431 (1960).

19 Tellier, R. Review of aerosol transmission of influenza A virus. *Emerg. Infect. Dis.* **12**, 1657-1662 (2006).

20 Bean, B. *et al.* Survival of influenza viruses on environmental surfaces. *J. Infect. Dis.* **146**, 47-51 (1982).

21 Shiomori, T., Miyamoto, H. & Makishima, K. Significance of airborne transmission of methicillin-resistant *Staphylococcus aureus* in an otolaryngology–head and neck surgery unit. *Arch. Otolaryngol. Head Neck Surg.* **127**, 644-648 (2001).

22 WHO. *Antimicrobial Resistance: Global Report on Surveillance* (World Health Organization, 2014).

23 Sievert, D. M. *et al.* Antimicrobial-resistant pathogens associated with healthcare-associated infections: summary of data reported to the National Healthcare Safety Network at the Centers for Disease Control and Prevention, 2009-2010. *Infect. Control Hosp. Epidemiol.* **34**, 1-14 (2013).

24 Nichol, K. A. *et al.* Changing epidemiology of methicillin-resistant *Staphylococcus aureus* in Canada. *J. Antimicrob. Chemother.* **68**, 47-55 (2013).

25 Lledo, W. *et al.* Guidance for control of infections with carbapenem-resistant or carbapenemase-producing *Enterobacteriaceae* in acute care facilities. *MMWR Morb. Mortal. Wkly Rep.* **10**, 256-260 (2009).

26 WHO. *Antimicrobial Resistance*, <http://www.who.int/mediacentre/factsheets/fs194/en/> (2018).

27 Beggs, C. B. The airborne transmission of infection in hospital buildings: fact or fiction? *Indoor Built Environ.* **12**, 9-18 (2003).

28 Kibbler, C. C., Quick, A. & O'Neill, A. M. The effect of increased bed numbers on MRSA transmission in acute medical wards. *J. Hosp. Infect.* **39**, 213-219 (1998).

29 Schaal, K. P. Medical and microbiological problems arising from airborne infection in hospitals. *J. Hosp. Infect.* **18**, 451-459 (1991).

30 WHO. *Global Tuberculosis Report 2019* (World Health Organization, 2019).

31 Riley, R. L., Wells, W. F., Mills, C. C., Nyka, W. & Mclean, R. L. Air hygiene in tuberculosis—quantitative studies of infectivity and control in a pilot ward—cooperative study between the Veterans Administration, the Johns-Hopkins-University School of Hygiene and Public Health, and the Maryland-Tuberculosis-Association. *Am Rev Tuberc Pulm* **75**, 420-431 (1957).

32 Moro, M. L. *et al.* An outbreak of multidrug-resistant tuberculosis involving HIV-infected patients of two hospitals in Milan, Italy. *AIDS* **12**, 1095-1102 (1998).

33 Gandhi, N. R. *et al.* Nosocomial transmission of extensively drug-resistant tuberculosis in a rural hospital in South Africa. *J. Infect. Dis.* **207**, 9-17 (2013).

34 Mongkolrattanothai, T., Lambert, L. A. & Winston, C. A. Tuberculosis among healthcare personnel, United States, 2010–2016. *Infect. Control Hosp. Epidemiol.* **40**, 701-704 (2019).

35 Oberg, T. & Brosseau, L. M. Surgical mask filter and fit performance. *Am. J. Infect. Control* **36**, 276-282 (2008).

36 Cohen, H. J. & Birkner, J. S. Respiratory protection. *Clin. Chest Med.* **33**, 783-793 (2012).

37 Bollinger, N. J. & Schutz, R. H. *NIOSH Guide to Industrial Respiratory Protection* (Publications Dissemination, DSDTT, 1987).

38 Martyny, J., Glazer, C. S. & Newman, L. S. Respiratory protection. *N. Engl. J. Med.* **347**, 824-830 (2002).

39 FDA, Guidance for Industry and FDA Staff: Surgical Masks—Premarket Notification [510(k)] Submissions (2004).

40 ASTM International, ASTM F1862 / F1862M - 13. Standard Test Method for Resistance of Medical Face Masks to Penetration by Synthetic Blood (Horizontal Projection of Fixed Volume at a Known Velocity) (2013).

41 Underwriters Laboratories, UL 2154 Fire Tests of Surgical Fabric (2000).

42 Consumer Product Safety Commission, 16 CFR Part 1610. Standard for the Flammability of Clothing Textiles (2008).

43 Gruendemann, B. J. & Mangum, S. S. *Infection Prevention in Surgical Settings* (Elsevier Health Sciences, 2001).

44 ASTM International, ASTM F1215-89. Test Method for Determining the Initial Efficiency of a Flatsheet Filter Medium in an Airflow Using Latex Spheres (Withdrawn 1998) (1989).

45 ASTM International, ASTM F2299 / F2299M - 03(2010). Standard Test Method for Determining the Initial Efficiency of Materials Used in Medical Face Masks to Penetration by Particulates Using Latex Spheres (2010).

46 Greene, V. W. & Vesley, D. Method for evaluating effectiveness of surgical masks. *J. Bacteriol.* **83**, 663-667 (1962).

47 ASTM International, ASTM F2101 - 14 Standard Test Method for Evaluating the Bacterial Filtration Efficiency (BFE) of Medical Face Mask Materials, Using a Biological Aerosol of *Staphylococcus aureus* (2014).

48 ASTM International, ASTM F2101 - 19, Standard Test Method for Evaluating the Bacterial Filtration Efficiency (BFE) of Medical Face Mask Materials, Using a Biological Aerosol of *Staphylococcus aureus* (2019).

49 Military Specification, MIL-M-36945C 4.4.1.1.1, Method 1 Military Specifications: Surgical Mask, Disposable (1975).

50 NIOSH. *Standard Respirator Testing Procedures. Air-Purifying Respirators*, <http://www.cdc.gov/niosh/npptl/stps/apresp.html> (2014).

51 NIOSH, Determination of Particulate Filter Efficiency Level for R100 Series Filter Against Liquid Particulates for Non-Powered, Air-Purifying Respirators Standard Testing Procedure (STP) (2016).

52 NIOSH, Determination of Particulate Filter Efficiency Level for R99 Series Filter Against Liquid Particulates for Non-Powered, Air-Purifying Respirators Standard Testing Procedure (STP) (2016).

53 NIOSH, Determination of Particulate Filter Efficiency Level for P100 Series Filter Against Liquid Particulates for Non-Powered, Air-Purifying Respirators Standard Testing Procedure (STP) (2016).

54 NIOSH, Determination of Particulate Filter Efficiency Level for N99 Series Filter Against Liquid Particulates for Non-Powered, Air-Purifying Respirators Standard Testing Procedure (STP) (2016).

55 NIOSH, Determination of Particulate Filter Efficiency Level for N100 Series Filter Against Liquid Particulates for Non-Powered, Air-Purifying Respirators Standard Testing Procedure (STP) (2016).

56 NIOSH, Determination of Particulate Filter Efficiency Level for R95 Series Filter Against Liquid Particulates for Non-Powered, Air-Purifying Respirators Standard Testing Procedure (STP) (2016).

57 NIOSH, Determination of Particulate Filter Efficiency Level for P95 Series Filter Against Liquid Particulates for Non-Powered, Air-Purifying Respirators Standard Testing Procedure (STP) (2016).

58 NIOSH, Determination of Particulate Filter Efficiency Level for N95 Series Filter Against Liquid Particulates for Non-Powered, Air-Purifying Respirators Standard Testing Procedure (STP) (2016).

59 NIOSH, Determination of Particulate Filter Efficiency Level for P99 Series Filter Against Liquid Particulates for Non-Powered, Air-Purifying Respirators Standard Testing Procedure (STP) (2016).

60 Flagan, R. C. & Seinfeld, J. H. *Removal of Particles from Gas Streams. Fundamentals of Air Pollution Engineering* (Prentice-Hall, Inc., 1988).

61 Zhu, C., Lin, C. H. & Cheung, C. S. Inertial impaction-dominated fibrous filtration with rectangular or cylindrical fibers. *Powder Technol.* **112**, 149-162 (2000).

62 Stenhouse, J. I. T., Gradon, L. & Marijnissen, J. C. M. *Electret Filters, Production and Properties; Proceedings of the International Workshop on Electret Filters, Production and Properties, Warsaw, Poland, January 29 and 30, 1999* (Delft University Press, 1999).

63 Natanson, G. L. Diffusional precipitation of aerosols on a streamlined cylinder with a small capture coefficient. *Proc. Acad. Sci. USSR, Phys. Chem. Sec* **112**, 21-25 (1957).

64 Langmuir, I. *Report on Smokes and Filters* (Pergamon Press, 1961).

65 Friedlander, S. K. Mass and heat transfer to single spheres and cylinders at low Reynolds numbers. *AIChE J.* **3**, 43-48 (1957).

66 Stechkina, I. B. & Fuchs, N. A. Studies on fibrous aerosol filters—I. Calculation of diffusional deposition of aerosols in fibrous filters. *Ann. Occup. Hyg.* **9**, 59-64 (1966).

67 Lee, K. W. & Liu, B. Y. H. Theoretical study of aerosol filtration by fibrous filters. *Aerosol Sci. Technol.* **1**, 147-161 (1982).

68 Spielman, L. & Goren, S. L. Model for predicting pressure drop and filtration efficiency in fibrous media. *Environ. Sci. Technol.* **2**, 279-287 (1968).

69 Shapiro, M., Gutfinger, C. & Laufer, G. Electrostatic mechanisms of aerosol collection by granular filters—a review. *J. Aerosol Sci.* **19**, 651-677 (1988).

70 Ranz, W. E. & Wong, J. B. Impaction of dust and smoke particles on ourface and body collectors. *Ind. Eng. Chem.* **44**, 1371-1381 (1952).

71 Kraemer, H. F. & Johnstone, H. F. Collection of aerosol particles in presence of electrostatic fields. *Ind. Eng. Chem.* **47**, 2426-2434 (1955).

72 Belkin, N. L. The evolution of the surgical mask: filtering efficiency versus effectiveness. *Infect. Control Hosp. Epidemiol.* **18**, 49-57 (1997).

73 Lenhart, S. W., Seitz, T., Trout, D. & Bollinger, N. Issues affecting respirator selection for workers exposed to infectious aerosols: emphasis on healthcare settings. *Appl. Biosaf.* **9**, 20-36 (2004).

74 Seto, W. H. *et al.* Effectiveness of precautions against droplets and contact in prevention of nosocomial transmission of severe acute respiratory syndrome (SARS). *Lancet* **361**, 1519-1520 (2003).

75 Goodwin, R., Haque, S., Neto, F. & Myers, L. B. Initial psychological responses to influenza A, H1N1 ("Swine flu"). *BMC Infect. Dis.* **9**, 166 (2009).

76 Lau, J. T., Griffiths, S., Choi, K. C. & Tsui, H. Y. Widespread public misconception in the early phase of the H1N1 influenza epidemic. *J. Infect.* **59**, 122-127 (2009).

77 Fitzgerald, D. A. Human swine influenza A [H1N1]: practical advice for clinicians early in the pandemic. *Paediatr. Respir. Rev.* **10**, 154-158 (2009).

78 Elachola, H., Assiri, A. M. & Memish, Z. A. Mass gathering-related mask use during 2009 pandemic influenza A (H1N1) and Middle East respiratory syndrome coronavirus. *Int. J. Infect. Dis.* **20**, 77-78 (2014).

79 Zumla, A. & Hui, D. S. Infection control and MERS-CoV in health-care workers. *Lancet* **383**, 1869-1871 (2014).

80 Feng, S. *et al.* Rational use of face masks in the COVID-19 pandemic. *Lancet Respir. Med.* (2020).

81 Balazy, A. *et al.* Do N95 respirators provide 95% protection level against airborne viruses, and how adequate are surgical masks? *Am. J. Infect. Control* **34**, 51-57 (2006).

82 Loeb, M. *et al.* Surgical mask vs N95 respirator for preventing influenza among health care workers: a randomized trial. *JAMA* **302**, 1865-1871 (2009).

83 Huang, C.-Y., Sun, C.-T., Hsieh, J.-L. & Lin, H. Simulating SARS: small-world epidemiological modeling and public health policy assessments. *J. Artif. Soc. Soc. Simul.* **7** (2004).

84 Chung, S. J., Ling, M. L., Seto, W. H., Ang, B. S. & Tambyah, P. A. Debate on MERS-CoV respiratory precautions: surgical mask or N95 respirators? *Singapore Med. J.* **55**, 294-297 (2014).

85 Diaz, K. T. & Smaldone, G. C. Quantifying exposure risk: surgical masks and respirators. *Am. J. Infect. Control* **38**, 501-508 (2010).

86 Chen, C.-C. & Willeke, K. Aerosol penetration through surgical masks. *Am. J. Infect. Control* **20**, 177-184 (1992).

87 Simmerman, J. M. *et al.* Findings from a household randomized controlled trial of hand washing and face masks to reduce influenza transmission in Bangkok, Thailand. *Influenza Other Respir. Viruses* **5**, 256-267 (2011).

88 Tang, J. W., Liebner, T. J., Craven, B. A. & Settles, G. S. A schlieren optical study of the human cough with and without wearing masks for aerosol infection control. *J. R. Soc. Interface* **6**, S727-736 (2009).

89 Cowling, B. J., Zhou, Y., Ip, D. K., Leung, G. M. & Aiello, A. E. Face masks to prevent transmission of influenza virus: a systematic review. *Epidemiol. Infect.* **138**, 449-456 (2010).

90 MacIntyre, C. R. *et al.* A cluster randomized clinical trial comparing fit-tested and non-fit-tested N95 respirators to medical masks to prevent respiratory virus infection in health care workers. *Influenza Other Respir. Viruses* **5**, 170-179 (2011).

91 Baer, E. T. Iatrogenic meningitis: the case for face masks. *Clin. Infect. Dis.* **31**, 519-521 (2000).

92 Chellamani, K. P., Veerasubramanian, D. & Vignesh Balaji, R. S. Surgical face masks: manufacturing methods and classification. *JAIR* **2**, 320-324 (2013).

93 Maturaporn, T. *Disposable Face Mask with Multiple Liquid Resistant Layers* US patent 5467765 A (1995).

94 Davison, A. M. Pathogen inactivation and filtration efficacy of a new anti-microbial and anti-viral surgical facemask and N95 against dentistry-associated microorganisms. *International dentistry Australasian edition* **7**, 36-42 (2012).

95 Li, Y. *et al. In vivo* protective performance of N95 respirator and surgical facemask. *Am. J. Ind. Med.* **49**, 1056-1065 (2006).

96 Hegde, R. R., Dahiya, A. & Kamath, M. G. *Olefin Fiber*, <https://web.archive.org/web/20080407003419/http://web.utk.edu/~mse/pages/Textiles/Olefin%20fibers.htm> (2004).

97 Kamath, M. G., Dahiya, A. & Hegde, R. R. *Development of Metallocene Based Polypropylene*, <https://web.archive.org/web/20080407003419/http://web.utk.edu/~mse/pages/Textiles/Olefin%20fibers.htm> (2004).

98 Ellison, C. J., Phatak, A., Giles, D. W., Macosko, C. W. & Bates, F. S. Melt blown nanofibers: fiber diameter distributions and onset of fiber breakup. *Polymer* **48**, 3306-3316 (2007).

99 Kothari, V. K. *Technical Textiles: Technology, Developments and Applications* (IAFL Publications, 2008).

100 Crosstex. *MaskEnomics: The Crosstex Guide to Face Mask Selection and Use*, <https://www.crosstex.com/sites/default/files/public/educational-resources/technical-specifications/maskenomics_2.pdf> (2014).

101 FDA. FLUIDSHIELD Surgical Mask with Expanded Chamber. Section 510(k) Premarket Notification (2015).

102 Nanjundappa, R. & Bhat, G. S. Effect of processing conditions on the structure and properties of polypropylene spunbond fabrics. *J. Appl. Polym. Sci.* **98**, 2355-2364 (2005).

103 Kamath, M. G., Dahiya, A. & Hegde, R. R. *Thermal Bonding of Nonwoven Fabrics*, <https://web.archive.org/web/20161204203040/http://www.engr.utk.edu/mse/Textiles/Thermal%20Bonding.htm> (2004).

104 Dahiya, A., Kamath, M. G. & Hegde, R. R. *Melt Blown Technology*, <https://web.archive.org/web/20161021060047/http://www.engr.utk.edu/mse/Textiles/Melt%20Blown%20Technology.htm> (2004).

105 Bird, W. *Surgical Face Mask* US patent 3802429 A (1974).

106 Skaria, S. D. & Smaldone, G. C. Respiratory source control using surgical masks with nanofiber media. *Ann. Occup. Hyg.* **58**, 771-781 (2014).

107 Shokri, A. *et al.* Evaluation of physical characteristics and particulate filtration efficiency of surgicalmasks used in Iran's hospitals. *IJOH* **7**, 10-16 (2015).

108 Leonas, K. K., Jones, C. R. & Hall, D. The relationship of fabric properties and bacterial filtration efficiency for selected surgical face masks. *JTATM* **3**, 1-8 (2003).

109 Qian, Y., Willeke, K., Grinshpun, S. A. & Donnelly, J. Performance of N95 respirators: reaerosolization of bacteria and solid particles. *Am. Ind. Hyg. Assoc. J.* **58**, 876-880 (1997).

110 OSHA. *Respirator Types*, <https://www.osha.gov/video/respiratory_protection/resptypes_transcript.html> (2012).

111 NIOSH. *42 CFR Part 84 Respiratory Protective Devices*, <http://www.cdc.gov/niosh/npptl/topics/respirators/pt84abs2.html> (1997).

112 Borkow, G., Zhou, S. S., Page, T. & Gabbay, J. A novel anti-influenza copper oxide containing respiratory face mask. *Plos One* **5**, e11295 (2010).

113 Viscusi, D. J., Bergman, M. S., Eimer, B. C. & Shaffer, R. E. Evaluation of five decontamination methods for filtering facepiece respirators. *Ann. Occup. Hyg.* **53**, 815-827 (2009).

114 Balazy, A. *et al.* Manikin-based performance evaluation of N95 filtering-facepiece respirators challenged with nanoparticles. *Ann. Occup. Hyg.* **50**, 259-269 (2006).

115 Fisher, E. M., Richardson, A. W., Harpest, S. D., Hofacre, K. C. & Shaffer, R. E. Reaerosolization of MS2 bacteriophage from an N95 filtering facepiece respirator by simulated coughing. *Ann. Occup. Hyg.* **56**, 315-325 (2012).

116 Roberge, R. J. *et al.* Effect of exhaled moisture on breathing resistance of N95 filtering facepiece respirators. *Ann. Occup. Hyg.* **54**, 671-677 (2010).

117 Chen, S.-C., Wang, J., Bahk, Y. K., Fissan, H. & Pui, D. Y. H. Carbon nanotube penetration through fiberglass and electret respirator filter and nuclepore filter media: experiments and models. *Aerosol Sci. Technol.* **48**, 997-1008 (2014).

118 Fjeld, R. A. & Owens, T. M. The effect of particle charge on penetration in an electret filter. *IEEE Trans. Ind. Appl.* **24**, 725-731 (1988).

119 Tsai, P. P., Schreuder-Gibson, H. & Gibson, P. Different electrostatic methods for making electret filters. *J. Electrostat.* **54**, 333-341 (2002).

120 Yang, Z. Z., Lin, J. H., Tsai, I. S. & Kuo, T. Y. Particle filtration with an electret of nonwoven polypropylene fabric. *Text. Res. J.* **72**, 1099-1104 (2002).

121 Wiwanitkit, V. N-95 face mask for prevention of bird flu virus: an appraisal of nanostructure and implication for infectious control. *Lung* **184**, 373-374 (2006).

122 Kravtsov, A. G. & Brunig, H. Characteristics of electret charge formation in polypropylene fibres. *Fibre Chem.* **32**, 180-186 (2000).

123 Huang, C., Willeke, K., Qian, Y., Grinshpun, S. & Ulevicius, V. Method for measuring the spatial variability of aerosol penetration through respirator filters. *Am. Ind. Hyg. Assoc. J.* **59**, 461-465 (1998).

124 Lee, S. A., Grinshpun, S. A. & Reponen, T. Respiratory performance offered by N95 respirators and surgical masks: human subject evaluation with NaCl aerosol representing bacterial and viral particle size range. *Ann. Occup. Hyg.* **52**, 177-185 (2008).

125 OSHA. Assigned Protection Factors for the Revised Respiratory Protection Standard (2009).

126 WHO. *Influenza (Seasonal)*, <https://www.who.int/en/news-room/fact-sheets/detail/influenza-(seasonal)> (2018).

127 CDC. *Past Pandemics*, <https://www.cdc.gov/flu/pandemic-resources/basics/past-pandemics.html> (2018).

128 Murray, C. J., Lopez, A. D., Chin, B., Feehan, D. & Hill, K. H. Estimation of potential global pandemic influenza mortality on the basis of vital registry data from the 1918-20 pandemic: a quantitative analysis. *Lancet* **368**, 2211-2218 (2006).

129 Ferguson, N. M. *et al.* Strategies for mitigating an influenza pandemic. *Nature* **442**, 448-452 (2006).

130 Peiris, J. S., Guan, Y. & Yuen, K. Y. Severe acute respiratory syndrome. *Nat. Med.* **10**, S88-97 (2004).

131 Coulliette, A. D., Perry, K. A., Edwards, J. R. & Noble-Wang, J. A. Persistence of the 2009 pandemic influenza A (H1N1) virus on N95 respirators. *Appl. Environ. Microbiol.* **79**, 2148-2155 (2013).

132 Birkner, J. S., Fung, D., Hinds, W. C. & Kennedy, N. J. Particle release from respirators, part I: determination of the effect of particle size, drop height, and load. *J. Occup. Environ. Hyg.* **8**, 1-9 (2011).

133 Viscusi, D. J., King, W. P. & Shaffer, R. E. Effect of decontamination on the filtration efficiency of two filtering facepiece respirator models. *J. Int. Soc. Respir. Prot.* **24**, 93-107 (2007).

134 Salter, W. B. *et al.* Analysis of residual chemicals on filtering facepiece respirators after decontamination. *J. Occup. Environ. Hyg.* **7**, 437-445 (2010).

135 Grinshpun, S. A. *et al.* Performance of an N95 filtering facepiece particulate respirator and a surgical mask during human breathing: two pathways for particle penetration. *J. Occup. Environ. Hyg.* **6**, 593-603 (2009).

136 Li, Y. *et al.* Effects of wearing N95 and surgical facemasks on heart rate, thermal stress and subjective sensations. *Int. Arch. Occup. Environ. Health.* **78**, 501-509 (2005).

137 Farquharson, C. & Baguley, K. Responding to the severe acute respiratory syndrome (SARS) outbreak: lessons learned in a Toronto emergency department. *J. Emerg. Nurs.* **29**, 222-228 (2003).

138 Radonovich, L. J., Cheng, J., Shenal, B. V., Hodgson, M. & Bender, B. S. Respirator tolerance in health care workers. *JAMA* **301**, 36-38 (2009).

139 Luximon, Y., Anne Sheen, K. & Luximon, A. Time dependent infrared thermographic evaluation of facemasks. *Work* **54**, 825-835 (2016).

140 Harber, P. *et al.* Respirator physiologic impact in persons with mild respiratory disease. *J. Occup. Environ. Med.* **52**, 155-162 (2010).

141 Rengasamy, A., Zhuang, Z. & Berryann, R. Respiratory protection against bioaerosols: literature review and research needs. *Am. J. Infect. Control* **32**, 345-354 (2004).

142 Barhate, R. & Ramakrishna, S. Nanofibrous filtering media: filtration problems and solutions from tiny materials. *J. Memb. Sci.* **296**, 1-8 (2007).

143 Urbaniak-Domagala, W., Wrzosek, H., Szymanowski, H., Majchrzycka, K. & Brochocka, A. Plasma modification of filter nonwovens used for the protection of respiratory tracts. *Fibres Text. East. Eur.* **18**, 94-99 (2010).

144 Tiliket, G. *et al.* A new material for airborne virus filtration. *Chem. Eng. J.* **173**, 341-351 (2011).

145 Zhang, Q. *et al.* Improvement in nanofiber filtration by multiple thin layers of nanofiber mats. *J. Aerosol Sci.* **41**, 230-236 (2010).

146 Podgorski, A., Balazy, A. & Gradon, L. Application of nanofibers to improve the filtration efficiency of the most penetrating aerosol particles in fibrous filters. *Chem. Eng. Sci.* **61**, 6804-6815 (2006).

147 Qin, X. H. & Wang, S. Y. Filtration properties of electrospinning nanofibers. *J. Appl. Polym. Sci.* **102**, 1285-1290 (2006).

148 Ratnesar-Shumate, S. *et al.* Evaluation of physical capture efficiency and disinfection capability of an iodinated biocidal filter medium. *Aerosol Air Qual. Res.* **8**, 1-18 (2008).

149 Estrela, C. *et al.* Mechanism of action of sodium hypochlorite *Braz. Dent. J.* **13** 113-117 (2002).

150 Hui, F. & Debiemme-Chouvy, C. Antimicrobial N-halamine polymers and coatings: a review of their synthesis, characterization, and applications. *Biomacromolecules* **14**, 585-601 (2013).

151 Badrossamay, M. R. & Sun, G. Acyclic halamine polypropylene polymer: effect of monomer structure on grafting efficiency, stability and biocidal activities. *React. Funct. Polym.* **68**, 1636-1645 (2008).

152 Zhao, N. & Liu, S. Thermoplastic semi-IPN of polypropylene (PP) and polymeric N-halamine for efficient and durable antibacterial activity. *Eur. Polym. J.* **47**, 1654-1663 (2011).

153 Cerkez, I., Worley, S. D., Broughton, R. M. & Huang, T. S. Antimicrobial surface coatings for polypropylene nonwoven fabrics. *React. Funct. Polym.* **73**, 1412-1419 (2013).

154 Lee, J. H., Wu, C. Y., Wysocki, K. M., Farrah, S. & Wander, J. Efficacy of iodine-treated biocidal filter media against bacterial spore aerosols. *J. Appl. Microbiol.* **105**, 1318-1326 (2008).

155 Tseng, C. C., Pan, Z. M. & Chang, C. H. Application of a quaternary ammonium agent on surgical face masks before use for pre-decontamination of nosocomial infection-related bioaerosols. *Aerosol Sci. Technol.* **50**, 199-210 (2016).

156 Borkow, G. & Gabbay, J. Putting copper into action: copper-impregnated products with potent biocidal activities. *FASEB J.* **18**, 1728-1730 (2004).

157 Li, Y., Leung, P., Yao, L., Song, Q. W. & Newton, E. Antimicrobial effect of surgical masks coated with nanoparticles. *J. Hosp. Infect.* **62**, 58-63 (2006).

158 Rengasamy, S., Fisher, E. & Shaffer, R. E. Evaluation of the survivability of MS2 viral aerosols deposited on filtering face piece respirator samples incorporating antimicrobial technologies. *Am. J. Infect. Control* **38**, 9-17 (2010).

159 Kamiyama, Y. *et al.* Protection from avian influenza H5N1 virus infection with antibody-impregnated filters. *Virol. J.* **8**, 54 (2011).

160 Nicas, M. & Best, D. A study quantifying the hand-to-face contact rate and its potential application to predicting respiratory tract infection. *J. Occup. Environ. Hyg.* **5**, 347-352 (2008).

161 Duy, J. *et al.* Circulating microRNA profiles of Ebola virus infection. *Sci. Rep.* **6**, 24496 (2016).

162 Morse, S. S., Garwin, R. L. & Olsiewski, P. J. Public health. Next flu pandemic: what to do until the vaccine arrives? *Science* **314**, 929 (2006).

163 CDC. Laboratory performance evaluation of N95 filtering facepiece respirators, 1996. *MMWR Morb. Mortal. Wkly Rep.* **47**, 1045 (1998).

164 Duarte Fo, O. B., Marra, W. D., Kachan, G. C. & Coury, J. R. Filtration of electrified solid particles. *Ind. Eng. Chem. Res.* **39**, 3884-3895 (2000).

165 Siegel, J. D., Rhinehart, E., Jackson, M., Chiarello, L. & Health Care Infection Control Practices Advisory Committee. 2007 Guideline for isolation precautions: preventing transmission of infectious agents in health care settings. *Am. J. Infect. Control* **35**, S65-164 (2007).

166 Lee, J. H. *et al.* Assessment of iodine-treated filter media for removal and inactivation of MS2 bacteriophage aerosols. *J. Appl. Microbiol.* **107**, 1912-1923 (2009).

167 Lore, M. B. *et al.* Performance of conventional and antimicrobial-treated filtering facepiece respirators challenged with biological aerosols. *J. Occup. Environ. Hyg.* **9**, 69-80 (2012).

168 Song, J. M. *et al.* Protective immunity against H5N1 influenza virus by a single dose vaccination with virus-like particles. *Virology* **405**, 165-175 (2010).

169 Quan, F. S. *et al.* A bivalent influenza VLP vaccine confers complete inhibition of virus replication in lungs. *Vaccine* **26**, 3352-3361 (2008).

170 Windisch, W., Hennings, E., Sorichter, S., Hamm, H. & Criée, C. P. Peak or plateau maximal inspiratory mouth pressure: which is best? *Eur. Respir. J.* **23**, 708-713 (2004).

171 Choi, H. J. *et al.* Stability of influenza vaccine coated onto microneedles. *Biomaterials* **33**, 3756-3769 (2012).

172 Choi, H. J., Ebersbacher, C. F., Kim, M. C., Kang, S. M. & Montemagno, C. D. A mechanistic study on the destabilization of whole inactivated influenza virus vaccine in gastric environment. *Plos One* **8**, e66316 (2013).

173 Greenspan, P., Mayer, E. P. & Fowler, S. D. Nile red: a selective fluorescent stain for intracellular lipid droplets. *J. Cell Biol.* **100**, 965-973 (1985).

174 Choi, H. J. *et al.* Stability of whole inactivated influenza virus vaccine during coating onto metal microneedles. *J. Control Release* **166**, 159-171 (2013).

175 Baldwin, R. L. How Hofmeister ion interactions affect protein stability. *Biophys. J.* **71**, 2056-2063 (1996).

176 Choi, H.-J. *et al.* Effect of osmotic pressure on the stability of whole inactivated influenza vaccine for coating on microneedles. *Plos One* **10**, e0134431 (2015).

177 Adams, J. R. & Merz, A. R. Hygroscopicity of fertilizer materials and mixtures. *Ind. Eng. Chem. Res.* **21**, 305-307 (1929).

178 WHO. *Urgent Health Challenges for the Next Decade*, <https://www.who.int/news-room/photo-story/photo-story-detail/urgent-health-challenges-for-the-next-decade> (2020).

179 WHO. *WHO Director-General's Opening Remarks at the Media Briefing on COVID-19 - 11 March 2020*, <https://www.who.int/dg/speeches/detail/who-director-general-s-opening-remarks-at-the-media-briefing-on-covid-19---11-march-2020> (2020).

180 Xia, J., Gao, J. & Tang, W. Nosocomial infection and its molecular mechanisms of antibiotic resistance. *BioSci. Trends* **10**, 14-21 (2016).

181 Kelsen, S. G. & McGuckin, M. The role of airborne bacteria in the contamination of fine particle nebulizers and the development of nosocomial pneumonia. *Ann. N. Y. Acad. Sci.* **353**, 218-229 (1980).

182 Grieble, H. G., Bird, T. J., Nidea, H. M. & Miller, C. A. Chute-hydropulping waste disposal system: a reservoir of enteric bacilli and pseudomonas in a modern hospital. *J. Infect. Dis.* **130**, 602-607 (1974).

183 Rubino, I. & Choi, H. J. Respiratory protection against pandemic and epidemic diseases. *Trends Biotechnol.* **35**, 907-910 (2017).

184 Quan, F. S., Rubino, I., Lee, S. H., Koch, B. & Choi, H. J. Universal and reusable virus deactivation system for respiratory protection. *Sci. Rep.* **7**, 39956 (2017).

185 Cotes, J. E. *Lung Function: Assessment and Application in Medicine* (Blackwell Publishing, 1965).

186 Hasan, J. *et al.* Multi-scale surface topography to minimize adherence and viability of nosocomial drug-resistant bacteria. *Mater. Des.* **140**, 332-344 (2018).

187 Barrett, C. R., Nix, W. D. & Tetelman, A. S. *The Principles of Engineering Materials* (Prentice Hall, 1973).

188 Mullin, J. *Crystallization (Fourth Edition)* (Butterworth-Heinemann, 2001).

189 Lodish, H. *et al. Transport across Cell Membranes. Molecular Cell Biology* (Macmillan, 2000).

190 Hoffmann, E. K., Lambert, I. H. & Pedersen, S. F. Physiology of cell volume regulation in vertebrates. *Physiol. Rev.* **89**, 193-277 (2009).

191 Pau, K. S. *Thermoluminescence Studies of Naturally Ocurring Salts Relevant to Dosimetry Obtained from Mizoram* PhD thesis, Mizoram University (2013).

192 Robinson, M. T. The crystal structures of β-K2SO4 and β-K2PO3F. *J. Phys. Chem.* **62**, 925-928 (1958).

193 Ott, H. Die Strukturen von Mn O, Mn S, Ag F, Ni S, Sn I4, Sr Cl2, Ba F2, Oraezisionsmessungen einiger Alkalihalogenide. *Z. Kristallogr. Krist*, 144 (1977).

194 Zhao, J., Miao, H., Duan, L., Kang, Q. & He, L. The mass transfer process and the growth rate of NaCl crystal growth by evaporation based on temporal phase evaluation. *Opt. Lasers Eng.* **50**, 540-546 (2012).

195 Rodriguez-Clemente, R. *Crystal Growth Kinetics of Sodium Chloride from Solution. Industrial Crystallization* (Springer, 1976).

196 Al-Jibbouri, S. & Ulrich, J. The influence of impurities on crystallization kinetics of sodium chloride. *Cryst. Res. Technol.* **36**, 1365-1375 (2001).

197 Garside, J., Gaska, C. & Mullin, J. W. Crystal growth rate studies with potassium sulphate in a fluidized bed crystallizer. *J. Cryst. Growth* **13-14**, 510-516 (1972).

198 Mullin, J. W. & Gaska, C. The growth and dissolution of potassium sulphate crystals in a fluidized bed crystallizer. *Can. J. Chem. Eng.* **47**, 483-489 (1969).

199 Mullin, J. W. & Gaska, C. Potassium sulfate crystal growth rates in aqueous solution. *J. Chem. Eng. Data* **18**, 217-220 (1973).

200 Kardum, J. P., Sander, A. & Glasnoviæ, A. Batch crystallization of KCl: the influence of the cooling and mixing rate on the granulometric properties of obtained crystals. *Chem. Biochem. Eng. Q.* **19**, 39-48 (2005).

201 Sarig, S., Glasner, A., Epstein, J. A. & Eidelman, N. Growth of potassium chloride crystals. *J. Cryst. Growth* **39**, 255-266 (1977).

202 Hidalgo, A. F. & Orr Jr, C. Homogeneous nucleation of sodium chloride solutions. *Ind. Eng. Chem. Res.* **7**, 79-83 (1968).

203 Nývlt, J. Kinetics of nucleation in solutions. *J. Cryst. Growth* **3-4**, 377-383 (1968).